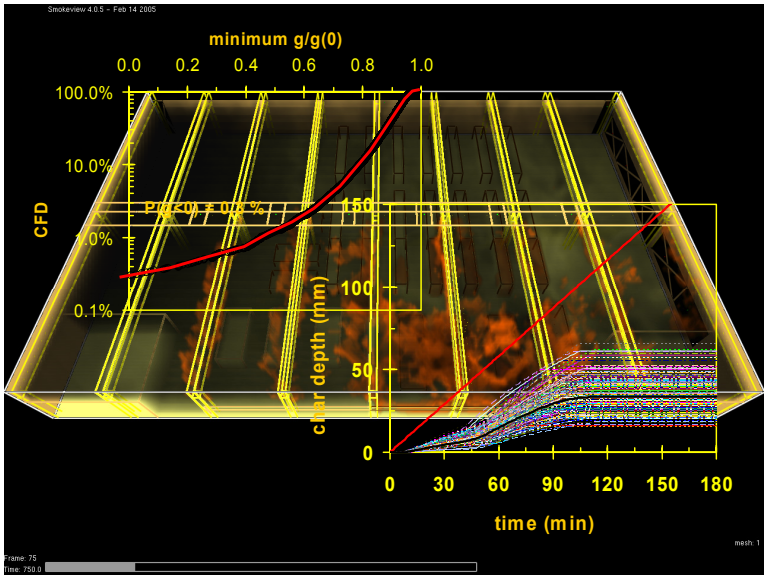

Application of reliability analysis and fire simulation to probabilistic assessment of fire endurance of wooden structures

Jukka Hietaniemi & Tomi Toratti
VTT

Simon Schnabl & Goran Turk
University of Ljubljana, Slovenia

ISBN 951–38–6606–8 (URL: http://www.vtt.fi/publications/index.jsp)
ISSN 1459–7683 (http://www.vtt.fi/publications/index.jsp)

JULKAISIJA – UTGIVARE – PUBLISHER

VTT, Vuorimiehentie 5, PL 2000, 02044 VTT
puh. vaihde (09) 4561, faksi (09) 456 4374

VTT, Bergsmansvägen 5, PB 2000, 02044 VTT
tel. växel (09) 4561, fax (09) 456 4374

VTT Technical Research Centre of Finland, Vuorimiehentie 5, P.O.Box 2000, FIN–02044 VTT, Finland
phone internat. + 358 9 4561, fax + 358 9 456 4374

VTT, Kivimiehentie 4, PL 1000, 02044 VTT
puh. vaihde 020 722 111, faksi 020 722 4815

VTT, Stenkarlsvägen 4, PB 1000, 02044 VTT
tel. växel 020 722 111, fax 020 722 4815

VTT Technical Research Centre of Finland, Kivimiehentie 4, P.O. Box 1000, FI-02044 VTT, Finland
phone internat. +358 20 722 111, fax +358 20 722 4815

Technical editing Maini Manninen

Published by

Series title, number and
report code of publication

VTT Working Papers 54
VTT–WORK–54

Author(s)
Hietaniemi, Jukka, Toratti, Tomi, Schnabl, Simon & Turk, Goran

Title

Application of reliability analysis and fire simulation to probabilistic assessment of fire endurance of wooden structures

Abstract

This report gives an exposition of the application of advanced, probabilistic calculation methods to assess of the fire endurance of structures. The particular application case that we address is glulam wooden structures in a hall-like large single-space building. The first method used is a reliability analysis based on the approximation of the fire exposure by the standard time-temperature curve and the second method is a novel simulation-based probabilistic approach integrating passive and active fire safety measures to an estimate of the risks involved.

Keywords
reliability analysis, wooden structures, fire simulation, charring, probabilistic models, Monte Carlo, fire resistance, beams, columns, glulam

ISBN
951–38–6606–8 (URL: http://www.vtt.fi/publications/index.jsp)

Series title and ISSN		Project number
VTT Working Papers 1459–7683 (URL: http://www.vtt.fi/publications/index.jsp)		R4SU00235
Date June 2006	Language English	Pages 97 p. + app. 23 p.
Name of project New simulation methods for fire safety analysis		Commissioned by Tekes & VTT

Contact
VTT Technical Research Centre of Finland
Kivimiehentie 4, P.O. Box 1000
FI-02044 VTT, Finland
Phone internat. +358 20 722 111
Fax +358 20 722 4815

Publisher
VTT Technical Research Centre of Finland
P.O. Box 1000
FI-02044 VTT, Finland
Phone internat. +358 20 722 4404
Fax +358 20 722 4374

Preface

This report gives an exposition of the application of advanced, probabilistic calculation methods to assess of the fire endurance of structures. The particular application case that we address is glulam wooden structures in a hall-like large single-space building. The first method used is a reliability analysis based on the approximation of the fire exposure by the standard time-temperature curve and the second method is a novel simulation-based probabilistic approach integrating passive and active fire safety measures to an estimate of the risks involved.

The work has been out at VTT Building and Transport, Finland. It forms a part of a larger research project launched to develop new tools for fire simulation with the aim set at producing generally acceptable and valid science-based tools to meet the needs of fire safety design and risk assessment within the industry and other stakeholders.

The project is funded by the National Technology Agency of Finland (Tekes) and VTT Building and Transport.

Contents

Preface 4

1. Introduction....7

2. Description of the building and structures....9

3. Statistical models for the variables treated as stochastic quantities....10
   - 3.1 Recommendations on the distributions....10
   - 3.2 Distributions and characteristic values used in this study....10
     - 3.2.1 Glulam strength distribution....11
     - 3.2.2 Permanent load distribution....12
     - 3.2.3 Snow load distribution....13
       - 3.2.3.1 About the different approach to modelling variable loads....13
       - 3.2.3.2 Data on the amount of snow at the location of the building....14
     - 3.2.4 Geometrical factors and model uncertainty distributions....19

4. Limit-state function for the beam....20
   - 4.1 Limit state for the normal-temperature analysis....20
   - 4.2 Limit state for the fire-condition analysis....22

5. Reliability analysis for normal-temperature conditions....24
   - 5.1 Reliability analysis using the annual maximum snow load distribution....24
   - 5.2 Reliability analysis for each month....25
   - 5.3 Comparison to target reliability values....27

6. Reliability analysis of the beam for the standard fire exposure conditions....28

7. Approach based on fire simulation....32
   - 7.1 Modelling of the example building....32
   - 7.2 Results of fire simulation....33
     - 7.2.1 Heat release rate....33
     - 7.2.2 Temperature....35
     - 7.2.3 Smoke density and flow field....40
       - 7.2.3.1 Smoke density....40
       - 7.2.3.2 Flow velocity....42
   - 7.3 Oxygen concentration....46
   - 7.4 Charring of the wooden structures evaluated on the basis the fire simulation results....46
     - 7.4.1 Heat transfer from the fire to the wooden members....47
     - 7.4.2 Calculation of wood charring....52

7.4.2.1 Formulation 52
7.4.2.2 The initial charring rate 53
7.4.2.3 Charring rate curves 55
7.4.2.4 Char depth 57
7.4.2.5 Limit state functions vs. time 59
7.4.2.6 Analysis of the most severe case: heating of a beam at position y = 30 m and x = 36 m 62
7.5 Interpretation of the likelihood of structural failure taking into account the wholeness of the building fire-safety 65
7.5.1 Risks to life and their reduction 65
7.5.1.1 The threat 65
7.5.1.2 The threatened 67
7.5.1.3 Risk to life 75
7.5.2 Influence of the fire brigade 78
7.5.2.1 Turnout time 79
7.5.2.2 Travel time 80
7.5.2.3 Water set-up time 81
7.5.2.4 Search and rescue time 81
7.5.2.5 Time from fire detection to the fire brigade intervention 82
7.5.2.6 Time from fire initiation the to fire brigade intervention 83
7.5.3 Analysis of the structural failure probabilities using the Time-Dependent Event Tree Method 85

8. Summary 91

Acknowledgements 92

References 93

Appendices:

Appendix A: Further analysis of the snow-load data
Appendix B: Detailed presentation of the FDS4 fire simulation results
Appendix C: Thermal properties of air
Appendix D: The time-dependent event tree risk analysis method

1. Introduction

This report gives an exposition of the application of advanced, probabilistic calculation methods to assess of the fire endurance of structures. The particular application case that we address is glulam wooden structures in a hall-like large single-space building.

The first part of the report presents a reliability analysis based on the approximation of the fire exposure by the standard time-temperature curve [Toratti & Turk 2005]. The Eurocode 5 and the norm B10 of the Finnish building code are used as the deterministic methods to which the probabilistic method is compared to. The calculations address the effect of the strength variation of the glulam material as well as the treatment of the variability of the snow load. The results show that the probability of failure resulting from a deterministic design based on Eurocode 5 is low compared to the target values and lower sections are possible if applying a probabilistic design method. In fire design, if a 60 minute resistance is required, this is not the case. Stochastic charring rates have a significant influence on the results as well.

The second part of this report deals with an approach based on fire simulation. The novelty of the approach lies in several features:

- use of the state-of-art fire simulation program FDS4 [McGrattan 2004a, 2004b] to assess the course and influence of a natural fire,
- analysis of the deterministic results obtained from the FDS4 simulations to a stochastic description of the natural fire and subsequent probabilistic calculations using the Probabilistic Fire Simulator developed at VTT [Hietaniemi *et al*. 2004c, Hostikka & Keski-Rahkonen 2003, Hostikka *et al.* 2003],
- the use of the Time-Dependent Event Tree (TDET) method developed at VTT [Hietaniemi *et al.* 2002, Korhonen *et al.* 2002, Hietaniemi *et al.* 2004, Hietaniemi *et al.* 2005] to integrate the influence of fire-safety measures to the fire safety analysis.

In the case of analysis of wooden structures, the uncertainties pertaining to the properties of the structures are considerable, both with regard to the response of wood to heating as well as the mechanical response of the wooden structure. Further uncertainties arise from deficiencies in our knowledge and models. Hence, the simulation-based probabilistic integrated fire safety approach is useful to the analysis of the structural adequacy of wooden structures in case of fire. Probabilistic fire simulation calls for use of the Monte Carlo technique, *i.e*., executing a vast number of simulations with parameter values drawn from the distributions characterising their scatter. This requires a lot of computing power which has only recently become available for the fire engineers as a result of the enormous growth in the computing power during the last

decade. As there are readily available software packages such as the Probabilistic Fire Simulator (PFS) developed by the Fire Research Group of VTT [Hietaniemi *et al*. 2004c, Hostikka & Keski-Rahkonen 2003, Hostikka *et al.* 2003] that can be used to carry out probabilistic fire simulation and, hence, it can be foreseen that this technique will in the near future become a standard fire safety engineering design tool. When combined with risk-analytical tools, probabilistic fire simulation can also be used in order to accomplish such far reaching goals as updating the fire regulations [Hietaniemi et al. 2004] towards a more risk-based system [Hietaniemi *et al.* 2005]. The simulation-based probabilistic fire endurance assessment presented in this report is intended to give the reader a comprehensive and concrete exposition of the use of the methodology which represents the leading edge of modern fire technology. The results of the fire risks obtained using the simulation-based probabilistic fire endurance assessment show that the glulam structures are actually able to withstand the fire exposure throughout the whole fire duration up to the burn-out of the fire load.

2. Description of the building and structures

The building considered in this study is a grocery shop located in the South-West region of Finland. It consists basically of a single space with length of 50 m, width 34 m and height 5,5 m. The building is a timber beam-column structure constructed of glued laminated wood (see Figure 1). The glulam columns support 17 m long beams which compose the roof structure (see Figure 2). The cross section height h varies between 854 mm and 1215 mm and its width is $b = 165$ mm. The beam spacing is $s = 6{,}3$ m. Deterministic design calculations using 50 % of the snow load characteristic to that part of Finland, *i.e.*, 1,4 kN/m^2, show that unprotected the beam would survive standard fire exposure for 30 minutes.

There are smoke vents opening at 100 ˚C on the roof of the building. Activation of these smoke vents send also an alarm signal to the community fire brigade located close to the building (at distance of about 500 m).

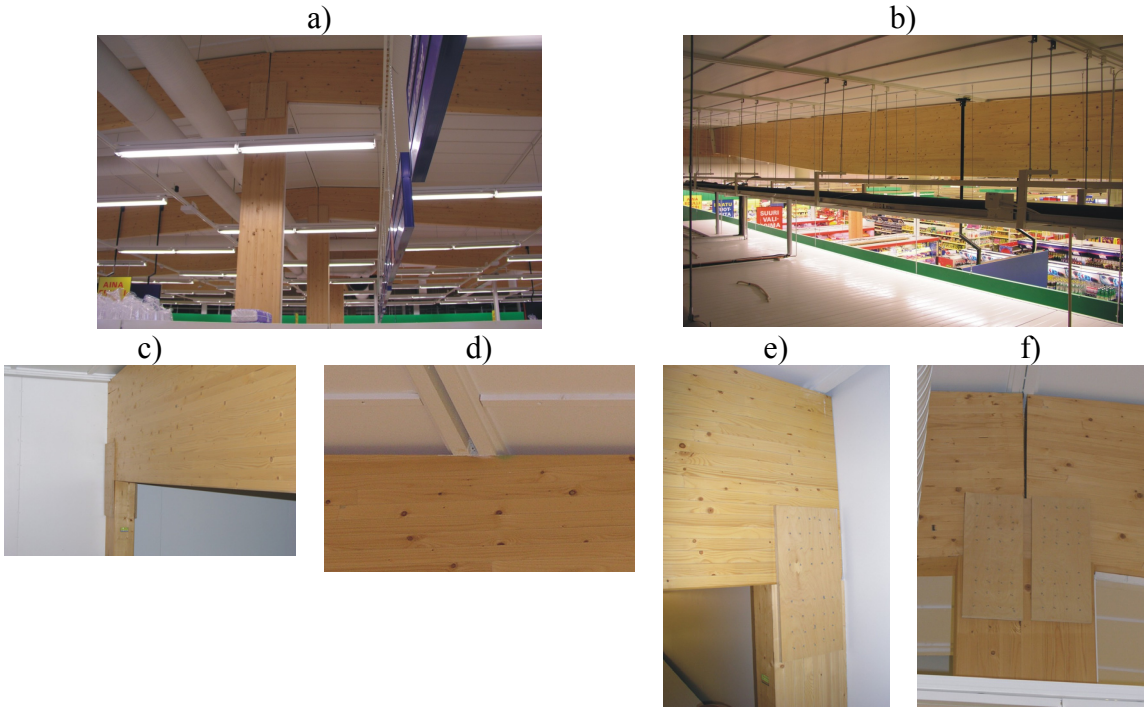

Figure 1. Photographs of the structures.

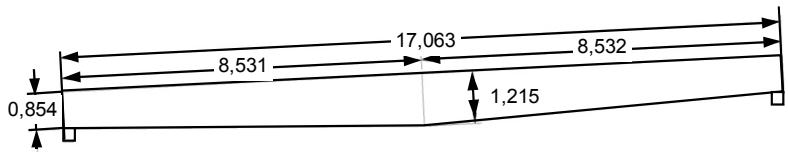

Figure 2. The glulam beam spanning between the columns. Dimensions are given in meters; the width is 0,165 m.

3. Statistical models for the variables treated as stochastic quantities

3.1 Recommendations on the distributions

For the present analysis we consider two mainly sources of input data, *i.e.*, the probabilistic model code [JCSS 2001] and [SAKO 1999], which is a Nordic study on the calibration of partial safety factors for various building materials. Table 1 summarises the input recommended in [SAKO 1999]. Extensive reliability studies have also been carried out by Thelandersson *et al*. [Thelandersson *et al.* 1999] and Ranta-Maunus [2001.]. In Ranta-Maunus [2001], the emphasis was on the precise description of the strength lower tail distribution for wooden products and on the calibration of partial safety factors for wooden structures. In Thelandersson *et al*. [1999], the emphasis was on the long-term load analysis and related calibration of the strength modification factors.

Table 1. Statistical distributions and coefficients of variation recommended in [SAKO 1999].

Type of parameter		**Parameter**	**Coefficient of variation**			**Distri-bution**
			Concrete	**Steel**	**Glulam**	
Loads	Permanent	– Self-weight	0,06	0,02	0,06	Normal
		– Other	0,10	0,10	0,10	Normal
	Variable	– Environmental	0,40	0,40	0,40	Gumbel
		– Imposed	0,20	0,20	0,20	Gumbel
Strength		Concrete	0,10			Log-Normal
		Reinforcement	0,04			Log-Normal
		Structural Steel		0,05		Log-Normal
		Glulam			0,15	Log-Normal
Geometry		Effective depth	0,02			Normal
		Beam depth	0,02	0,01	0,01	Normal
		Beam width	0,02	0,01	0,01	Normal
		Plate thickness		0,04		Normal
Model uncertainties		R-model	0,05	0,05	0,05	Normal

3.2 Distributions and characteristic values used in this study

In the following we elaborate further the distributions concerning the glulam strength, permanent load, snow load, geometrical factors and model uncertainty.

3.2.1 Glulam strength distribution

There exists few test data which could be used to describe the glulam strength distribution. (Much more is available for other wooden materials like structural timber, LVL or plywood). To obtain the lower tail strength distribution with enough accuracy, a high number of tests are required. The largest test sample available to the authors is described in Table 2. This data was obtained in a joint Nordic project on the reliability of timber. The tests were carried out in NTI Norway.

Table 2. Available glulam test data. [Ranta-Maunus A., Summary report of NI project on reliability of timber structures. October 2001. Joint Nordic wood project meeting and Cost E24 workshop. Copenhagen]

Target $f_{0.05}$ [N/mm^2]	$f_{0.05}$ in test [N/mm^2]	Explanation of test	Sample size	Tail fitted [%]	Fitting distribution	COV [%]
30	33.5	Edgewise bending	126	10	Normal Log-normal	11 13
37	39.9	Edgewise bending	109	10	Normal Log-normal	14 19

In these test samples, the target characteristic values were achieved. The tail fitting of the strength distribution resulted in a coefficient of variation of 13 % and 19% when using the log-normal distribution. It was concluded in the above reference, that until further evidence, a log-normal distribution with a coefficient of variation of 15 % may be recommended. More test results on glulam are however needed.

For this study we adapt for bending strength F the lognormal distribution with the probability density function given by

$$f_F(x) = \frac{1}{\beta\sqrt{2\pi}\cdot x}\cdot\exp\left[-\tfrac{1}{2}\left(\frac{\ln x-\alpha}{\beta}\right)^2\right], \qquad (1)$$

with the basic of the value coefficient of variation of V_F = 15 %. To see the influence of the coefficient of variation, it is subjected to a parametric study in which its value is varied from 5 % to 40 %. The parameters α and β of the lognormal distribution may be evaluated from the $V_F = m_F/\sigma_F$ where m_F is the mean value and σ_F is the standard deviation and the characteristic strength of the particular glulam material considered. As the glulam material is of structural quality L40, we may assume that the characteristic value if the bending strength is $f_k = F_{0.05}$ = 39 N/mm^2 (short term strength). Solving for α and β we obtain the values given in Table 3 for the different coefficient of variation values considered. Figure 3 shows the distribution functions for V_F = 15 %.

Table 3. Parameters of the lognormal distribution used to characterise the glulam bending strength. The values printed in bold face type correspond to the basic case, others are relevant for the parametric study of the influence of V_F.

V_F	α	β	V_F	α	β
5 %	3,746	0,0499	25 %	4,068	0,246
10 %	3,828	0,0997	30 %	4,146	0,293
15 %	**3,909**	**0,149**	35 %	4,222	0,340
20 %	3,988	0,197	40 %	4,297	0,385

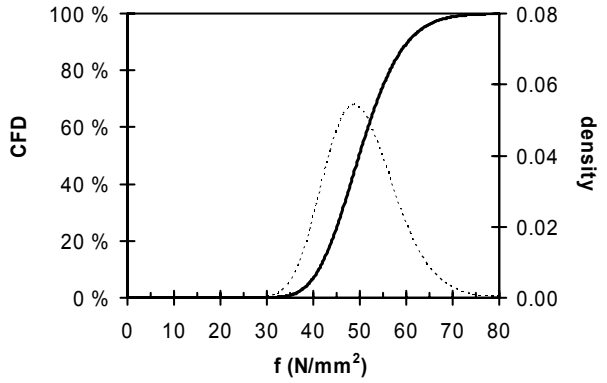

Figure 3. The cumulative frequency distribution (CFD) and the probability density function used to characterise the bending strength in the case V_F = 15 %.

3.2.2 Permanent load distribution

According to the recommendations given in Table 1, the permanent load G is normally distributed. We take the coefficient of variation to be V_G = 5 %. The mean value m_G of the permanent load may be calculated on the basis of the glulam beam and the roof self-weights. The glulam beam self-weight is assumed to be 0,88 kN/m acting on the beam as a line-load and the roof self-weight 0,44 kN/m^2 acting on the whole roof area. Since the beams are 6.3 m apart the width of the roof loading lumped to each beam is 6.3 m. Therefore, the mean value m_G and the standard deviation σ_G of the normally distributed permanent load are

$$\begin{aligned} m_G &= 6.3 \cdot 0.44 + 0.88 = 3.65 \,\text{kN/m.}, \\ \sigma_G &= m_G \, V_G = 0.18 \,\text{kN/m.} \end{aligned} \tag{2}$$

Figure 4 shows the permanent load distribution functions.

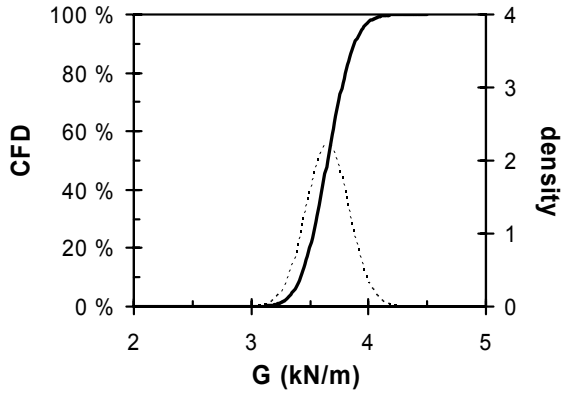

Figure 4. The cumulative frequency distribution (CFD) and the probability density function used to characterise the permanent load.

3.2.3 Snow load distribution

3.2.3.1 About the different approach to modelling variable loads

The possibility that there is additional load due to snow on the roof is usually tackled by using the methods stipulated in norms, e.g., the national norms or the Eurocodes. These approaches are based on the potential *maximum* amount of snow that there can be on the roof. In practise the values used are obtained from statistics on annual maxima, from which then some suitable high percentile value is chosen as the design value. The fact that buildings are not loaded with full snow load throughout the whole year – even in Finland the snow lad in the summertime is usually negligible – is taken into account by multiplying the snow load design value by suitable reduction factor. In principle this approach is straightforward and the amount of computational labour is usually so low that they could be carried out even with the computers of the 1970's or 1980's. This may be the main reason for the popularity of these approaches even today, the fact these methods were rooted because of mere practical reasons into the structural fire analysis back those days. Yet, there are some pitfalls in these approaches: in the description given above, the phrase "suitable" occurred twice. However, there is no consensus of what is suitable: what is suitable for one stakeholder may be utmost unsuitable to another. As a result of this circumstance, there is a quite a bit of "political" arguing behind the selection of the "suitable" values. This is not to say that it is necessarily wrong, because actually on the average the situation settles to a generally balanced situation in which one stakeholder side wins while some other looses. What the horse-trading concerning the suitable factors does introduce to the approaches is a significant un-scientific component.

As this report after all is a report produced in a project with its objective to develop new generally acceptable, i.e., science-based, technical tool to tackle the fire problem, we present also another approach to treat the snow load problem: this approach entirely based on simulation which suits very well with the spirit of the project that this work belongs to. This approach is very simple, even much simpler than the approaches that have found their way to the norms. The only drawback is that it requires more computational power, but today there is plenty of that available, not to mention the situation in the future. In this approach one first uses snow statistics to assemble a distribution charactering the snow situation through one year – a year is the natural basic time unit as the snow situation repeats itself on a one-year period – and then, secondly, one executes Monte Carlo sampling from this annual snow distribution with a fire simulation and the associated structural analysis carried using the sampled snow load. When this is repeated sufficiently many times, a comprehensive probabilistic picture of the structural performance emerges. The question how many times is "sufficient" is not a question of suitability, but the required number of the Monte Carlo runs depends on how small probabilities we need to resolve in the analysis.

3.2.3.2 Data on the amount of snow at the location of the building

3.2.3.2.1 Distribution of annual maximum values

The basic data available for the determination of the loading caused by the snow is the measurements of the snow water equivalent in the region corresponding to the geographic location of the building. If one follows the approach based on the annual maxima, the data displayed in Figure 5 suffices. This data can be modelled using the extreme value distribution (or Gumbel distribution) the probability density function given by

$$f_{Q_{\max}}(x) = \frac{\exp\left[-(x-a)/b - \exp\left[-(x-a)/b\right]\right]}{b}, \tag{3}$$

where the parameters a and b can be determined using the data. One piece of information on a and b is given in Table 1, *i.e.*, that the coefficient of variation can be assumed to V_Q = 40 % and another piece of information can be read from Figure 5 which shows that we may estimate the 98 % fractile of the distribution (corresponding to 50 years return period) to be 220 mm. The resulting values of a and b are a = 88,558 mm and b = 33,683 mm.

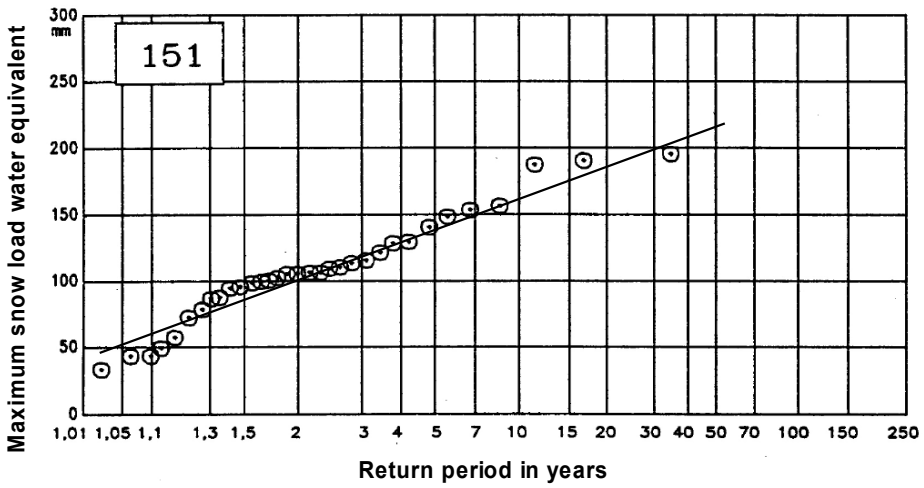

Figure 5. Data of Perälä & Reuna [1990] on the maximum annual snow in the region of the building considered expressed as water equivalents.

The snow loading expressed in water equivalents (in mm) can be converted to a line snow roof load (in kN/m) by multiplying by the acceleration of gravity 9,81 m/s^2 and diving by 1000 (giving units of kN/m^2) and multiplying by the spacing of the columns s = 6,3 m and finally, by using a conversion factor of 0,8 to transform the ground snow-load value to a roof-snow load value. The resulting values of a and b for the Gumbel distribution used to characterise the annual maximum snow load are:

- a = 4,38 kN/m
- b = 1,67 kN/m.

Figure 6 shows the distribution functions of the annual maximum value of the snow load.

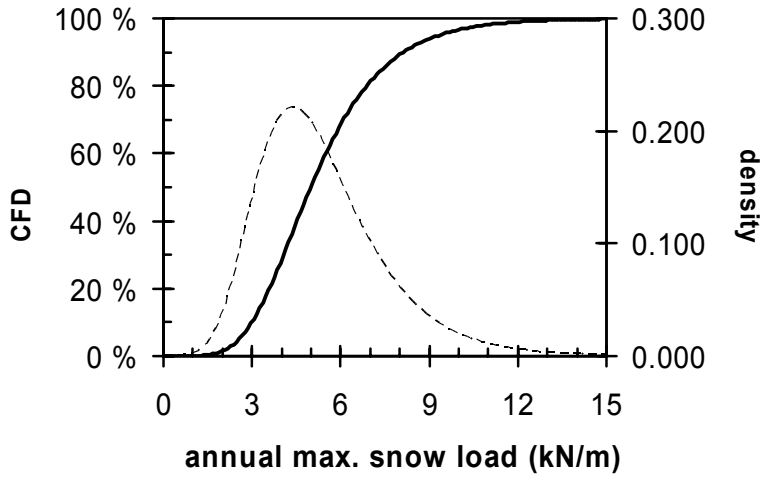

Figure 6. The cumulative frequency distribution (CFD) and the probability density function used to characterise the annual maximum snow load.

3.2.3.2.2 Distribution of annual values

In the simulation treatment of the snow load we need a more detailed picture of the snow loading. The most well-resolved data available is the data measured every month. This data reflects the actual snow loading that one would find on a randomly selected moment of time. The basic data we use is the monthly snow water equivalent data in the region no. 35312 ranging from the city of Nokia to the city of Harjavalta shown in Figure 7.

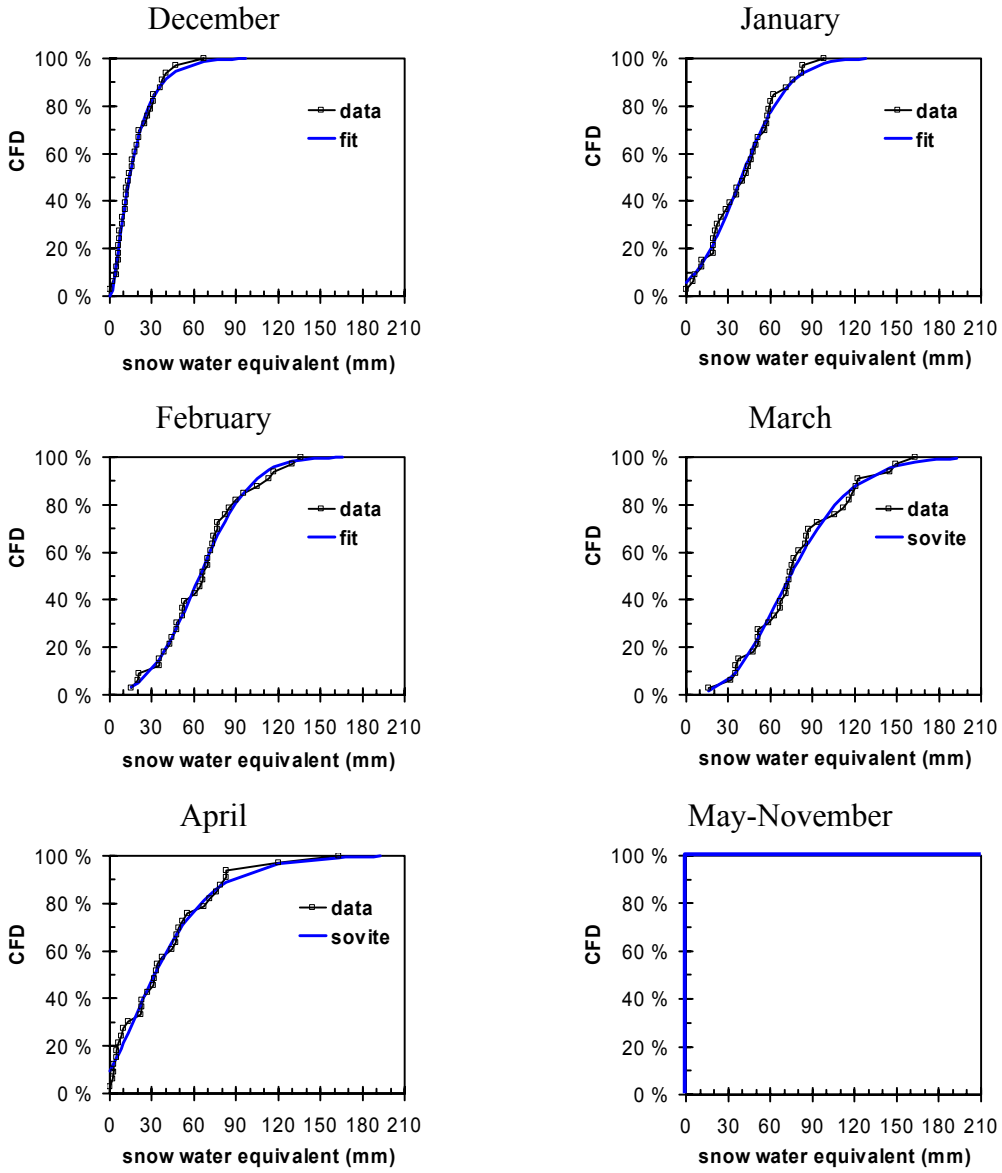

Figure 7. The distributions of the snow water equivalent values measured in the region of Finland close to the building considered in this study. Data from winters 1960/1961 to 1992/1993. The dotted curves represent the data and the smooth curves are fits to the data using the gamma distribution.

The monthly data can be used to evaluate the annual snow loading distribution by using the Monte Carlo method, *i.e.*, selecting values randomly from the distributions shown in Figure 7 and analysing what kind of a distribution the Monte Carlo sample forms. Results of the Monte Carlo analysis[1] are shown Figure 8. The data Monte Carlo samples are modelled a combination of the Dirac delta distribution (that models the summer months with no snow) and a 3-parameter Weibull distribution that models the months with snow on the ground:

$$f_Q(x) = \eta \cdot \delta(x) + (1-\eta) \cdot \left(\frac{\alpha}{\beta^\alpha} \right) (x-c)^{\alpha-1} \exp\left[-\left(\frac{x-c}{\beta} \right)^\alpha \right]. \qquad (4)$$

The parameter η is the fraction of times when there is no snow and α, β and c are the Weibull distribution parameters. According to the Monte Carlo analysis and the curve fitting, $\eta = 61{,}0$ %, $\alpha = 2{,}014$, $\beta = 85{,}474$ mm and $c = -18{,}118$ mm (see Figure 8).

The conversion to snow load in units of kN/m goes as explained above and the parameters for the distribution describing the snow load are

- $\eta = 61{,}0$ %
- $\alpha = 2{,}014$
- $\beta = 4{,}226$ kN/m
- c = -0,8958 kN/m.

Figure 9 shows the distribution functions of the annual snow load.

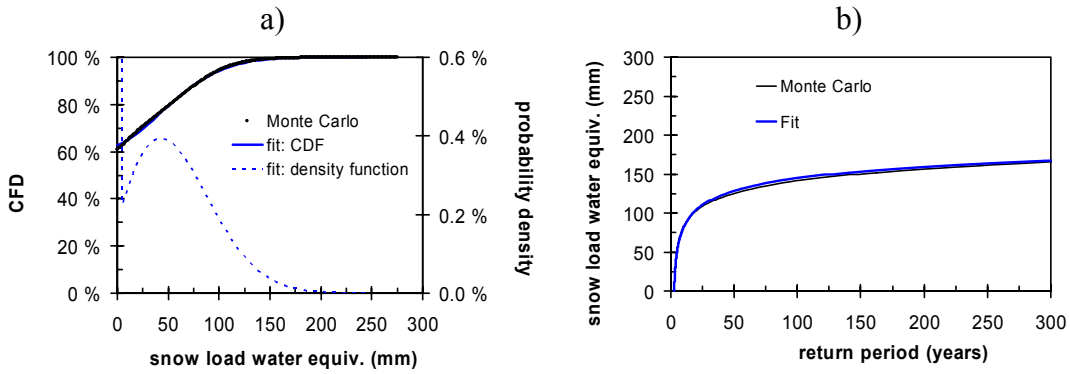

Figure 8. Distribution of the annual snow loading expressed as water equivalents obtained by Monte Carlo analysis of the monthly data: a) a conventional form of plotting the cumulative frequency distribution vs. the variable value and b) an inverted plot using the return-period concept.

[1] The sampling technique is not actually crude Monte Carlo, but Latin hypercube sampling.

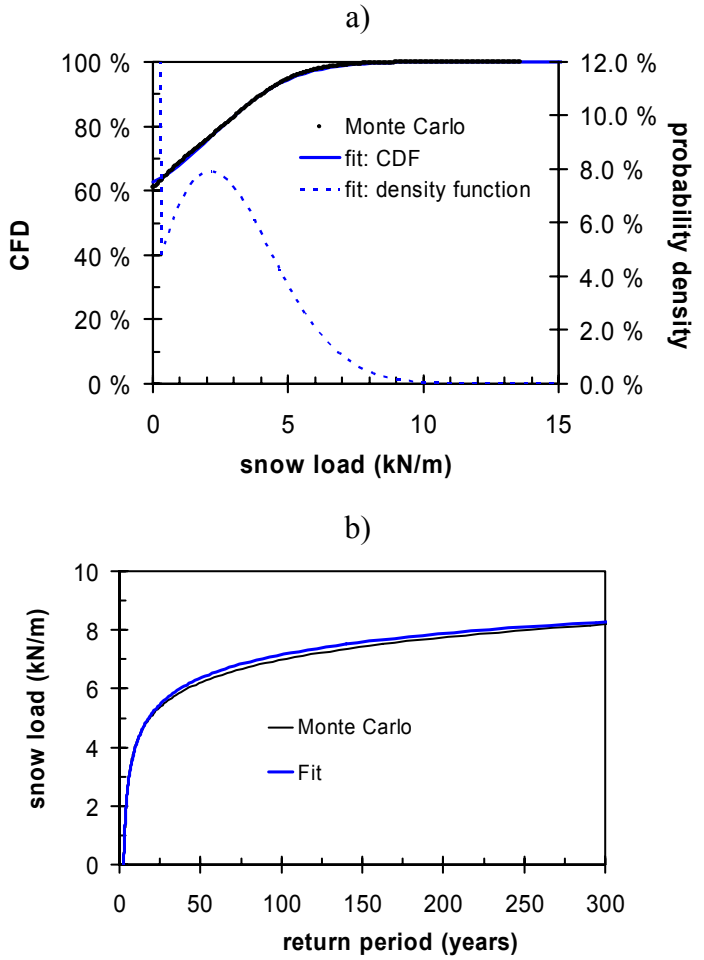

Figure 9. Distribution of the annual snow load obtained by Monte Carlo analysis of the monthly data: a) a conventional form of plotting the cumulative frequency distribution vs. the variable value and b) an inverted plot using the return-period concept.

It should be noted that the distributions obtained to characterise the monthly snow water equivalent data can be used – via Monte Carlo sampling – to obtain an estimate for the distribution of the annual maximum values. A comparison of a distribution obtained in this way to the data shown in is presented in Figure 5 is presented in Appendix A. The agreement is fairly good: the mean value and coefficient of variation for the data shown in Figure 5 are 108 mm and 38 % and those obtained on the basis of the monthly distributions are 97 mm and 32 %.

3.2.4 Geometrical factors and model uncertainty distributions

To characterise the variability in the cross section dimensions we adapt the suggestions given in Table 1 and assume that b and h are normally distributed with a coefficient of variation of 1 %.

Also the characterisation of the model uncertainties, a multiplication factor k_{model}, is done according Table 1 and thus we take its mean value to be unity and the standard deviation equal to 5 %.

4. Limit-state function for the beam

Since the beam is simply supported, the evaluation of internal forces is elementary. The structural analysis was carried out on bending at the critical cross section, bending at the apex section and shear. The initial analysis showed that the critical cross section is situated where the bending stresses are highest. The beam height at this point is h_{cr} = 1060 mm. Bending at the apex zone was not critical. Also the shear capacity resulted in much lower probabilities of failure. Therefore in the following, only the critical cross section in bending is analysed. The strength reducing factor for torsional buckling is not required for normal design, but it becomes necessary for the fire design were more slender sections are analysed.

The stresses in the critical cross section are calculated in two different ways: a) according to the Finnish building code on the design of timber structures B10 [RIL 2001] and b) according to Eurocode 5 [CEN 2002].

4.1 Limit state for the normal-temperature analysis

The design is based on the requirement that the normal stress σ_{xx} should not exceed the bending strength F (expressed in N/mm^2) taking into consideration a height effect in the critical cross section, *i.e.*,

$$\sigma_{xx} \le \zeta \cdot F \tag{5}$$

where the factor ζ is different in the two design norms.

In the Finnish national norm B10 a height effect in the critical cross section is taken into consideration as follows

$$\zeta = C_F = \left(\frac{300 \text{ mm}}{h_{cr}} \right)^{\frac{1}{9}}, \tag{6}$$

which for h_{cr} = 1060 mm gives C_F = 0,87.

In the Eurocode 5, Eq. (1) is applied to the outermost fibre of the tapered edge. The angle between the beam main axis and the fibre direction may deviate in the compressive side of the beam and this is taken into account by a strength-reduction factor $k_{m,\alpha}$, *i.e.*, the Eurocode 5,

$$\zeta = k_{m,\alpha} = \frac{1}{\sqrt{1 + \left(\frac{f_{m,k}}{1.5 f_{v,k}} \tan\alpha\right)^2 + \left(\frac{f_{m,k}}{f_{c,90,k}} \tan^2\alpha\right)^2}}, \tag{7}$$

where the factors $f_{m,k}$, $f_{v,k}$, and $f_{c,90,k}$ are the characteristic values of the bending strength, the shear strength, the compression strength perpendicular to the grain, respectively, and $\alpha = 2{,}5^{\circ}$ is the angle of taper. The following values were taken (short-term characteristic strengths):

- $f_{m,k} = 39{,}0$ N/mm^2,
- $f_{v,k} = 3{,}5$ N/mm^2,
- $f_{c,90,k} = 6$ N/mm^2,

resulting in $k_{m,\alpha} = 0{,}95$.

The design equation may be expressed in terms of the limit state function g_ζ as

$$g_\zeta \geq 0\,. \tag{8}$$

where for the maximum bending stress case g_ζ reads

$$g_\zeta = F\, k_{\mathrm{mod}} C_F - \left(\frac{N_{xp}\,(G+Q)}{bh} + \frac{6\,M_{yp}\,(G+Q)}{bh^2}\right) k_{\mathrm{model}}\,, \tag{9}$$

where the constant factors are:

- $k_{mod} = 1/1{,}3 \approx 0{,}77$ (B10) or 0,8 (Eurocode 5),
- $C_F = 0{,}87$ (B10) or $k_{m,\alpha} = 0{,}95$ (Eurocode 5)

and the stochastically treated quantities are

- G is the permanent load (in N/mm^2); normal distribution with $V_G = 0.05$
- Q: Snow Load (Gumbel, $C_Q = 0.40$)
- F: Glulam strength (log-normal, $V_f = 0.15$)
- b and h: Section dimensions, height and width (normal, $V_{b \text{ or } h} = 0.01$)
- k_{model}: Model uncertainty (normal, mean = 1.0, $V_m = 0.05$).

The force factors N_{xp} and M_{yp} are obtained by a mechanical analysis. Their values are treated as constants:

- $N_{xp} = 0{,}346$ [kN per unit load kN/m] and
- $M_{yp} = 29{,}144$ [kNm per unit load kN/m].

4.2 Limit state for the fire-condition analysis

In the fire conditions, the beam may become so slender that the torsional buckling becomes significant. This is taken into account by modifying the strength term in the limit state equation by the strength reduction factor for torsional buckling of the beam (as given in EC5) k_{crit} giving

$$g = F\, k_{crit}\, k_{\mathrm{mod},fi} \begin{matrix} k_{m,\alpha} \\ \text{or} \\ C_F \end{matrix} - \left(\frac{N_{xp}(G+Q)}{b_{red} h_{red}} + \frac{6\, M_{yp}\,(G+Q)}{b_{red} h_{red}^2} \right) k_{\mathrm{model}} \tag{10}$$

In the analysis of the torsional buckling we consider that the beam is supported at 2,4 m spacing from the top edge.

The fire exposure is taken into account by letting the section dimensions for height h_{red} and width b_{red} to reduce during time:

$$\begin{aligned} h_{red} &= h - d_{eff}\,, \\ b_{red} &= b - d_{eff}\,. \end{aligned} \tag{11}$$

For the standard fire conditions, according to the Eurocode 5 the charring depth d_{eff} is given by

$$d_{eff} = \beta_n t + K_0 d_0 \tag{12}$$

where β_n = 0,7 mm/min, K_o = 1, d_o = 7 mm and t is the time in minutes and according to the Finnish norm B10

$$d_{eff} = \beta_n t\,. \tag{13}$$

In the reliability analysis given in Chapter 6 we carry out also a parametric study of the influence of the variability of the charring rate by letting the charring rate β_n to be a normally distributed quantity with mean value of 0,7 mm/min and the coefficient of variation of 10 %, 20 % or 30 %.

For the fire design based on the standard fire design also the values of $k_{mod,fi}$, $k_{m,\alpha}$ and C_F differ from the normal-temperature analysis. In the fire design these factors have the following values:

- $k_{mod,fi}$ = 1.0, $k_{m,\alpha}$ = 0.95 (Eurocode 5)
- C_F = 1 (B10).

In the case of the simulated fire exposure, the char depth is calculated on the basis of the heat exposure to the structures as described in section 7.4.2. In this case, the charring rate is an inherent stochastic quantity.

5. Reliability analysis for normal-temperature conditions

5.1 Reliability analysis using the annual maximum snow load distribution

The reliability analysis using the limit state given in the previous Chapter was performed by the computer program Comrel [RCP GmbH 1999]. Initially, different reliability methods were tried. Since the problem is relatively simple, different methods (FORM, SORM, crude Monte Carlo, adaptive sampling, etc.) gave almost identical results. In adaptive sampling 20 000 repetitions of the calculation were performed, whereas the number of simulations in crude Monte Carlo was 5 000 000. There were clearly advantages with the other methods compared to crude Monte Carlo simulations: the solutions were more stable and the calculation was faster. In the following, the adaptive sampling procedure is used in the reliability analysis.

The probability of failure for the two different design codes as a function of the coefficient of variation of strength is shown in Figure 10. The relationship is not monotonic; instead it has a maximum between 0,125 and 0,15. The failure probability increases for larger or smaller coefficients of variation. From Figure 10 we may notice that the probability of failure increases over 10-fold as the coefficient of variation increases from 0,15 to 0,40.

The probability of failure P_f is close to a minimum at a strength variation of about 15 %, a value usually assumed for glulam, and it is not very sensitive to the strength variation in this range. Considering the failure probability, there seems to be no reason for attempting to decrease the strength variation, unless the material strength characteristic value is affected. This low sensitivity of the strength variation is also of advantage considering the accuracy of a reliability analysis of a glulam structure, because to start with the variation of strength is not very precisely known.

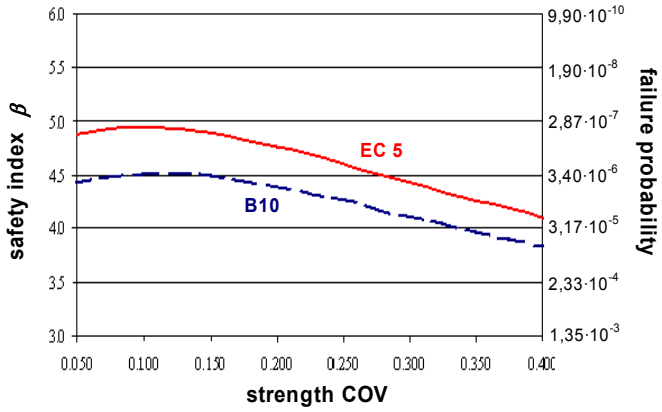

Figure 10. Dependence of the safety index β on the strength coefficient of variation for the two norms, Eurocode 5 and the Finnish norm B10.

The calculation shows that for a glulam having a strength COV of 15 %, according to B10 the β-value is 4,49 corresponding to a failure probability of Pf = 3,56·10-6 and according to EC5 the β-value is 4,89 corresponding to a failure probability of Pf = 0,51·10-6. In the following calculation the glulam strength coefficient of variation is 15 % in all cases.

5.2 Reliability analysis for each month

In the following, the monthly measured snow load water equivalents shown in Figure 7 were used as the basis of the analysis. This was done in order to see the variation of the reliability during a year and to compare the yearly maximum value with the results obtained according to the code format calculations given in the preceding section. The results are shown in Figure 11.

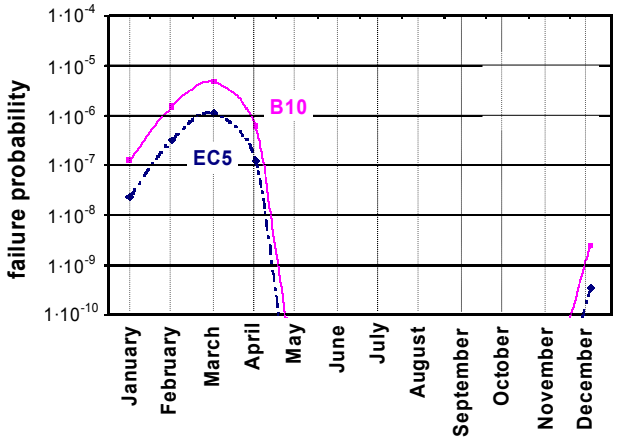

Figure 11. Probability of failure during one year (bending failure mode at maximum bending stress location).

The maximum probability of failure occurs during March in this case and the value is $P_f = 1{,}16 \cdot 10^{-6}$ according to EC5 and $P_f = 4.80 \cdot 10^{-6}$ according to B10. The annual probability of failure is:

$$P_{f,year} = 1 - (1 - P_{f,January})(1 - P_{f,February}) \cdots (1 - P_{f,December}). \quad (14)$$

These probabilities are compared with the results of the previous section in Table .

As may be observed from Table 4, there is some effect of the distribution model used for the snow load. The differences are not high when the β-values are compared. The monthly normal distribution method gave a double failure probability, in case of B10, and triple, in case of EC5. These differences may be due to the different ways to describe the snow load data and/or to the different distributions used.

Table 4. Annual probability of failure: comparison between the values obtained using two descriptions for the snow load, the distribution of the annual maximum values and the distributions monthly measured values.

Code used	β value and $P_{f,year}$ based on annual maximum snow load	β value and $P_{f,year}$ based on monthly snow loads
EC5	4.885 ($5.18 \cdot 10^{-7}$)	4.654 ($1.63 \cdot 10^{-6}$)
B10	4.489 ($3.58 \cdot 10^{-6}$)	4.344 ($7.05 \cdot 10^{-6}$)

5.3 Comparison to target reliability values

The calculated reliabilities may be compared to the target values given in Table 5 for reliability class 2 (moderate consequences of failure). The probabilistic model code gives a safety index value of 4,2, and prEN 1990 [CEN 2001] gives a value of 4,7 . The calculated reliabilities are higher than the target levels given in probabilistic model code [JCCS 2001].

Table 5. Recommended target β-values in ultimate limit state for a one year period according to the probabilistic model code [JCCS 2001.] and prEN 1990 [CEN 2001].

	Relative cost of safety measure	Class 1 Minor consequences of failure		Class 2 Moderate consequences of failure		Class 3 Large consequences of failure	
		β	P_f	β	P_f	β	P_f
Probab. model code	Large (A)	3,1	$\approx 9{,}7\cdot10^{-4}$	3,3	$\approx 4{,}8\cdot10^{-4}$	3,7	$\approx 1{,}1\cdot10^{-4}$
	Normal (B)	3,7	$\approx 1{,}1\cdot10^{-4}$	**4,2**	$\approx 1{,}3\cdot10^{-5}$	4,4	$\approx 5{,}4\cdot10^{-6}$
	Small (C)	4,2	$\approx 1{,}3\cdot10^{-5}$	4,4	$\approx 5{,}4\cdot10^{-6}$	4,7	$\approx 1{,}3\cdot10^{-6}$
prEN 1990		4,2	$\approx 1{,}3\cdot10^{-5}$	**4,7**	$\approx 1{,}3\cdot10^{-6}$	5,2	$\approx 10^{-7}$

Dimensioning this beam using the deterministic design code method results in a β-value of 4,5 using the B10 code and in a β-value of 4,9 using the EC5 code design procedures (snow load characterised by the annual maximum values). These values are rather close to the target values. However, it would be possible to reduce the section height especially in the case of EC5, if the target reliabilities defined above are applied instead (see Figure 12).

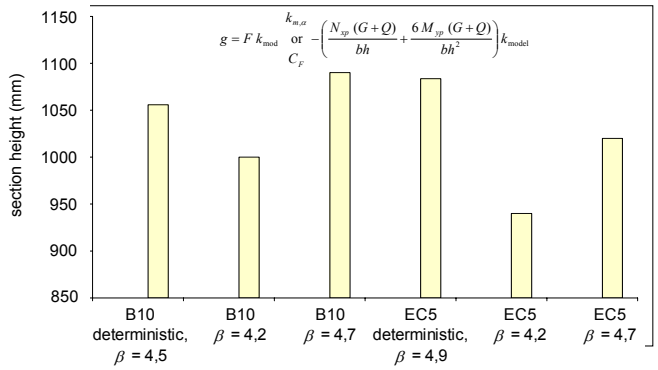

Figure 12. Required beam section heights based on the Finnish timber design code B10 and Eurocode 5). The β values from a deterministic analyses based on the design codes are also given. If target β values of Table are applied, the required heights are shown.

6. Reliability analysis of the beam for the standard fire exposure conditions

In the following, several reliability analyses are carried out for the same beam under a fire condition characterised by the standard temperature-time curve [ISO 834]. The analyses are done based on the methods given in prEN 1995-1-2 [5] on loading conditions under fire and on the charring rate of the wood section. Based on the previous example, only the most critical section is analysed for bending stresses, since this will be the determining section also in a fire condition. The limit-state function used in the analysis is presented in section 4.2.

The results of the reliability analyses are shown in Figure 13. The winter months have the highest probability of failure due to snow loads and March is most critical in this sense. The fire design according to EC5 is more conservative than according to B10.

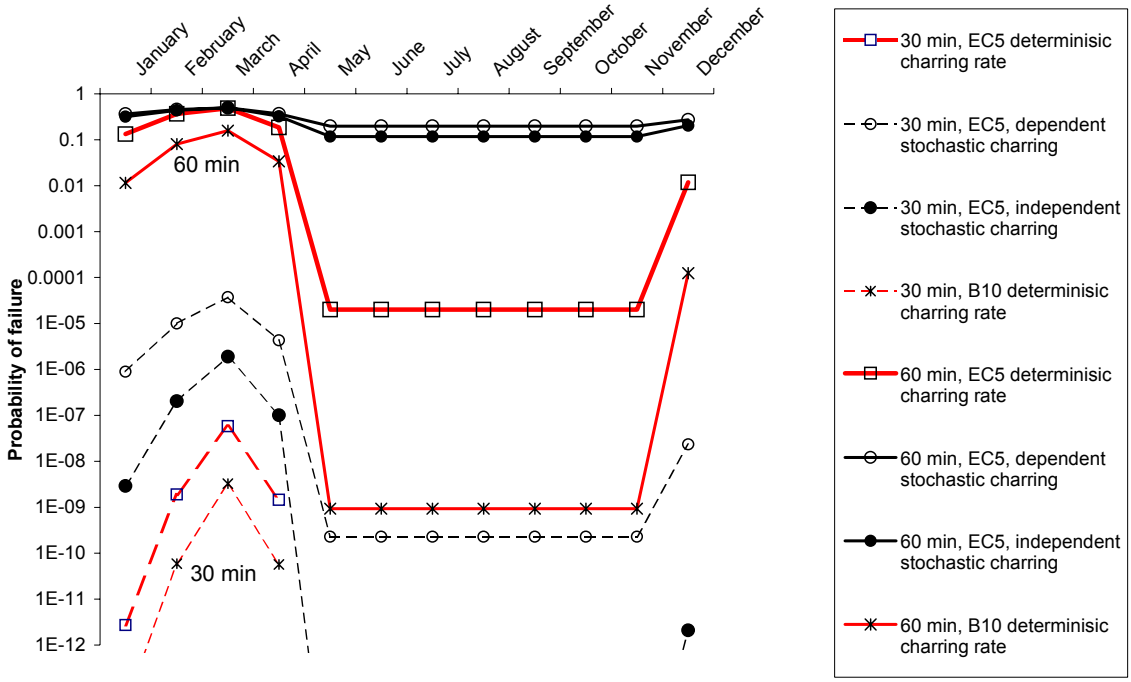

Figure 13. Results of the reliability analysis during a fire situation at different months of a year. This figure also includes results obtained using a stochastic charring rate with COV = 20 %.

It has been observed from previous charring experiments that charring rates are variable between test pieces. Variabilities in the order of COV=20 % have been observed for glulam, but higher and lower variabilities have also been observed [Hietaniemi 2005].

The influence of the variability of the charring rate on the probability of failure was analysed using a parametric study assigning values of 0 % (deterministic), 10 %, 20 % and 30 % to the coefficient of variation of the charring rate, see Figure 14. As the three different charring depths of the different sides of the beam, may or may not be independent, two separate calculations were done, one assuming these are independent and the other dependent.

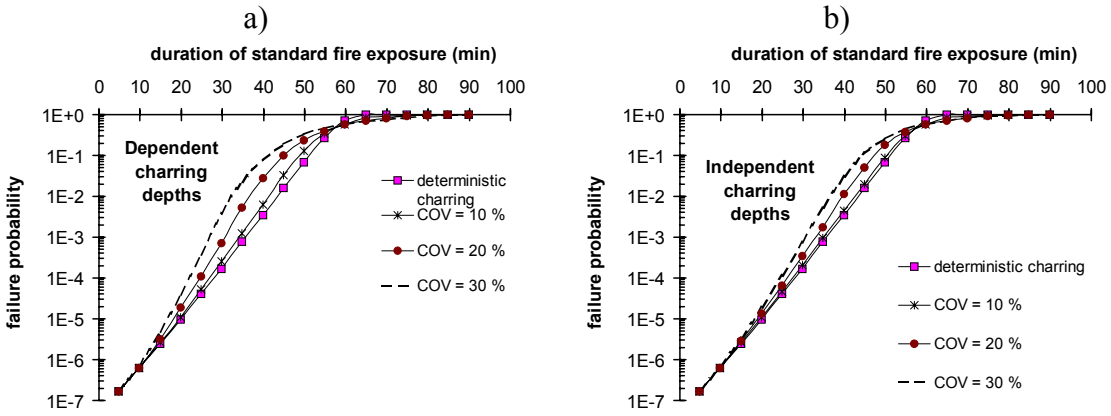

Figure 14. Parametric study of the influence of the variability of the charring rate on the probability of failure: a) dependent and b) independent charring depths of the different sides of the beam.

Comparing the results obtained with the deterministic charring rate to the stochastic rate with a variability of COV = 20 %, the following may be observed (see Table 6). The effect of the charring rate being a stochastic variable is significant only after a fire duration of about 15 to 30 minutes, for shorter fire duration the failure probabilities are small and the differences small. At a fire duration approaching 60 min, the effect of stochastic charring decreases again. This is true for high loads (Figure 9), for low loads (Figure 8 summer period) there is a high difference also at a 60 minute fire duration time. Also whether the charring rates between the sides are dependent or independent is of significance. This is a characteristic not well known, that is, whether the variability is more pronounced between different glulam beams (dependent or fully correlated) or within a glulam beam (independent or non-correlated).

Table 6. Ratios of the failure probability of the deterministic and stochastic charring rates (COV = 20 %) for four standard fire exposures. (Annual max. snow loads).

	15 min	30 min	45 min	60 min
Deterministic	1	1	1	1
Stochastic, independent	1,2	2,0	3,5	0,9
Stochastic, dependent	1,4	4,3	6,8	0,8

Next we assess the beam failure probability after a 30-minute or 60-minute standard fire exposure employing the following assumptions:

- a deterministic value 0,7 mm/min as given the codes is used for the charring rate,
- the upper supporting structure is assumed to function during the fire in prevention of lateral buckling at the 2,4 m spacing points,
- the snow load is modelled using the monthly distributions,
- failure is defined as structural failure with the bending stresses exceeding the capacity.

Based on prEN 1990 [3], the annual target probability of failure level is recommended as $P_{f,year} = 1{,}3 \cdot 10^{-6}$. Based on the probabilistic model code [6] the following probabilities for a dangerous fire scenario are assumed:

- P_i(ignition) = 10^{-6}/year/m^2 (value for shops/offices); with area of 1768 m^2 we obtain an estimate of $1{,}8 \cdot 10^{-3}$/year for the annual fire frequency,
- P_f(flashover|ignition) = 10^{-1} (in the case of a public fire brigade).

Based on the above information, the annual probability of failure of the structure can be calculated as

$$P_{f,fire,year} = \\ = 1 - \left((1 - P_i \, P_f \, P_{f,fire,January}) \, (1 - P_i \, P_f \, P_{f,fire,February}) \, \cdots \, (1 - P_i \, P_f \, P_{f,fire,December}) \right) \tag{15}$$

and results summarised in Table 7 are obtained for the two different codes, EC5 and B10.

Table 7. Annual probability of failure due to fire.

$P_{f,fire,year}$	EC5 method			B10 method Deterministic charring
	Deterministic charring	Stochastic dependent charring	Stochastic independent charring	
Fire duration 30 min	9.04×10^{-13}	7.77×10^{-10}	3.27×10^{-12}	5.00×10^{-14}
Fire duration 60 min	1.74×10^{-5}	4.91×10^{-5}	3.82×10^{-5}	4.18×10^{-6}

Considering the limit state equation for fire, the k_{crit} term, which reduces the strength due to lateral torsional buckling, becomes critical. This reduces the beam capacity at a fast rate as the charring progresses and the cross section becomes more slender. The fire design according to EC5 is conservative (compared to B10). Stochastic charring rates have a significant influence on the failure probabilities.

Summarising, if a R60 classification is required, then the fire design when based on Eurocode 5 becomes the determining factor. Stochastic charring rates have a significant influence on the probability of failure for a standard fire exposure of duration of approximately 30 minutes or more. In the case of shorter standard fire exposures the influence is relatively small. The fire design according to Eurocode 5 is more conservative than according to the Finnish norm B10 due to differences in the charring rate and the modelling of lateral torsional buckling.

7. Approach based on fire simulation

In this Chapter we present an analysis of the fire endurance of the structures based on a comprehensive use of fire simulation and the analysis of its results.

7.1 Modelling of the example building

The fire-simulation model of the building is shown in Figure 15. We have analysed several fire scenarios in this building using both a deterministic fire simulation with the FDS 3 (McGrattan *et al*. 2002a, McGrattan *et al*. 2002b) and FDS 4 (McGrattan 2004a, McGrattan 2004b) program and a probabilistic fire simulation using the PFS program (Hostikka & Keski-Rahkonen 2003, Hostikka *et al*. 2003, Hietaniemi *et al*. 2004). Some of these scenarios have been dealt with in earlier presentations (Hietaniemi & Korhonen 2004a, Hietaniemi & Korhonen 2004b). In this example we consider only one fire scenario, a fire which grows hot enough to break the large windows on the south wall of the building. In this case the HRR may grow up to hundreds of megawatts (see 7.2.1). It should be noted that the fire development is principally governed by the potential breakage of the large windows and the particular scenario we are considering here is one in which the temperature required for the window breakage *and fallout* is 300 °C. This is actually a rather low temperature for major glass breakage leading to a fallout which will be taken into account when we estimate probability of this particular fire scenario needed in the assessment of the overall probability of structural failure.

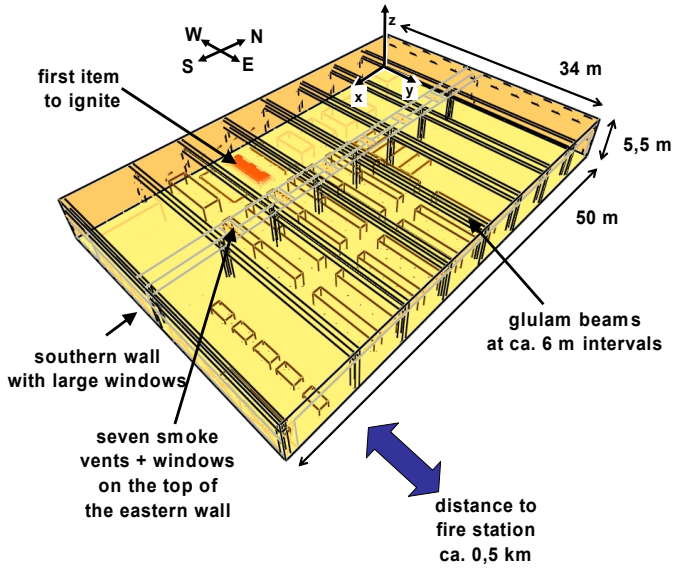

Figure 15. The target building. The principal fire safety measures are the smoke vents, which activate at 100 °C and simultaneously give an alarm signal to the fire station located in the near vicinity of the building.

7.2 Results of fire simulation

This section summarises the relevant fire characteristics obtained from the fire simulations. Some more detailed results are presented in Appendix A.

7.2.1 Heat release rate

Figure 16 shows heat release rate (HRR) curves for the fire scenarios with window breaking and fallout taking place at a) 400 ˚C and b) 500 ˚C. The steep increase in the HRR at *ca*. 45 min is due to the breaking and fallout of the large windows on the southern wall of the building.

The initial development of the HRR (Figure 17) shows the predetermined t^2 growth with time constant 150 s followed by a faster growth after *ca*. 7 minutes. At 10 minutes the HRR already approaches 50 MW.

The fire starts to decay after *ca*. 90 minutes. We model the burn out of the fire load by assuming that it is a rare event that the fire load would burn out before 120 minutes and that the fire load burns out mainly between 120 minutes and 180 minutes so that it is a rare event that the fire load would not have burnt out before 180 minutes. We model this event using a 3-parameter gamma distribution with the density function given by

$$f(x) = \frac{1}{\Gamma(\alpha)\beta^{\alpha}}(x - x_{\min})^{\alpha-1} e^{-\frac{x-x_{\min}}{\beta}}, \; x \geq x_{\min}$$
$$f(x) = 0, \; x < x_{\min}. \qquad (16)$$

where the parameters are $\alpha = 8{,}9$, $\beta = 6{,}2$ min and $x_{\min} = 91{,}9$ min (see Figure 18). It should be noted that the results obtained for the fire endurance of the structures are practically independent of these assumptions we have made on the fire load burnt; in fact, the results would be the same even if we assumed that the fire would burn infinitely.

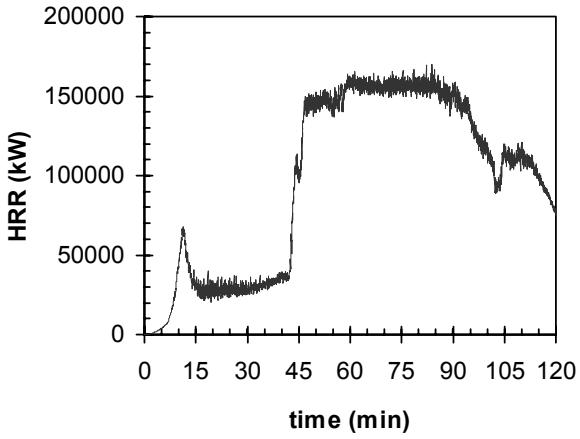

Figure 16. Heat release rate curves for the fire scenarios with window breaking and fallout taking place at 400 ˚C. For the scenario with window breaking and fallout occurring at 500 ˚C, the HRR curve is basically similar but the sharp increase at about 45 minutes in delayed by about 10 minutes.

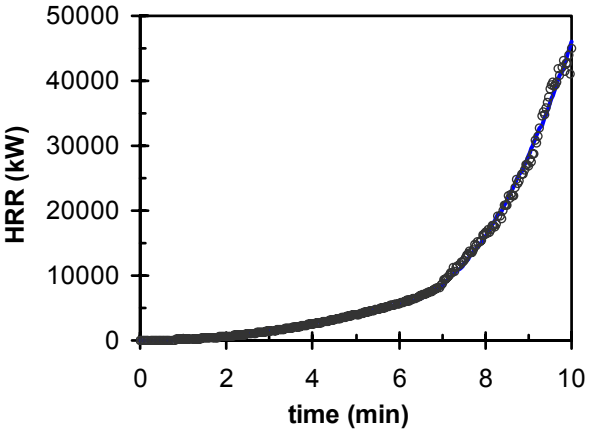

Figure 17. Initial growth of the heat release rate.

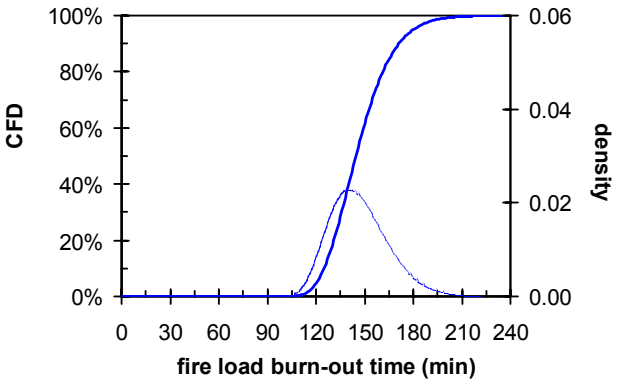

Figure 18. Statistical model for the fire load burn-out time.

7.2.2 Temperature

Examples of the dependence of the gas temperatures at different heights are shown in Figure 19. Figure 20 shows a simplified model abstracted from the FDS simulation results. Before the time t_1 the temperature is so low that has virtually no effect on the structures. During the period t_1-t_2, *i.e.*, before the window breakage and fallout at time t_2, the temperature, T_A, and thus charring are still relatively minute. As the windows break and fallout starting time t_2, there is drastic increase in the temperatures from T_A to T_B and hence also in the wood charring. At time t_3 the fire load is exhausted and the temperatures start to decay. Later on in this report, the periods t_1-t_2 and t_2-t_3 are referred to as "time before window breakage and fallout" and "time after window breakage and fallout", respectively.

In the following we represent the time factors t_1, t_2 and t_3 as stochastic factors characterised as follows:

- t_1 = 8 min ± 10 %, uniform distribution
- t_2 = 48 min ± 10 %, uniform distribution
- t_3 = 100 min ± 10 %, uniform distribution.

The temperature levels T_A and T_B depend on the horizontal and vertical position in the enclosure. These dependencies as well as the uncertainties involved are dealt with in Figure 21, Figure 22, Figure 23, Figure 24, Figure 25 and Figure 26.

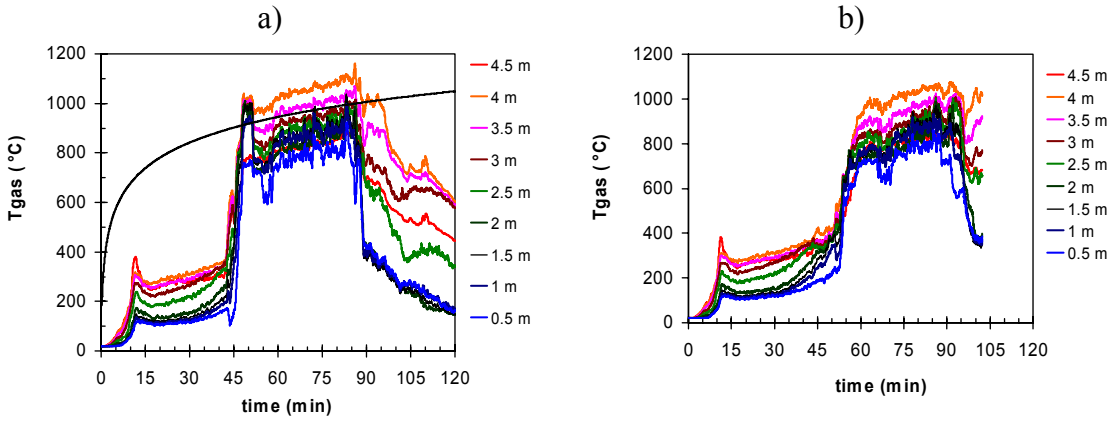

Figure 19. Examples of typical time-temperature curves at different heights for the fire scenarios with window breaking and fallout taking place at a) 400 ˚C and b) 500 ˚C. To clarify the curves, the simulation results have been smoothed by using a 30-s sliding averaging procedure.

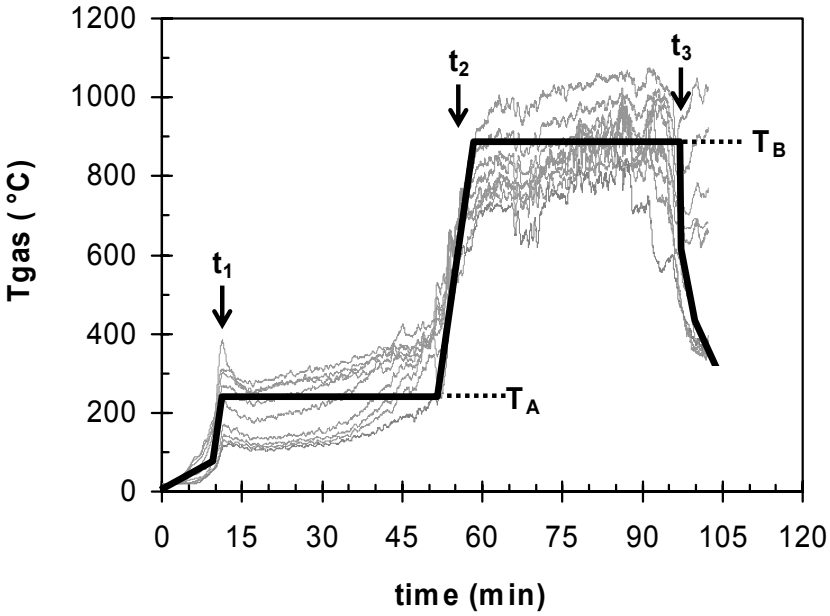

Figure 20. Simplified model of the time-temperature curves.

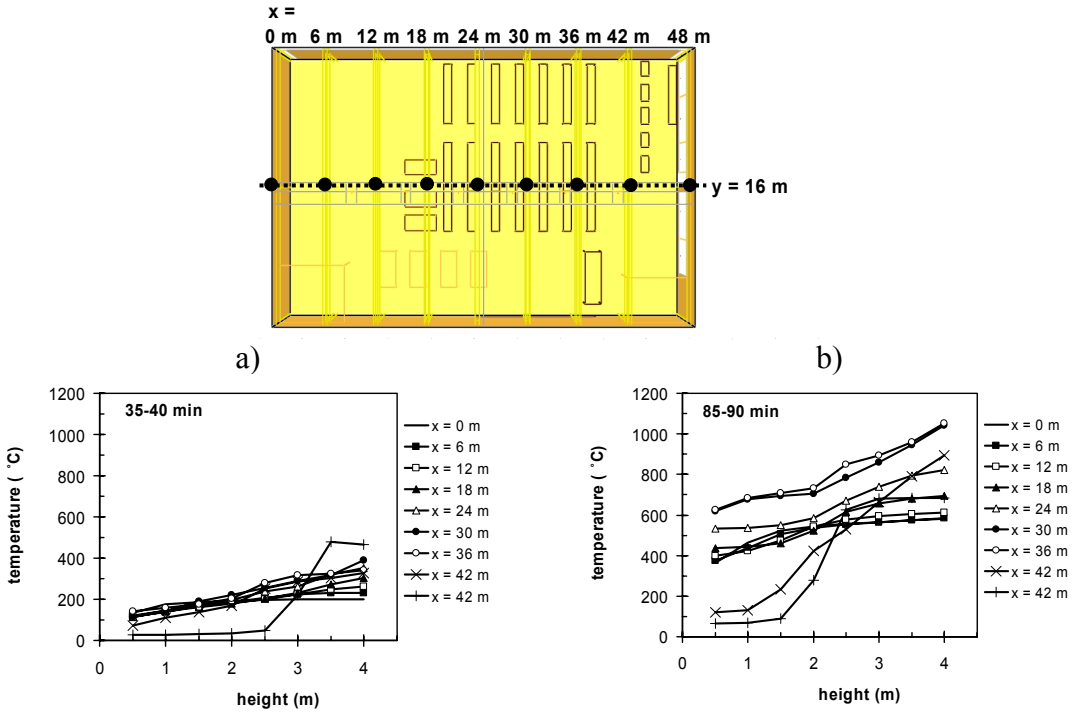

Figure 21. Dependence of the temperature on the height at the different locations in building shown in the top most figure in the fire scenario with window breaking and fallout at 400 ˚C: a) before and b) after the window breakage and fallout.

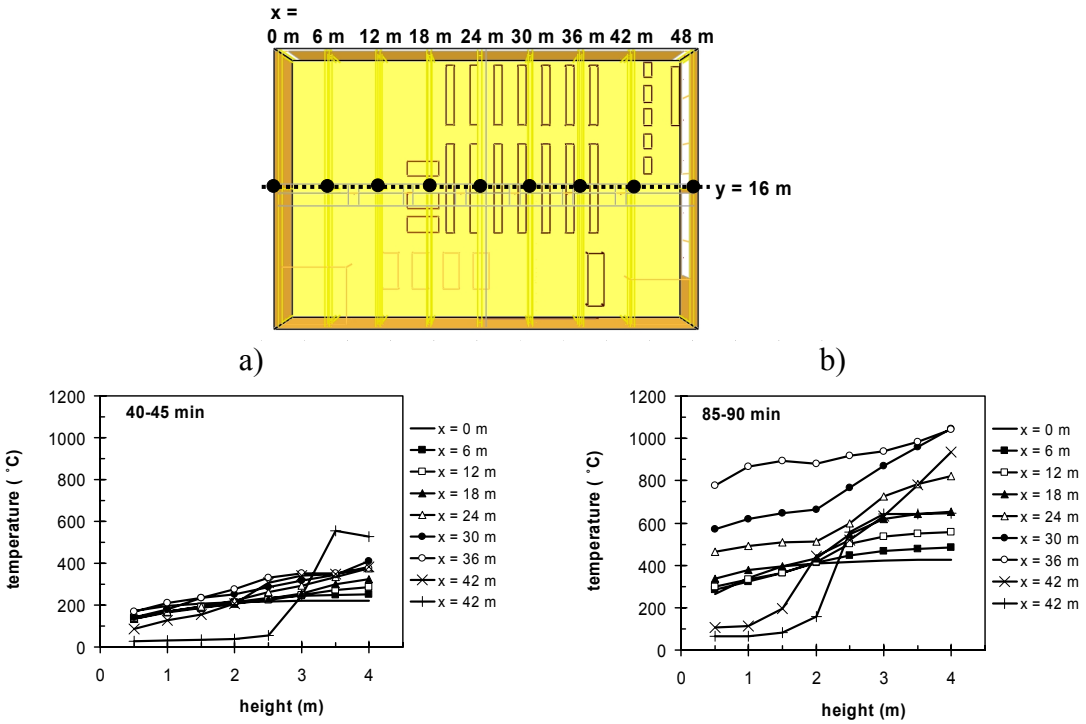

Figure 22. Dependence of the temperature on the height at the different locations in building shown in the top most figure in the fire scenario with window breaking and fallout at 500 ˚C: a) before and b) after the window breakage and fallout.

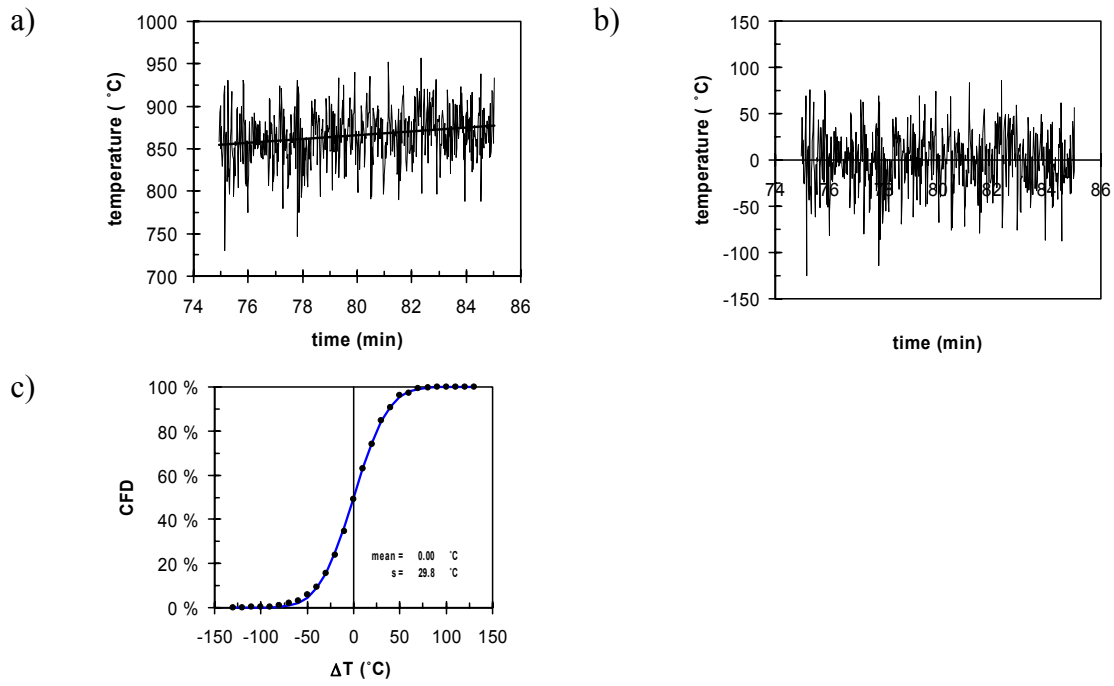

Figure 23. Example of the quantification of the uncertainty of the temperature data: a) non-smoothed time-temperature curve for 75-85 min in the fire scenario with window breakage and fallout at 500 ˚C, b) fluctuations of the temperature readings around the linear trend depicted in Fig. (a) and c) analysis of the fluctuations using a zero-mean normal distribution with the standard deviation equal to 30 ˚C.

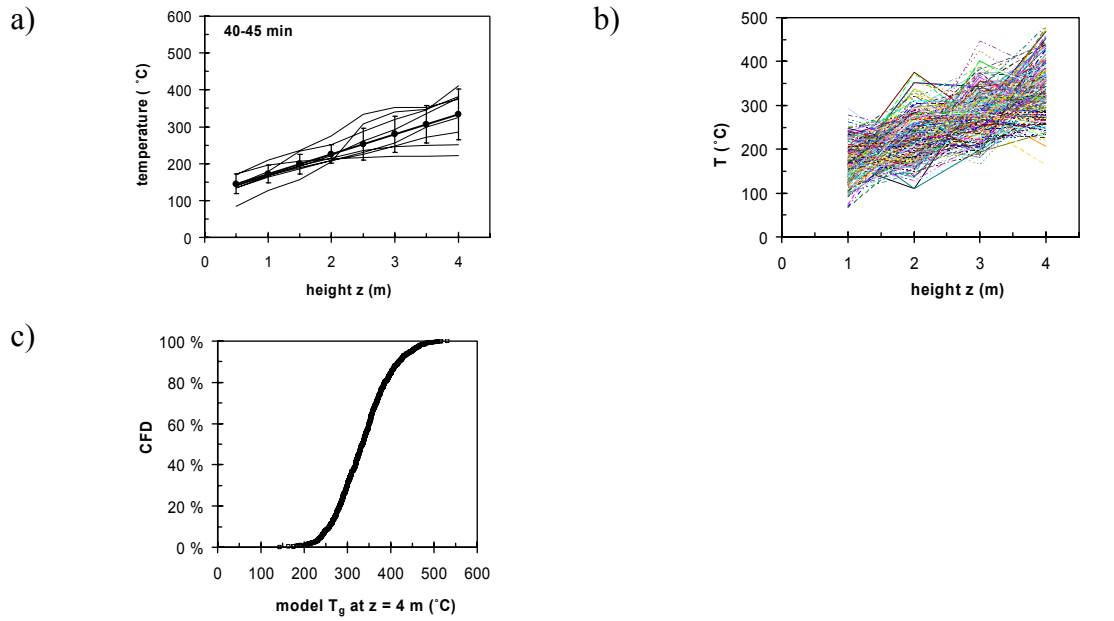

Figure 24. Temperature input to the heat transfer calculations to model times before the breakage and fallout of the windows: a) height dependence of the temperatures at different locations, b) the linear model with variability added to it and c) an example of the distribution of the temperatures.

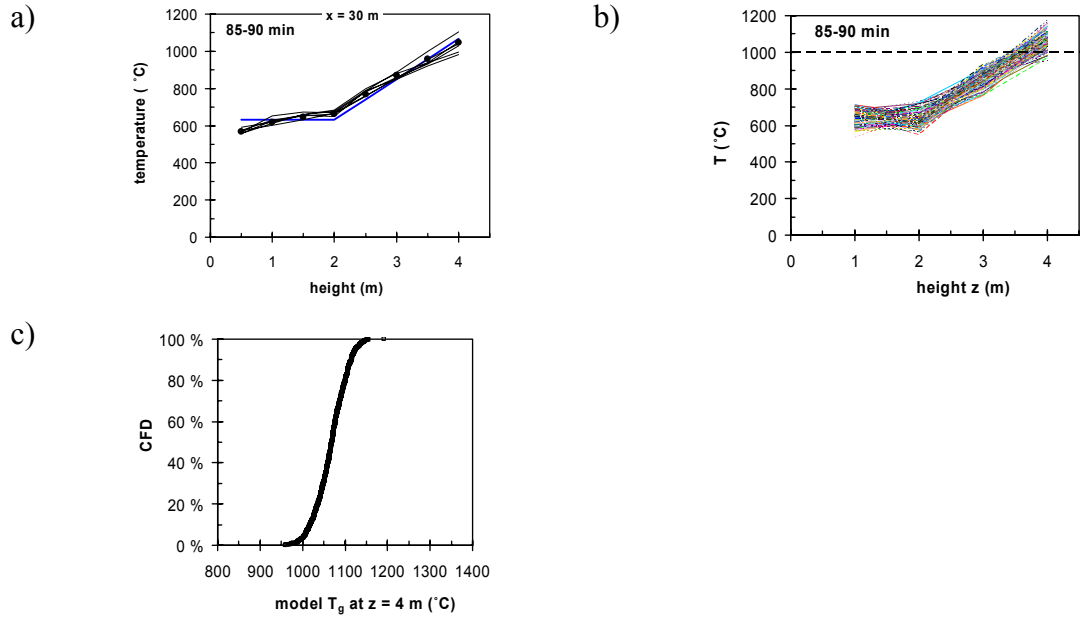

Figure 25. Temperature input to the heat transfer calculations to model times after the breakage and fallout of the windows at x = 30 m: a) height dependence of the temperatures at different locations, b) the linear model with variability added to it and c) an example of the distribution of the temperatures. The dotted line in (b) denotes the mean value of the standard temperature curve in this time window.

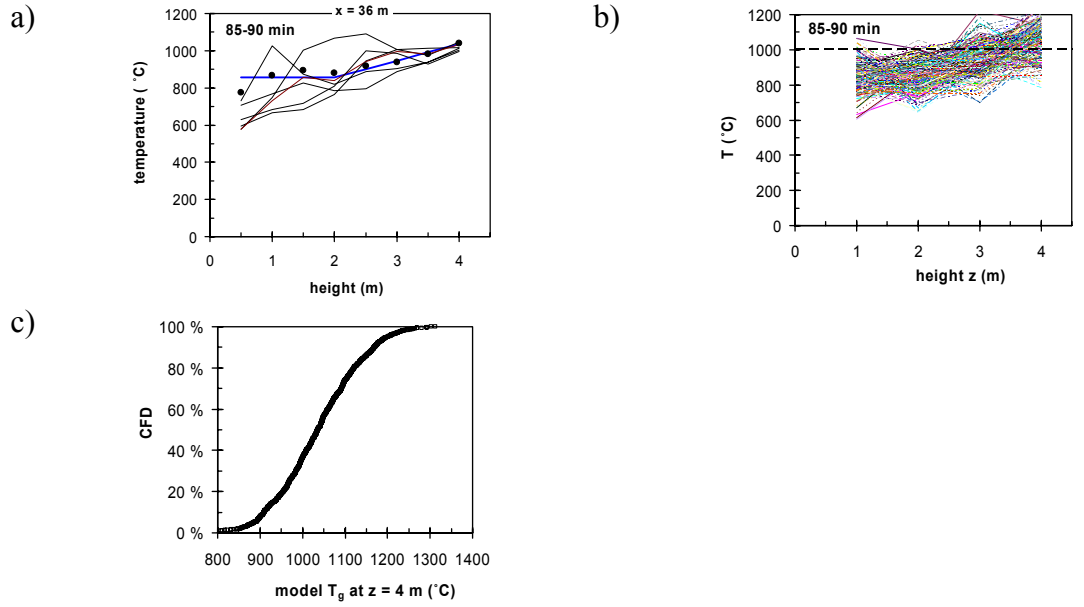

Figure 26. Temperature input to the heat transfer calculations to model times after the breakage and fallout of the windows at x = 36 m: a) height dependence of the temperatures at different locations, b) the linear model with variability added to it and c) an example of the distribution of the temperatures. The dotted line in (b) denotes the mean value of the standard temperature curve in this time window.

7.2.3 Smoke density and flow field

7.2.3.1 Smoke density

The results on the smoke density (Figure 27, Figure 28, Figure 29 and Appendix A) show that the space becomes very smoke between 10 and 15 minutes: during this time period, the extinction coefficient rises from essentially zero to 2–6 m^{-1}. In the hot upper smoky layer, the extinction coefficient k_g is about 4–6 m^{-1}, *i.e.*, the structures within the upper layer are surrounded by a quite thick smoke. For the heat transfer analysis we abstract the results as follows: for both window breakage and fallout scenarios we use the following values

- before window breakage and fallout $k_g = (6\pm1)$ m^{-1} (uniform distribution)
- after window breakage and fallout $k_g = (4\pm1)$ m^{-1} (uniform distribution).

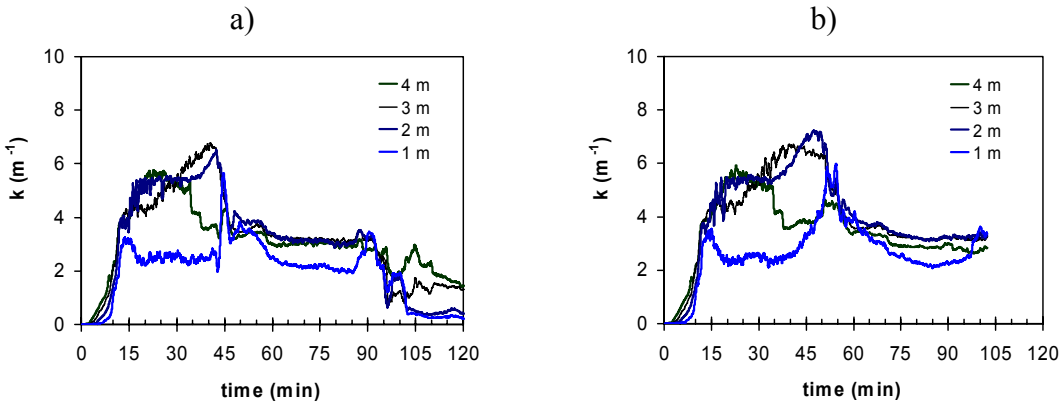

Figure 27. Examples of typical extinction coefficient curves at different heights for the three fire scenarios: window breaking and fallout at a) 400 ˚C and b) 500 ˚C. To clarify the curves, the simulation results have been smoothed by using a 30-s sliding averaging procedure.

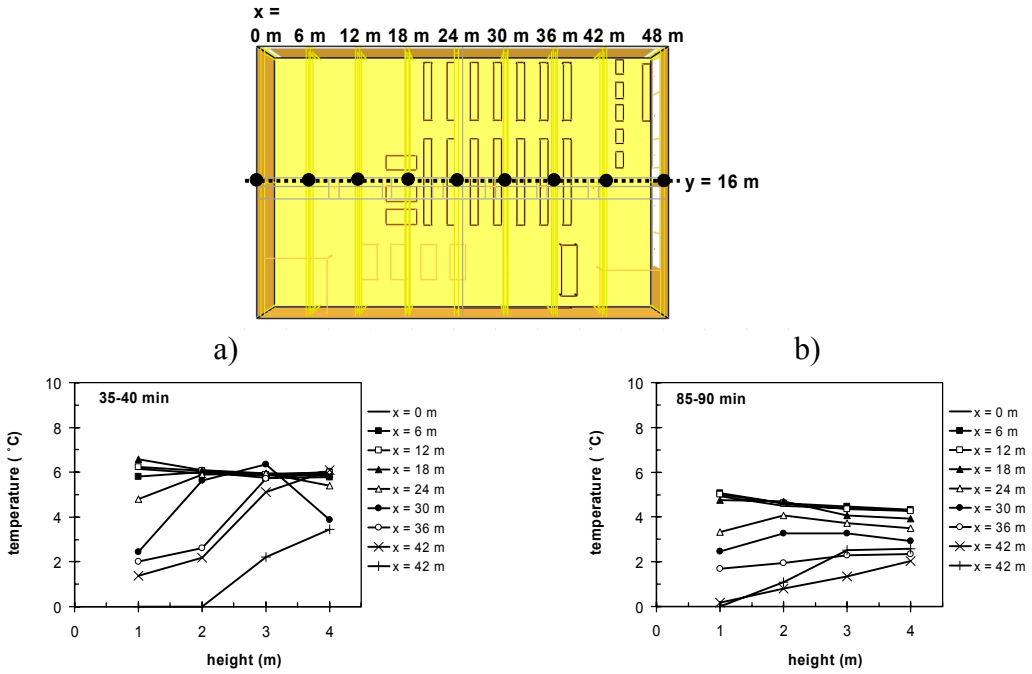

Figure 28. Dependence of the extinction coefficient on the height at the different locations in building shown in the top most figure in the fire scenario with window breaking and fallout at 400 ˚C: a) before and b) after the window breakage and fallout.

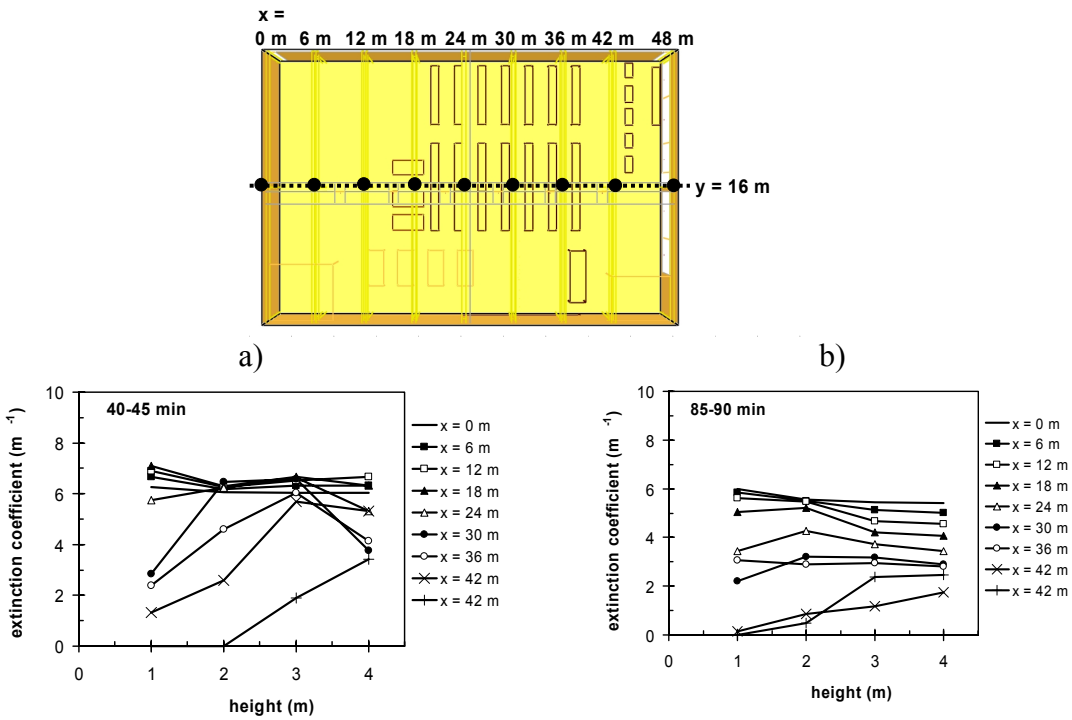

Figure 29. Dependence of the extinction coefficient on the height at the different locations in building shown in the top most figure in the fire scenario with window breaking and fallout at 500 ˚C: a) before and b) after the window breakage and fallout.

7.2.3.2 Flow velocity

The flow velocity varies considerably both temporally and spatially. A distinct change takes place at the time when the large windows on the south wall of the building break and fallout. This is demonstrated by Figure 30 which shows that before the window breakage and fallout, the average flow velocity in the building is ~ 0–3 m/s with higher flow velocities up to 6–7 m/s occurring in the vicinity of the initial fire, and after the window breakage and fallout the flow velocity the average flow velocity is clearly higher with high velocity regions of velocities reaching 8–9 m/s occurring in several locations. The velocity profiles depicted in Figure 31 show that before the window breakage and fallout the time-averaged velocities are distributed quite evenly with respect to the building centreline (line y = 16 m). The value of the velocity fluctuates between about 3 m/s and 6 m/s.

Figure 32 shows a more detailed analysis of the variability on the flow field: there are snapshots of the flow field taken at 5 consecutive times separated by a 1-minute interval. It can be seen that the velocity fluctuations go up to ca. 2 m/s. Figure 33 shows a more detailed quantification of the velocity fluctuations: it is seen that they can be described as a normally distributed noise with standard deviation of 0,5 m/s.

The results of the flow velocity field can be summarised to a simplified model of the flow velocity field to be used in the structural fire endurance calculations as follows (see Figure 33d):

- before the breakage and fallout of the windows the mean value $\overline{v}_g$ of the flow velocity varies uniformly from 3 m/s to 6 m/s;
- after the breakage and fallout of the windows the mean value $\overline{v}_g$ of the flow velocity varies uniformly from 4 m/s to 8 m/s;
- imposed on the mean velocity there is a normally distributed fluctuating component Δv_g with zero mean and standard deviation equal to 0,5 m/s.

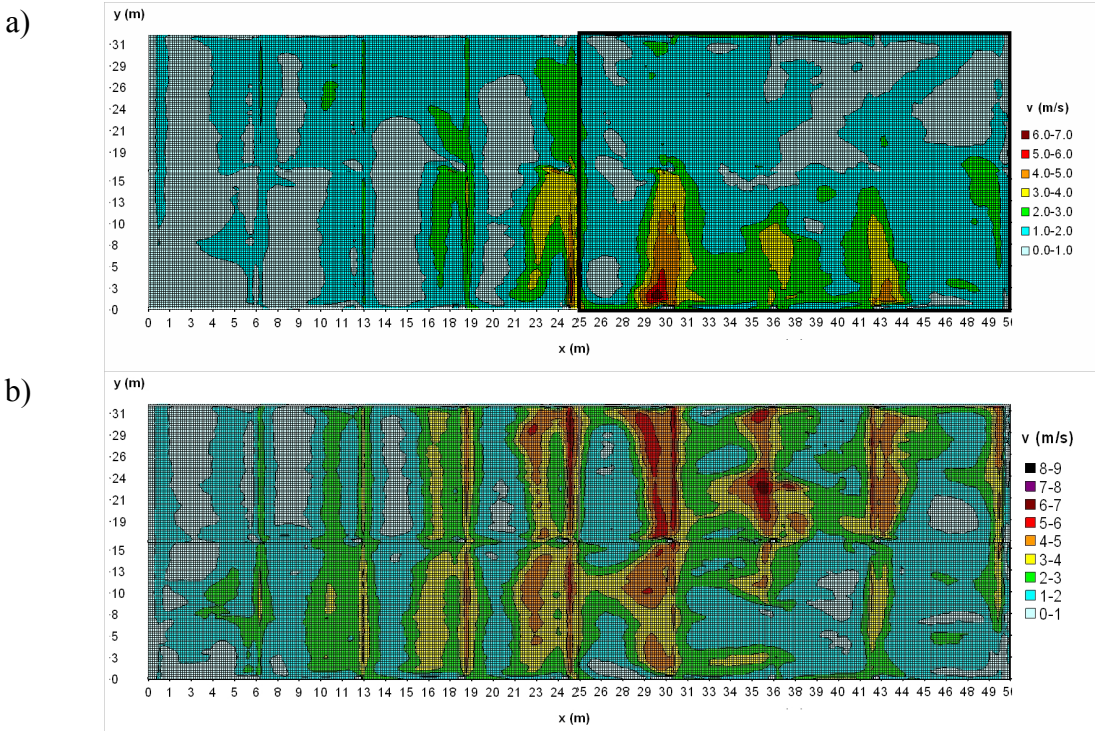

Figure 30. Examples of the flow velocity fields shown as planar cuts at height z = 4,0 m: average values during a) 35–40 and b) 85–90 minutes in the fire scenario with window breaking and fallout occurring at 500 ˚C.

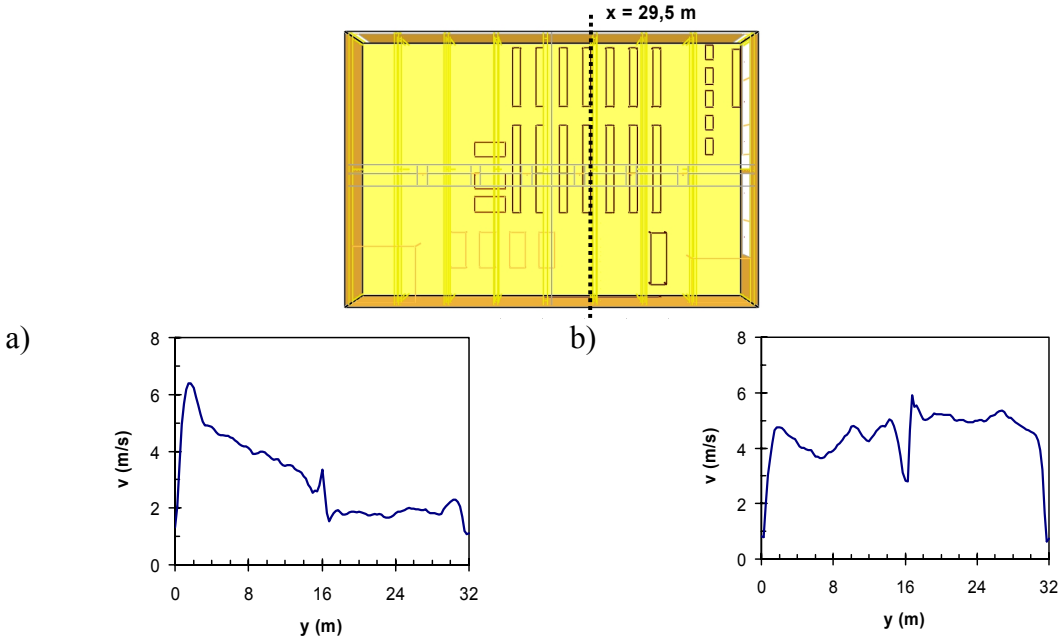

Figure 31. Flow velocity profiles along the line shown in the uppermost figure (x = 29,5 m and z = 4,0 m), average values during a) 35–40 and b) 85–90 minutes.

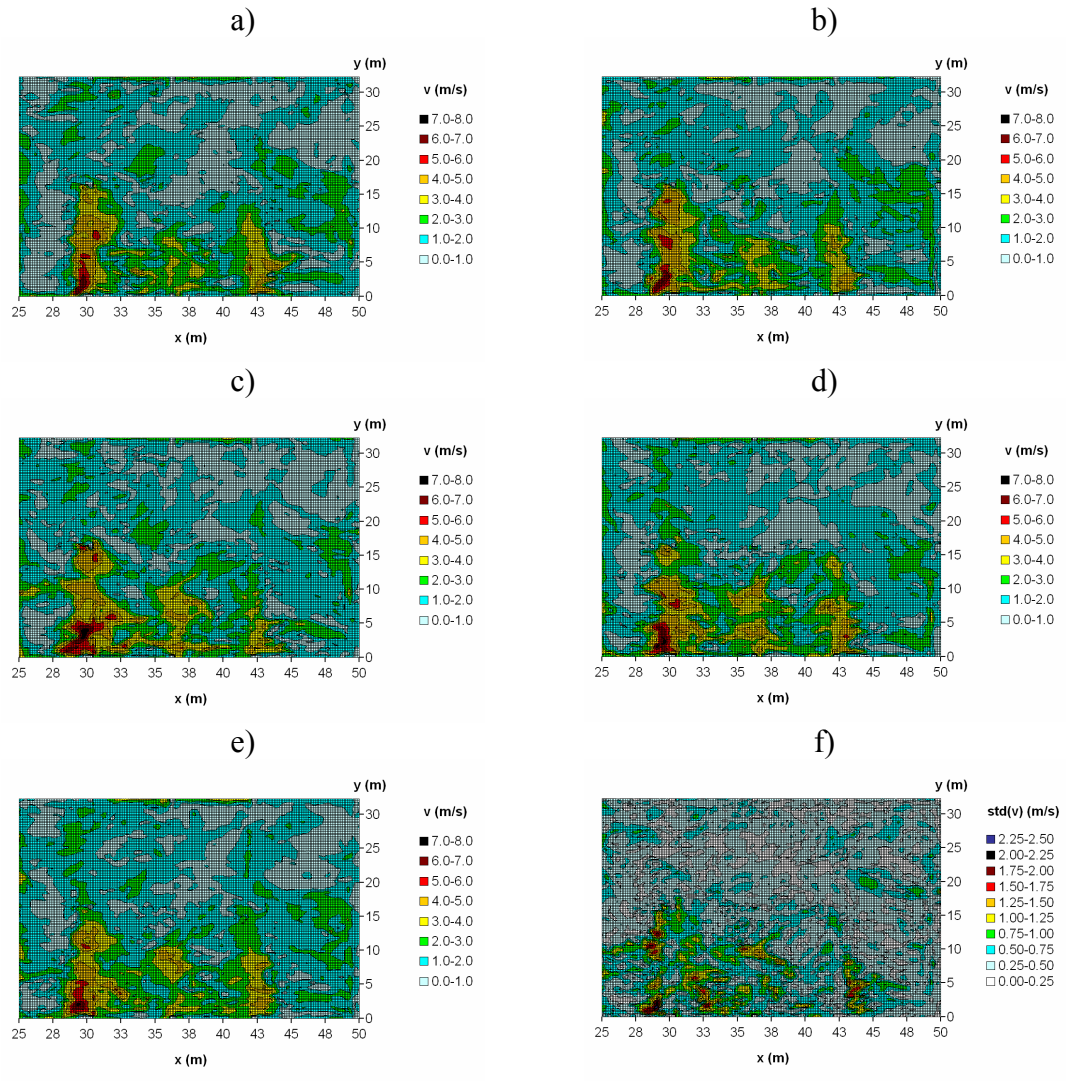

Figure 32. More detailed example of the variations of the flow field shown as planar cuts at height z = 4,0 m of the area shown by the thick-edge square in Figure 30a: instantaneous values during a) 35 minutes, b) 36 minutes, c) 37 minutes, d) 38 minutes and e) 39 minutes; f) shows the velocity fluctuations in terms of the standard deviation taken over the charts a)-e). The fire scenario is the one with window breaking and fallout at 500 ˚C.

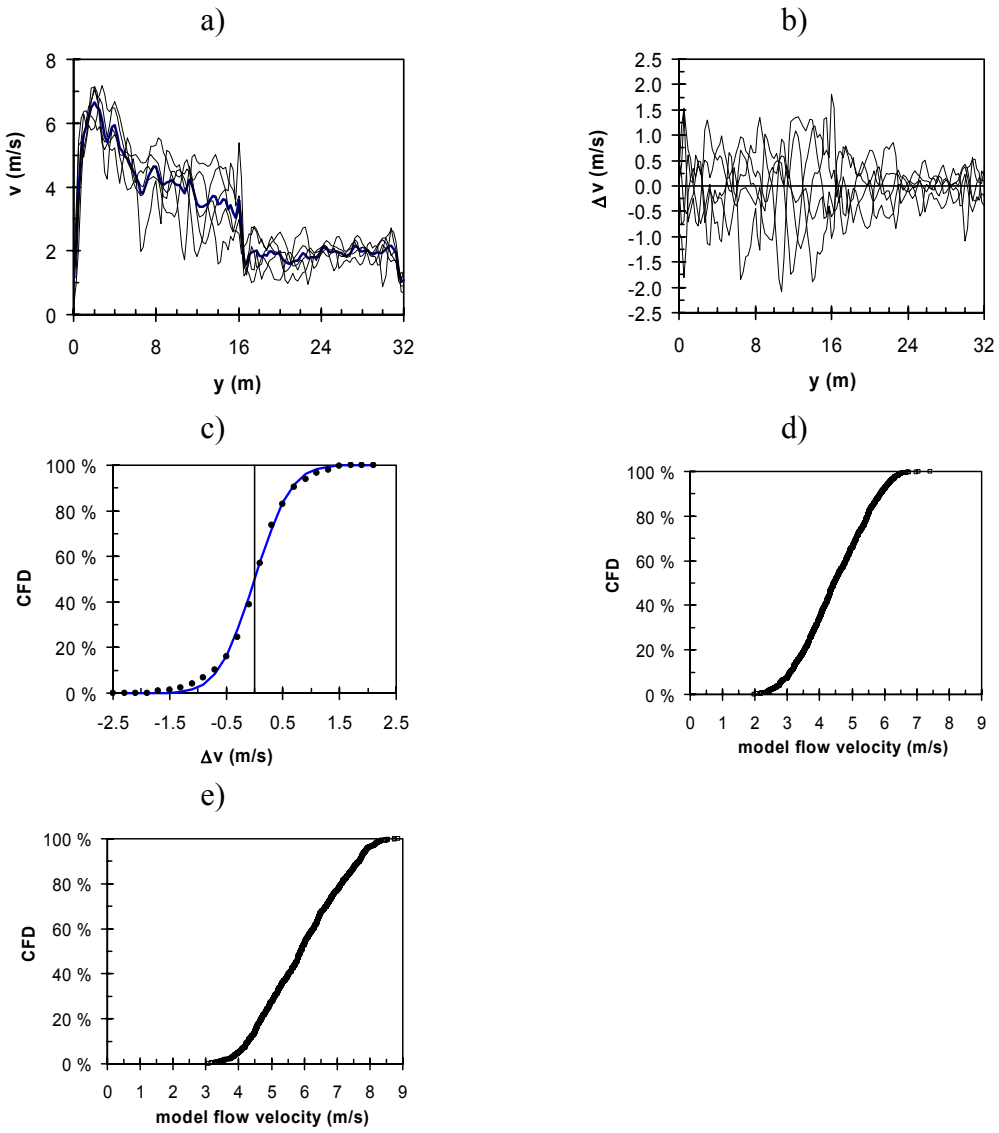

Figure 33. Quantification of the uncertainty of the flow velocity data: a) example of instantaneous velocity profiles taken at 1 minute intervals between 35 and 39 minutes in the fire scenario with window breakage and fallout at 500 ˚C, b) fluctuations of the velocities around the mean value depicted in Fig. (a), c) analysis of the temperature fluctuations using a zero-mean normal distribution with standard deviation equal to 0,5 m/s, d) the cumulative frequency distribution of the flow velocity used in the heat transfer calculations for times before the window breakage and fallout and e) the cumulative frequency distribution of the flow velocity used in the heat transfer calculations for times after the window breakage and fallout.

7.3 Oxygen concentration

We show that oxygen concentration just for the fire scenario with window breaking temperature set at 500 ˚C as the essential features are the same in the other fire scenarios, *i.e.*, during vigorous burning, the oxygen concentration in the hot smoke layer is low, according to the simulations dropping to zero at *ca*. 1 hour. Based on this result, we make a cautious assumption and assume that the oxygen concentration varies locally between 0 % and 5 %.

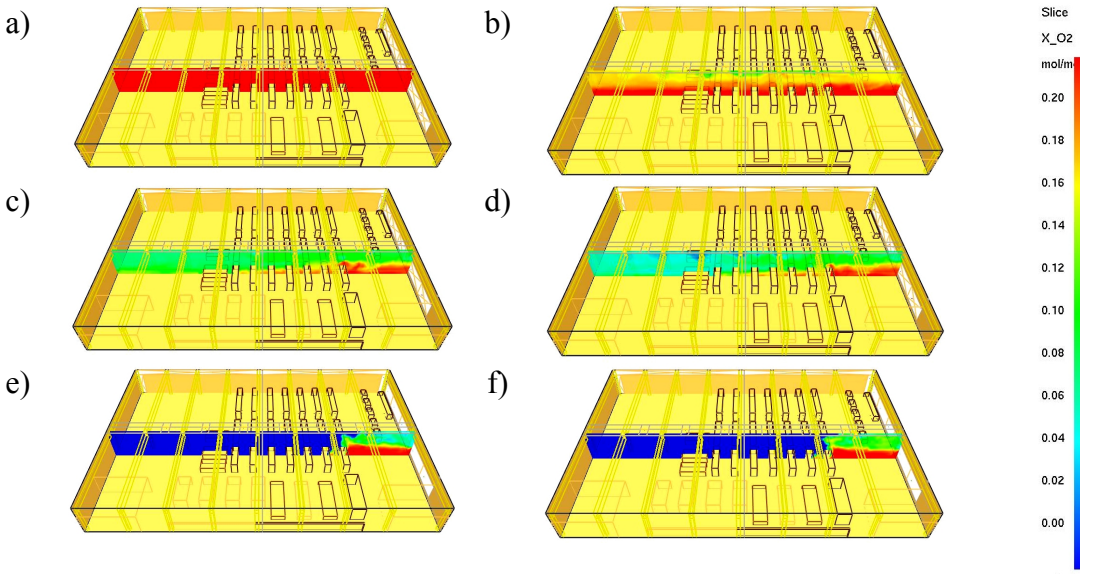

Figure 34. Oxygen concentration shown as a planar cut at y = 16,0 m for times a) 5, b) 10, c) 20, d) 40, e) 60 and f) 70 minutes.

7.4 Charring of the wooden structures evaluated on the basis the fire simulation results

In this Chapter we first carry out a heat transfer analysis to establish the heat flux to the structures and then convert the heat fluxes to charring rates using the model developed by Hietaniemi (2005). As the quantities involved in the analysis have considerable fluctuations, the analysis is carried on stochastic bases, *i.e.*, by treating the quantities as random parameters characterised by appropriate statistical distributions.

7.4.1 Heat transfer from the fire to the wooden members

In the heat-transfer analysis we treat the wooden structural member as an object with surface temperature of T_s immersed to a hot grey gas with uniform temperature T_g, flow velocity field characterised by a constant velocity v_g and optical thickness characterised by an extinction coefficient k_g (Figure 35).

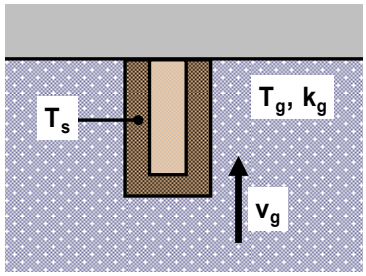

Figure 35. Schematic description of the heat transfer from the fire environment to the wooden structural member.

To describe the charring of the wooden structural members we employ the empirical model developed by Hietaniemi (2005), which works with the gross heat flux $\dot{q}''_G$ incident on the member surface, *i.e.*, the heat flux value not including the surface heat losses. This heat flux coincides with the heat flux which would be recorded by a cooled heat-flux gauge,

$$\dot{q}''_e = h\left(T_g - T_\infty\right) + \varepsilon\sigma\left(T_g^4 - T_\infty^4\right), \tag{17}$$

where h is the heat transfer coefficient, ε is the emissivity of the gas surrounding the member, $\sigma = 5{,}67 \cdot 10^{-8}$ WK^{-4}m^{-2} is the Stefan-Boltzmann constant and $T_\infty \sim 300$ K is the ambient temperature.

For the hot layer with relatively high extinction coefficient, the emissivity of the hot gases may be approximated as follows:

$$\varepsilon \approx 1 - \exp\left(-k_g D\right) \approx 1, \tag{18}$$

because the product of the extinction coefficient $k_g \sim 2$–6 m^{-1} and the dimension of the gas volume D ~ 10 m is ~ 20–60 rendering the exponential term negligibly small.

We emphasise that the treatment of the heat radiation used in this report is very coarse, selected on the basis of the focus of this report, which is the charring and mechanical response of the wooden structures. A more rigorous treatment of the heat radiation

would be to use the radiation transport equation, which for a grey non-scattering medium may be written as (Baum 2005, McGrattan *el al*. 2001):

$$\mathbf{u}\cdot\nabla I(\mathbf{r}) = \kappa(\mathbf{r})\left(\frac{\sigma T_g(\mathbf{r})^4}{\pi} - I(\mathbf{r})\right), \tag{19}$$

where I is the heat radiation intensity at position $\mathbf{r}$, $\mathbf{u}$ is a unit normal direction vector, $\kappa(\mathbf{r})$ is absorption coefficient and $\sigma = 5{,}67\cdot10^{-8}\ \mathrm{WK^{-4}m^{-2}}$ is the Stefan-Boltzmann constant.

The heat transfer coefficient depends on the flow velocity and gas temperature in the vicinity of the structural member as well as the member surface temperature T_s (Drysdale 1998, Atreya 2002):

$$h = \frac{\lambda_g(T_f)}{D}\cdot Nu(v_g, T_f) = \frac{\lambda_g(T_f)}{D}\cdot A\cdot \mathrm{Re}(v_g, T_f)^p\ \mathrm{Pr}(T_f)^{1/3}, \tag{20}$$

$$\mathrm{Re}(v_g, T_g) = \frac{D v_g}{\nu(T_f)} \tag{21}$$

$$\mathrm{Pr}(T_g) = \frac{\nu(T_f)}{\alpha(T_f)} \tag{22}$$

$$T_f = \frac{T_s + T_g}{2} \tag{23}$$

where the dependence of Nusselt number Nu, the Reynold Number Re and the Prandtl number Pr on the flow velocity v_g and the mean boundary layer temperature T_f either directly or through the kinematic viscosity ν or the thermal diffusivity α the has been written down explicitly. Quantity $\lambda_g(T_f)$ is the thermal conductivity of the gases and D is a characteristic dimension of the heat-transfer system, which we evaluate as the geometric mean of the width and depth of the member section. To calculate the mean boundary layer temperature T_f we use $T_s = T_\infty$.

The model parameters A and p depend on the flow configuration. We consider here the following two configurations (Atreya 2002)[2]:

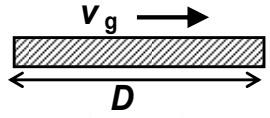

$$A = 0{,}66 \qquad p = 1/2 \,, \tag{24}$$

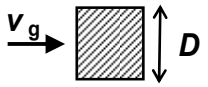

$$A = 0{,}102 \qquad p = 0{,}675 \,, \tag{25}$$

Hence we have the following two expressions for the heat transfer coefficient

$$h_1 = 0{,}66 \cdot \lambda_g\left(T_f\right) \cdot D^{-1/2} \cdot v_g{}^{1/2} \cdot \nu\left(T_f\right)^{-1/6} \alpha\left(T_f\right)^{-1/3}, \tag{26}$$

$$h_2 = 0{,}102 \cdot \lambda_g\left(T_f\right) \cdot D^{-0{,}325} \cdot v_g{}^{0{,}675} \cdot \nu\left(T_f\right)^{-0{,}3417} \alpha\left(T_f\right)^{-1/3}. \tag{27}$$

For simplicity we assume that the gas properties can be modelled using the properties of air which are summarised in Appendix C. As T_g and v_g are stochastic quantities (see sections 7.2.2 and 7.2.3), also the heat transfer coefficients are stochastic and, hence we evaluate their values using the Monte Carlo simulation. In these simulations we first calculate h_1 and h_2 and then determine h by selecting randomly either h_1 or h_2. The resulting heat transfer coefficient is practically the same for times before and after the window breakage and fallout: it ranges between ~10–20 W/m^2 with the mean value of about 15 W/m^2, see Figure 36.

The distributions of the resulting heat fluxes are presented in Figure 37, Figure 38 and Figure 39 corresponding to the following cases:

- Figure 37: heat flux for times before the breakage and fallout of the windows, y = 16 m (centre) and all x positions;
- Figure 38: heat flux for times after the breakage and fallout of the windows, y = 16 m (centre) and x = 30 m;
- Figure 39: heat flux for times after the breakage and fallout of the windows, y = 16 m (centre) and x = 36 m.

[2] As D ~ 1 m, v_g ~ 5 m/s and ν ~ 10^{-4} m^2/s, the Reynolds number Re ~ 50 000 and thus, the expression valid for laminar flow are used.

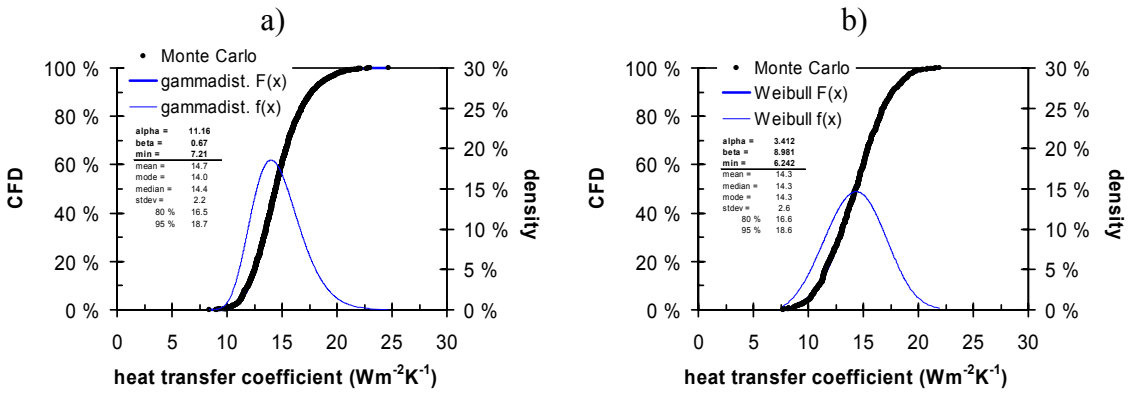

Figure 36. The heat transfer coefficient h for times a) before and b) after the window breakage and fallout.

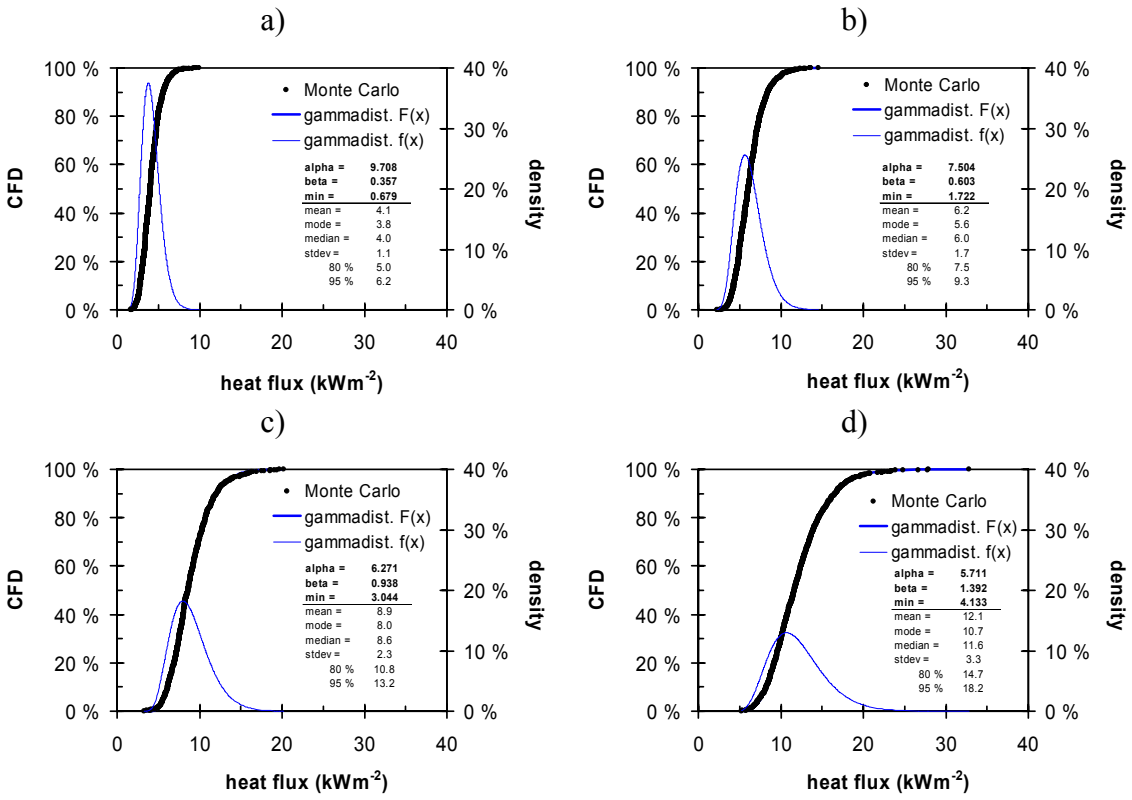

Figure 37. The gauge heat flux exposing the structures before the window breakage and fallout at heights a) z = 1 m, b) z = 2 m, c) z = 3 m and d) z = 4 m.

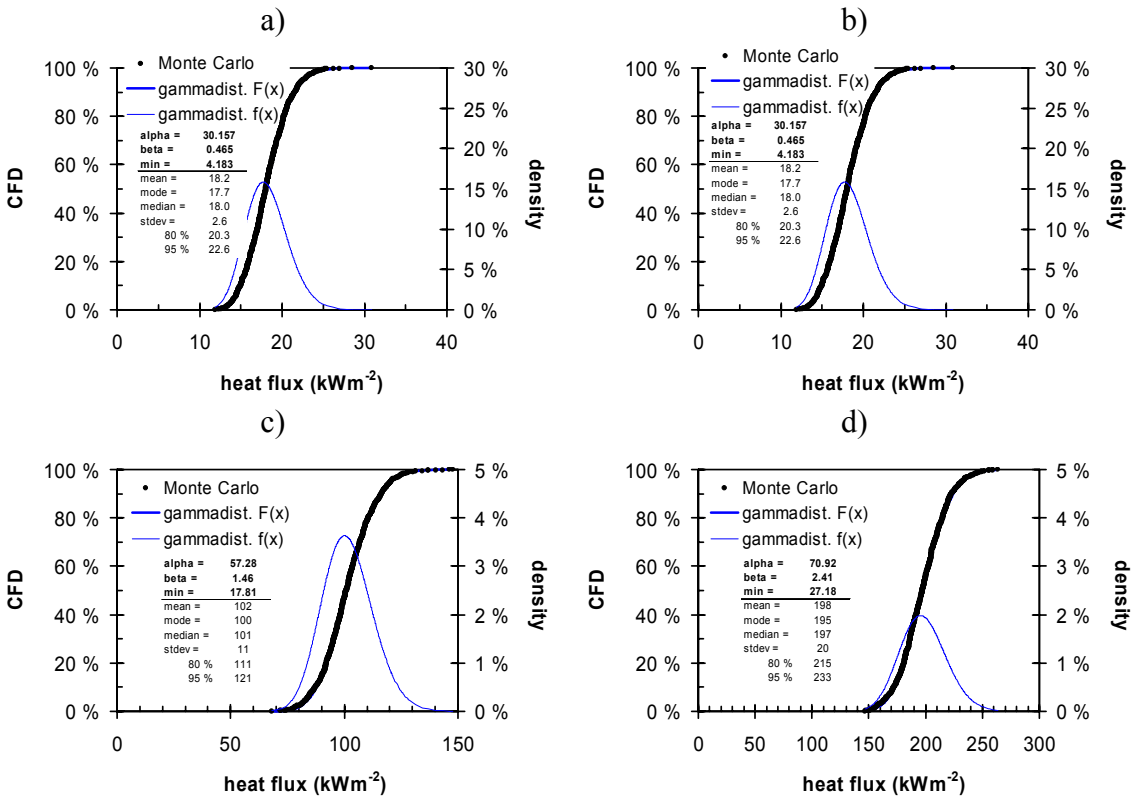

Figure 38. The gauge heat flux exposing the structures after the window breakage and fallout at position x = 30 m and at heights a) z = 1 m, b) z = 2 m, c) z = 3 m and d) z = 4 m.

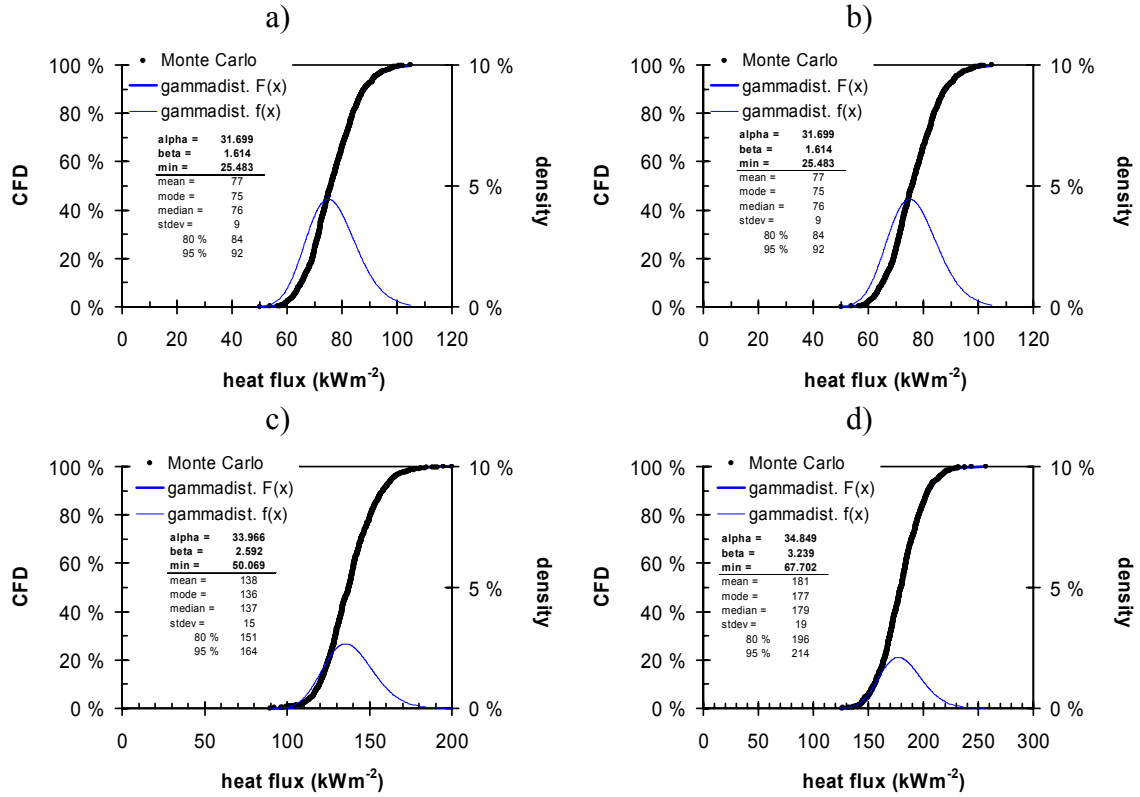

Figure 39. The gauge heat flux exposing the structures after the window breakage and fallout at position x = 36 m and at heights a) z = 1 m, b) z = 2 m, c) z = 3 m and d) z = 4 m.

7.4.2 Calculation of wood charring

7.4.2.1 Formulation

In the heat fluxes established by the heat transfer analysis can be converted to charring rate values by using the model developed by Hietaniemi (2005). As we assume that after and before, the heat fluxes are roughly constant, the relation between the charring rate β and the heat flux $\dot{q}''_e$ is

$$\beta = f(\chi_{O2}, t) \cdot \frac{C \cdot \dot{q}''^{p}_{e}}{(\rho + \rho_0)(A + B \cdot w)} \cdot \exp\left(-\frac{t}{\tau}\right) \equiv \beta_0 \cdot \exp\left(-\frac{t}{\tau}\right), \qquad (28)$$

where β_0 is the initial charring rate, ρ is density of the wooden member, w is the moisture content and χ_{O2} oxygen concentration, and the model parameters are[3]

$$f(\chi_{O2},t)=\xi+(1-\xi)\cdot\left(\frac{\chi_{O2}(t)}{\chi_{O2}^{(0)}}\right)^{0,737}. \tag{29}$$

$$C\propto\Delta(2{,}72;\,5{,}45;\,3{,}93)\,\mathrm{kW/m^2}, \tag{30}$$

$$\rho_0\propto N(465;93)\,\mathrm{kgm^{-3}}, \tag{31}$$

$$\begin{cases} A\propto U(505;1095)\,\mathrm{kJ/kg\ (average=800\ kJ/kg)} \\ B\propto U(2430;2550)\,\mathrm{kJ/kg\ (average=2490\ kJ/kg)} \end{cases}, \tag{32}$$

$$p\propto N(0{,}50;0{,}04)\ . \tag{33}$$

$$\tau\ \propto\Delta(90;110;100)\,\mathrm{min}. \tag{34}$$

$$\xi\propto U(0{,}50;0{,}65)\,(\mathrm{average}=0{,}575), \tag{35}$$

with $\chi_{O2}^{(0)}=21\%$ being the normal volumetric oxygen concentration.

7.4.2.2 The initial charring rate

We first determine the distributions of the initial charring rate β_0. When we assign a value of $\rho=500\ \mathrm{kg/m^3}$ for the density and $w=10\ \%$ for the moisture content and employ the heat flux distributions given in Figure 37, Figure 38 and Figure 39 we obtain the distributions of the initial charring rates corresponding to the following cases:

- Figure 40: the initial charring rate for times before the breakage and fallout of the windows, $y=16$ m (centre) and all x positions;
- Figure 41: the initial charring rate for times after the breakage and fallout of the windows, $y=16$ m (centre) and $x=30$ m;
- Figure 41: the initial charring rate for times after the breakage and fallout of the windows, $y=16$ m (centre) and $x=36$ m.

[3] $N(\mu;\sigma)$ is the Normal distribution with mean μ and standard deviation σ, $\Delta(x_{\min};x_{\max},x_{\mathrm{peak}})$ is the triangular distribution with minimum value $x_{\min}$, maximum value $x_{\max}$ and peak value x_{peak}; $U(x_{\min};x_{\max})$ is the uniform distribution with minimum value $x_{\min}$ and maximum value $x_{\max}$.

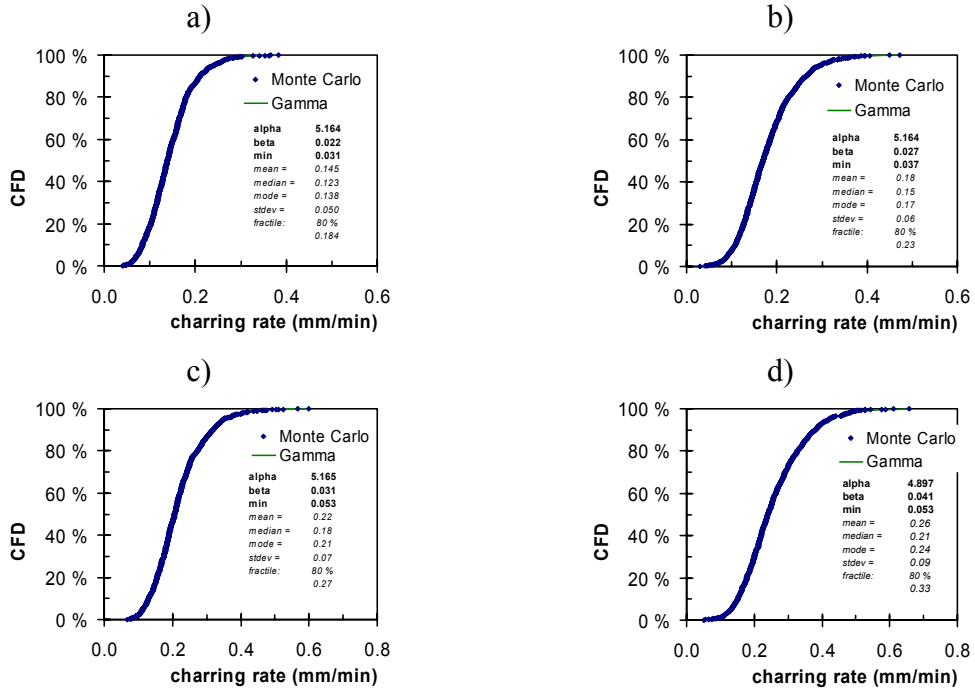

Figure 40. The initial charring rate β_0 of the structures before the window breakage and fallout at heights a) z = 1 m, b) 2 m, c) 3 m and d) 4 m.

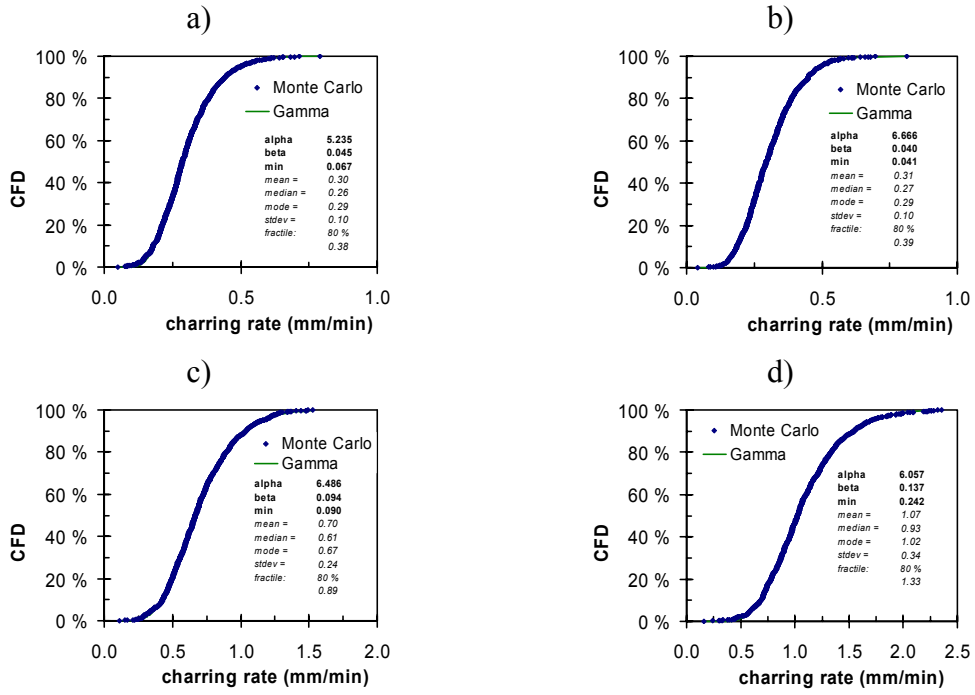

Figure 41. The initial charring rate β_0 of the structures after the window breakage and fallout at position x = 30 m and at heights a) z = 1 m, b) 2 m, c) 3 m and d) 4 m.

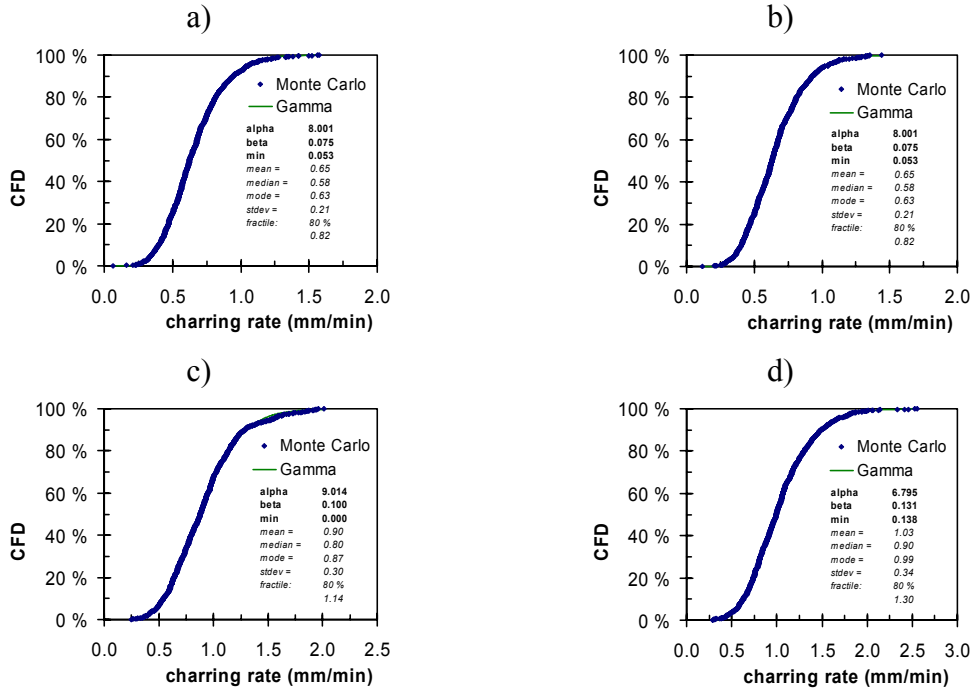

Figure 42. The initial charring rate β_0 of the structures after the window breakage and fallout at position x = 36 m and at heights a) z = 1 m, b) 2 m, c) 3 m and d) 4 m.

7.4.2.3 Charring rate curves

The model described by Eq. (12) includes an exponential attenuation factor to characterise the phenomenon that the charring rate decreased as a char layer builds on a wooden product. This attenuation factor together with the time dependence of the gas temperatures shown in Figure 20 determines the time dependence of the charring rate. Examples consisting of 250 samples of the resulting charring rate curves for the different cases considered are shown in the following:

- Figure 43: examples of the charring rates at position y = 16 m and x = 30 m;
- Figure 44: examples of the charring rates at position y = 16 m and x = 36 m.

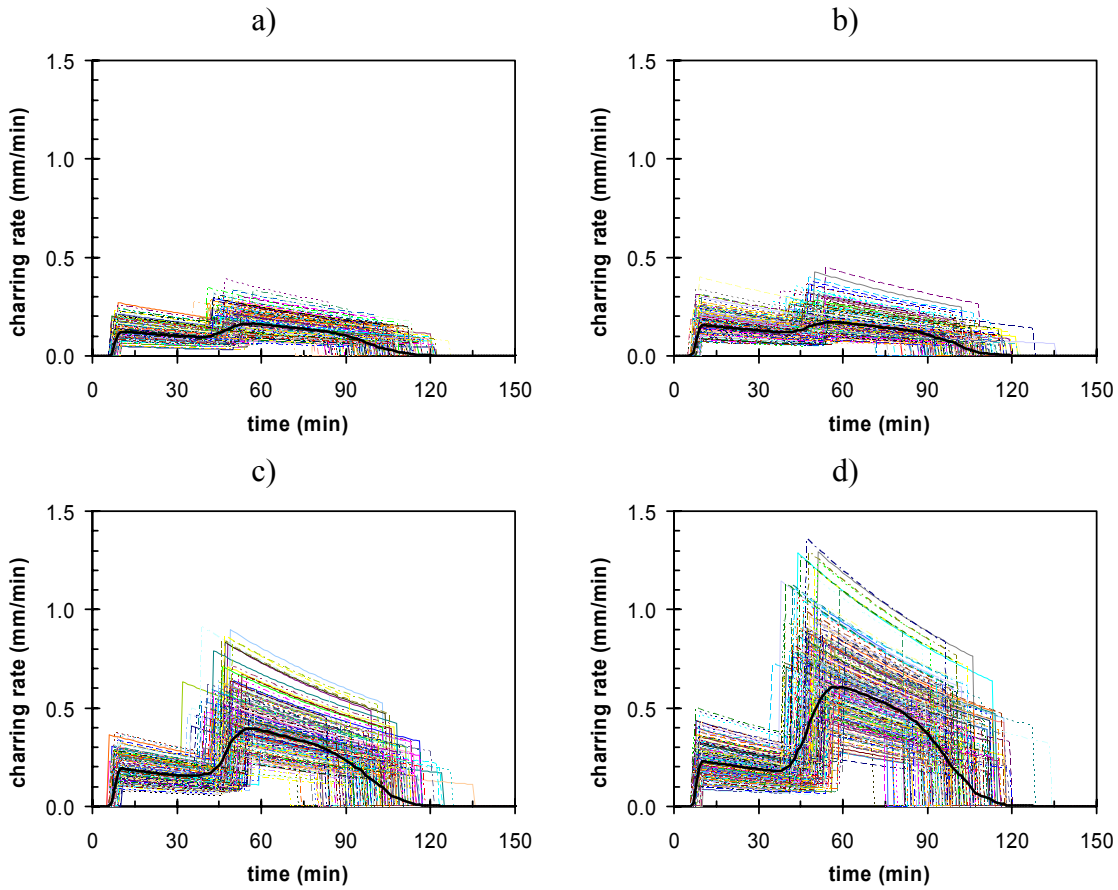

Figure 43. Examples of the charring rate curves of the structures at position x = 30 m and at heights a) z = 1 m, b) z = 2 m, c) z = 3 m and d) z = 4 m.

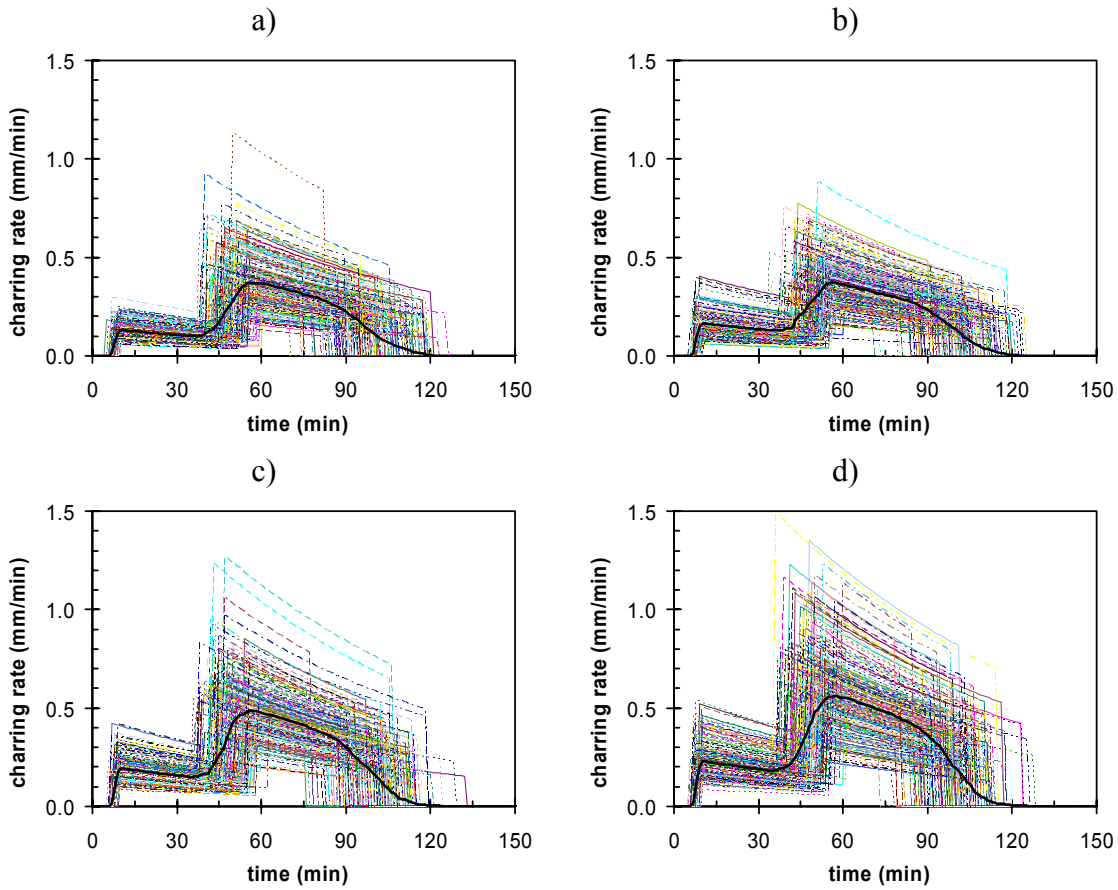

Figure 44. Examples of the charring rate curves of the structures at position x = 36 m and at heights a) z = 1 m, b) z = 2 m, c) z = 3 m and d) z = 4 m.

7.4.2.4 Char depth

The depth of the char is obtained by integrating the charring rate. Examples consisting of 250 samples of the temporal development char depths for the different cases considered are shown in the following:

- Figure 45: examples of the temporal development of the char depth at position $y = 16$ m (centre) and $x = 30$ m;
- Figure 46: examples of the temporal development of the char depth at position y = 16 m (centre) and $x = 36$ m.

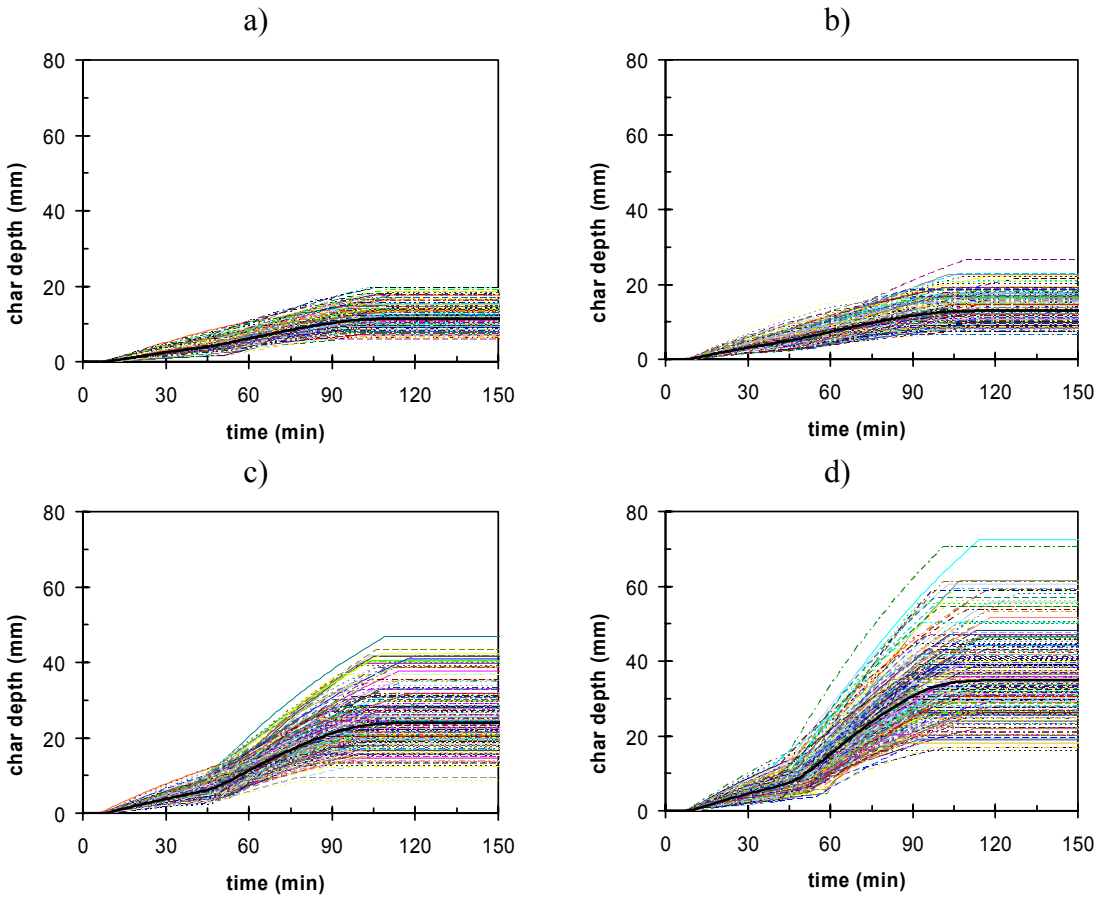

Figure 45. Examples of the charring rate curves of the structures at position x = 30 m and at heights a) z = 1 m, b) z = 2 m, c) z = 3 m and d) z = 4 m.

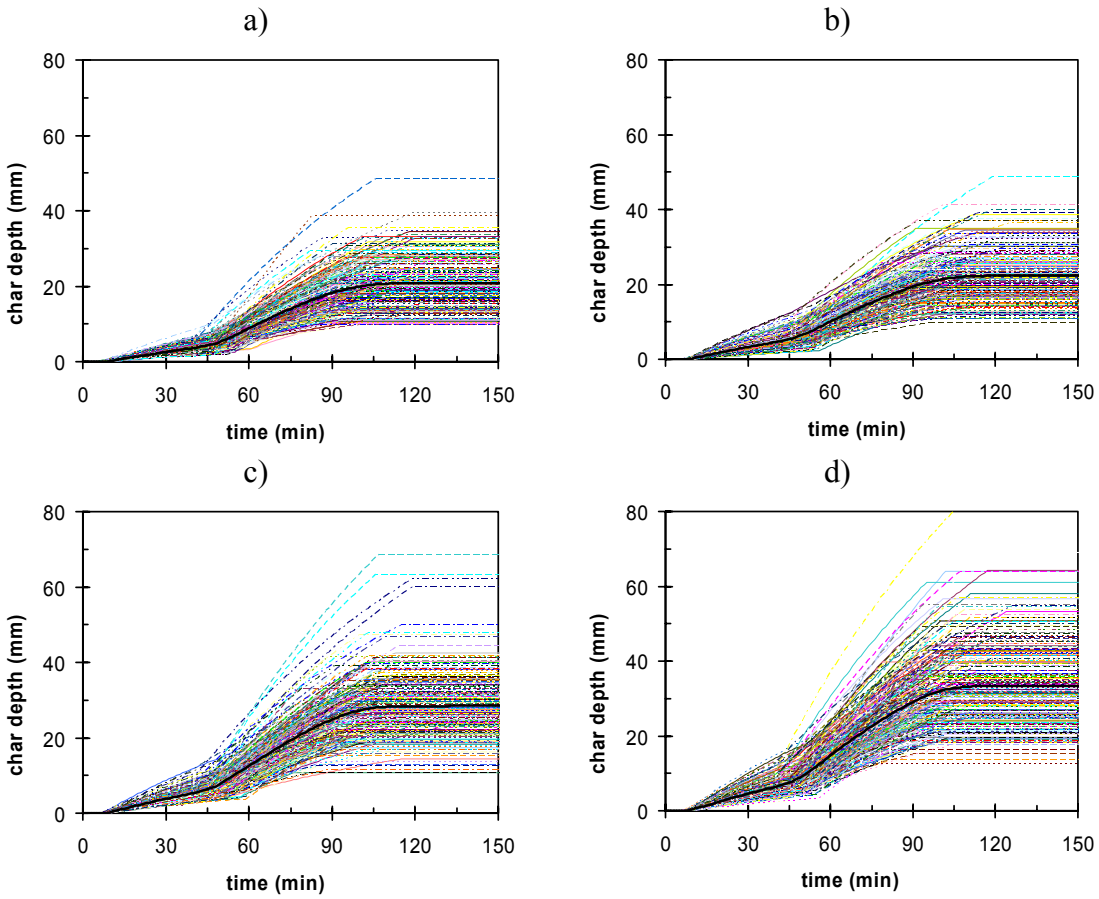

Figure 46. Examples of the charring rate curves of the structures at position x = 36 m and at heights a) z = 1 m, b) z = 2 m, c) z = 3 m and d) z = 4 m.

7.4.2.5 Limit state functions vs. time

When we insert the stochastic char-depth values to the limit-state function (Eqs. (10) and (11)), the following results exemplified by the 250 samples are obtained:

- Figure 47: examples of the temporal development of the limit state function at position $y = 16$ m (centre) and $x = 30$ m;
- Figure 48: examples of the temporal development of the limit state function at position $y = 16$ m (centre) and $x = 36$ m.

Figure 49 shows the values of the limit-state functions after the fire has ended because the fire load has burned out. It can be seen that fire exposure at position $x = 36$ m is more severe than that at $x = 30$ m as the limit-state function has negative value for both $z = 3$ m and $z = 4$ m. Thus, in following we analyse the structural failure probability at that position in more details.

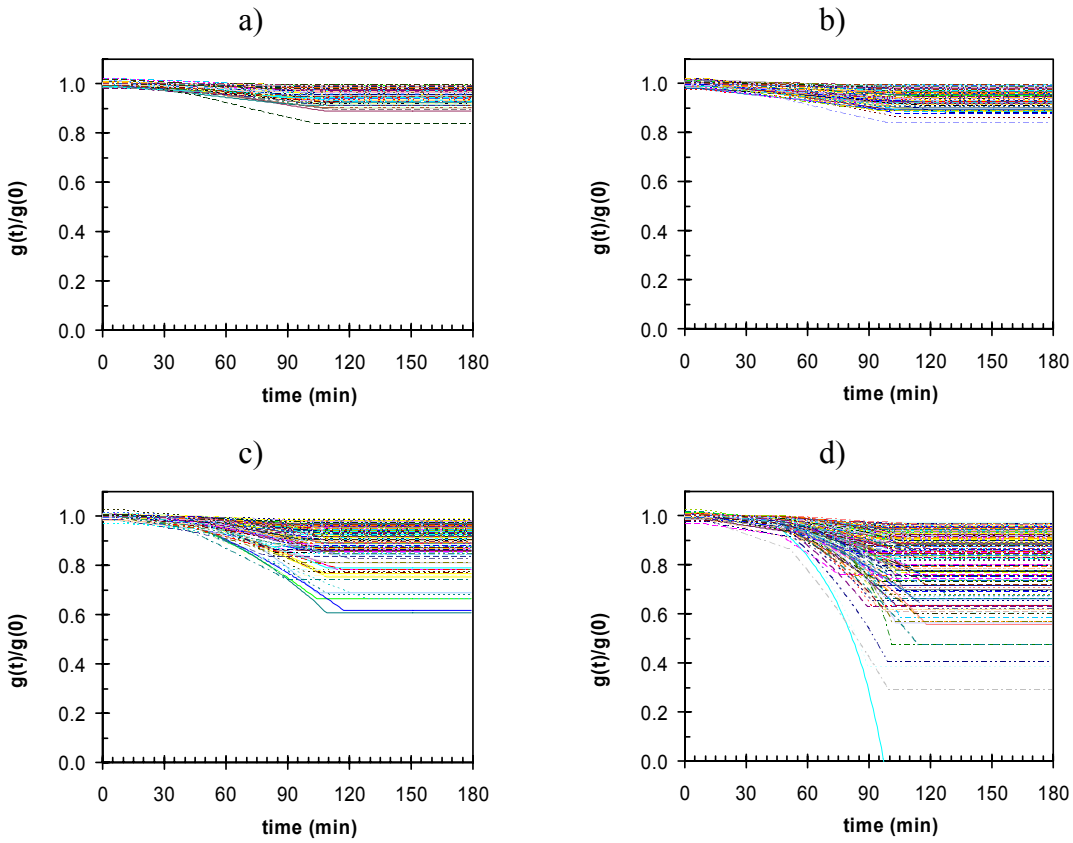

Figure 47. Examples of the limit-state functions of the structures at position x = 30 m and at heights a) z = 1 m, b) z = 2 m, c) z = 3 m and d) z = 4 m. The limit-state functions are shown in relation to their value at zero time.

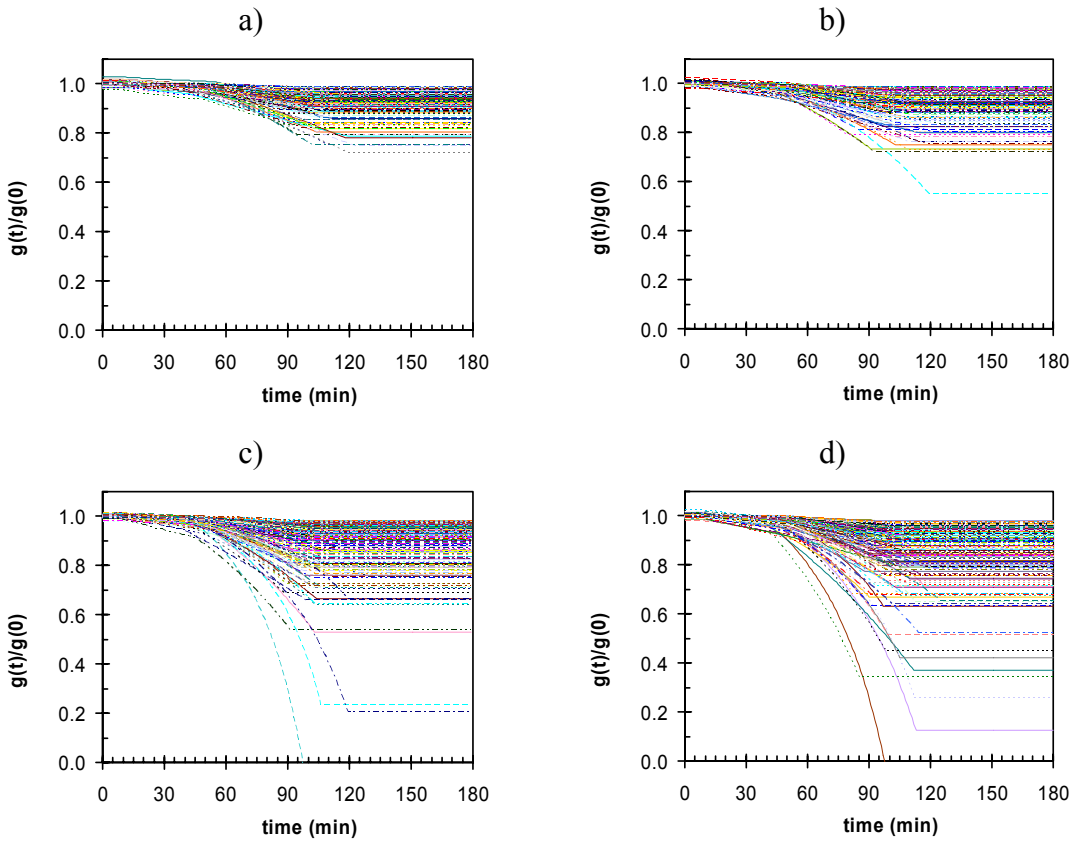

Figure 48. Examples of the limit-state functions of the structures at position x = 36 m and at heights a) z = 1 m, b) z = 2 m, c) z = 3 m and d) z = 4 m. The limit-state functions are shown in relation to their value at zero time.

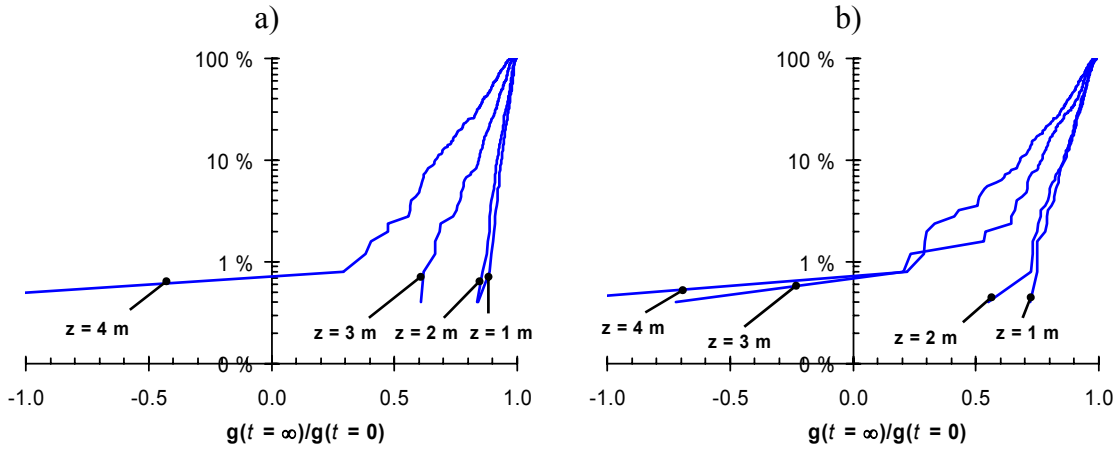

Figure 49. Examples of the values of limit-state functions after the fire has ended due to fire load burn out (formally at time equal to infinity): a)at position x = 30 m b) at position x = 36 m.

7.4.2.6 Analysis of the most severe case: heating of a beam at position y = 30 m and x = 36 m

Figure 50 shows a more detailed analysis of the most severe fire exposure case, the heating of a beam at position y = 30 m and x = 36 m. The results shown are based on a Monte-Carlo sample of size 10 000. It can be seen that the ultimate failure probability (at long times) is 0,6 % and that failures – if they take place – occur only after *ca*. 70–75 minutes.

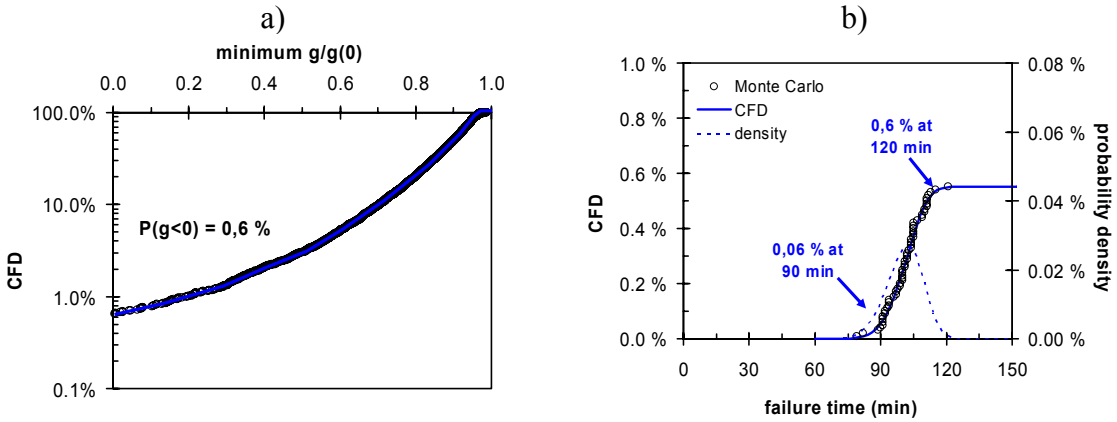

Figure 50. A more detailed analysis of the structural failure probability using the limit-state function of a beam at position x = 36 m, y =16 m and z = 4 m: a) the value of the limit-state functions after fire load burn out and) distribution of the beam failure times. The results are based on a Monte-Carlo sample of size 10 000.

It is worthwhile to elaborate in details what these results on the failure probability mean:

- They mean that if the fire would burn uninterrupted for a long time, longer than 2 hours, the chance of a structural failure would be 0,6 % per a fire that has grown as severe as the simulation depicts, which is rather severe. In particular, uninterrupted burning means that there would be no attempts by the fire brigade to fight the fire, which is not likely specifically as the fire brigade is located at only half a kilometre distance from the building. This issue is dealt in details in the following section.
- In other words one may expect that a structural failure would take place once out of about 170 severe (flashed out fires) in the population of such grocery stores as the one studied in this report;

- The meaning of the structural failure in this context is that the stress caused by the beam bending exceeds its bending strength. As the structural analysis concerns only the single structural element, we can not make any further estimates on whether the structural failure would lead to complete or partial collapse of the building. A cautious guess is that if the beam fails, the possibility of collapse cannot be ruled out.
- Even if we assume that the single-element failure leads to a progressive collapse, the collapse would not cause any significant threat to neighbouring buildings as the building is an isolated one with considerable distance to its neighbours.
- The time of failure here is the real time with zero time coinciding with the initiation of the fire growth at the prescribed growth rate, *i.e.*, we omit here any potential phase of minute, perhaps smouldering burning, which is a safe-side assumption. In particular we want to point out this time is not the same time as that used in the building product classification, e.g., the R60 or R90 classes and further that the assessment of the whether the structures satisfy the fire safety requirements must be based on the assessment of the whether they fulfil the performance requirements needed to ensure fire safety.
  - One set of such performance requirements is set in the Interpretative Document relating to Construction Product Directive (Council Directive 89/106/EEC of 21 December 1988) and included in Part E1, Fire Safety in Buildings, of the National Building Code of Finland [Ministry of the Environment 2002]. These requirements read: "The construction works must be designed and built in such a way that in the event of an outbreak of fire:

    - the load-bearing capacity of the construction can be assumed for a specific period of time,
    - the generation and spread of fire and smoke within the works are limited,
    - the spread of fire to neighbouring construction works is limited,
    - occupants can leave the works or be rescued by other means,
    - the safety of rescue teams is taken into consideration."

    The first of these essential requirements is elaborated further in Chapter 6 of E1 as:

    - A building and the building elements therein must not cause danger through collapse due to the effect of fire within a specified period of time after the start of fire. If necessary for the safety of persons or with regard to the extent of damage, the building shall sustain the combustion of the entire fire load and the cooling phase

without collapse [Ministry of the Environment 2002, section 6.1]. A further clarification especially for the performance-based fire designs sates that "When the design of load-bearing constructions is based on a design fire concept, a building is considered sufficiently fire safe with respect to load-bearing constructions if [Ministry of the Environment 2002, section 6.3]:

- a building of more than two storeys does not generally collapse during the fire or cooling phase or
- a building of not more than two storeys does not collapse during the period of time required for securing evacuation, rescue operations and controlling the fire.

– The Eurocode EN1991-1-2 states the requirement of fire safety using more generic phrases as "The general objectives of fire protection are to limit risks with respect to the individual and society, neighbouring property, and where required, environment or directly exposed property, in the case of fire" [CEN 2002b].

- The fact the beam failure becomes possible only about 70 minutes after the fire has started to grow means in practise that the structural performance poses negligible (virtually zero) hazard to life be it either that of the shop occupants or the rescue teams: if the are shop customers or staff inside the building after 70 minutes, they have been caught as victims of the fire long before that time, during the initial phases of the fire and if the fire brigade has not been able to suppress the fire within the 70 minutes, the firemen would neither be inside the building nor so close that they would be in danger even if the building would collapse, but they would hold the fire in control by cooling the building and its vicinity from the outside.

In short, the results that the building will not collapse within about 70 minutes from the fire initiation suffices to attest fire safety as put forward in the rules and requirements cited above: practically the only consequences are monetary and will most probably be covered by the insurance. In fact, the structural performance revealed in this study is not very critical even with respect to the property losses, because if the fire escalates as severe as our simulations depict, the building contents would be complete lost even if the building would survive the fire without collapse and also the building fabric would most likely be destroyed beyond reparability.

The conclusions quoted above do not take into account the probability aspect of the failure – they are derived on the basis of the failure timing. In the next section we delve into the probability dimension.

7.5 Interpretation of the likelihood of structural failure taking into account the wholeness of the building fire-safety

As any other safety issue, also fire safety is most naturally and comprehensively assessed in terms of the risks involved. Risks of a system such as a building and its neighbours, on the other hand, should be treated as different aspects of the one meaningful entity, the safety of the system. In a fire safety system, the different aspects of risks are

- risks to health and life, including all potentially threatened people, *i.e.*, staff, occupants, rescue teams, people in neighbouring facilities, passers-by, etc.
- property risks including direct, indirect and consequential risks of the system (the building that burns) or those of other systems (the neighbouring buildings or other linked facilities)
- environmental risks and risks related to any other hazards not mentioned here explicitly.

There is also a definite importance hierarchy in the risks, with the risks to health and life being the most important and those related to any other safety objectives being of secondary importance, which most often depends on the situation – while complete loss of an empty barn house may be just an advantage for its owner, total destruction of a shopping mall is a totally inconceivable and intolerable loss.

Thus, despite the fact that this report deals with structural fire safety, we start the risk analysis from the risks to life.

7.5.1 Risks to life and their reduction

In the following we assess the risks to life by comparing the distributions of the threat caused by the fire and the number of people potentially under risk.

7.5.1.1 The threat

We start by analysing the threat caused by the fire to life. For simplicity we assess the this threat through an assessment of the time when the conditions inside the building become critical for the evacuation safety and use the smoke layer height criterion used, *e.g.*, in the Swedish fire regulations [Boverket 2002, item 5:361] and adapted also to Finnish guidelines on fire engineering [RIL 2003]. Quantified as $z_{crit} = 1{,}6\ \text{m} + 0{,}1 \times \text{room height}$ (we use a rounded value of $z_{crit} = 2$ m), this criterion

that is based on the visibility considerations offers a conservative measure for the safety of the evacuation conditions. It should be noted that this criterion does not coincide with the onset of fatal conditions or even with conditions that may lead to injuries; it is more like a convenient way to assess the time when the occupants should better be out of the building in order to avoid any possible harm. Figure 51 shows an analysis of the critical time: the distribution derived shows that this varies from about 3 minutes to 10 minutes. For further use, the distribution is modelled using a 3-parameter gamma distribution with the density function defined in a piece-wise manner as:

$$
\begin{aligned}
f_C(x) &= 0\,,\ x < x_{\min,1} \\
f_C(x) &= \frac{1}{\Gamma(\alpha_1)\beta_1^{\alpha_1}}\left(x - x_{\min,1}\right)^{\alpha_1 - 1} e^{-\frac{x - x_{\min,1}}{\beta_1}}\,,\ x_{\min,1} \le x < x_A \\
f_C(x) &= \frac{1}{\Gamma(\alpha_2)\beta_2^{\alpha_2}}\left(x - x_{\min,2}\right)^{\alpha_2 - 1} e^{-\frac{x - x_{\min,2}}{\beta_2}}\,,\ x_A \le x < x_B \\
f_C(x) &= \frac{1}{\Gamma(\alpha_3)\beta_3^{\alpha_3}}\left(x - x_{\min,3}\right)^{\alpha_3 - 1} e^{-\frac{x - x_{\min,3}}{\beta_3}}\,,\ x_B \le x
\end{aligned}
\tag{36}
$$

with

$$
x_A = F_C^{-1}\left(p_A\right) \text{ and } x_B = F_C^{-1}\left(p_B\right) \tag{37}
$$

where $F_C^{-1}(\cdot)$ denotes the inverse of the corresponding cumulative distribution and p_A and p_B are parameters. Curve fit yields the following values for the distribution parameters α_i, β_i, $x_{\min,i}$, p_A and p_B: $\alpha_1 = 0{,}43$, $\beta_1 = 21{,}2$ min, $x_{\min,1} = 3{,}22$ min, $\alpha_2 = 41{,}4$, $\beta_2 = 0{,}31$ min, $x_{\min,2} = -5{,}80$ min, $\alpha_3 = 6{,}12$, $\beta_3 = 0{,}36$ min, $x_{\min,3} = 5{,}70$ min, $p_A = 0{,}53$ and $p_B = 0{,}80$.

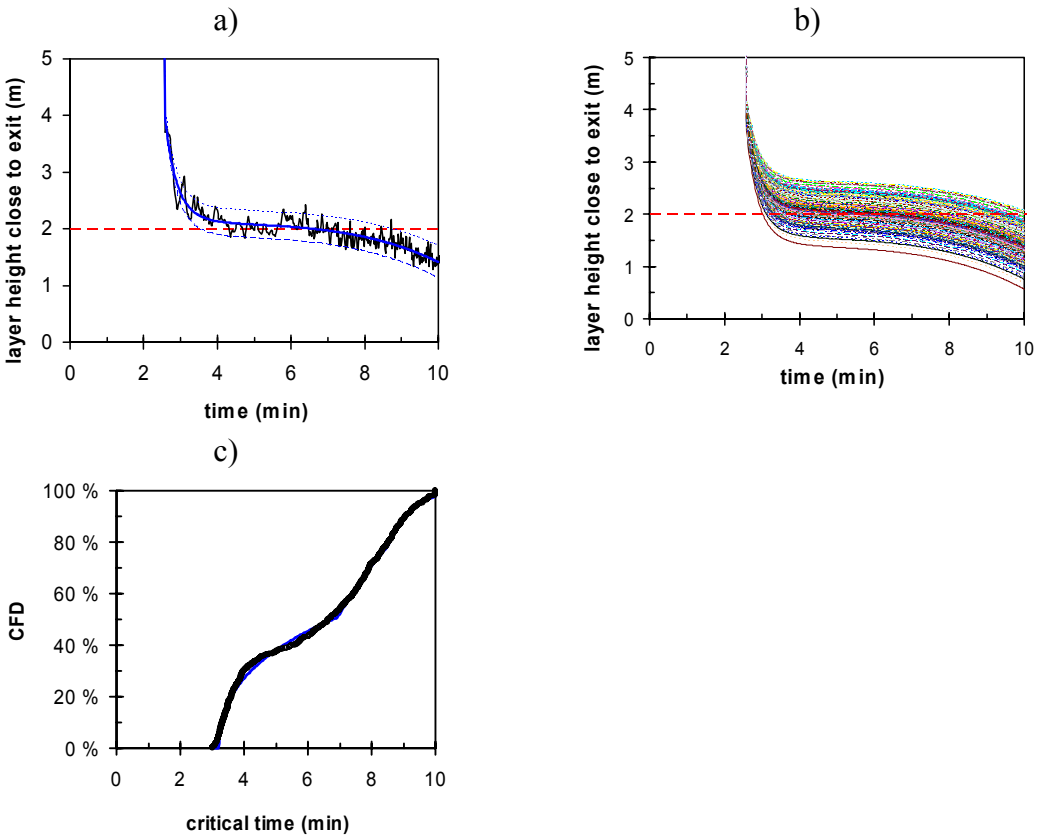

Figure 51. Analysis of the critical time for safe evacuation: a) the temporal evolution of the smoke layer height obtained from the fire simulations with the solid curve representing a least-squares fit to the data and the dotted and dashed curves showing a ±7 % scatter around the fitted curve; b) Stochastic model for the smoke layer height and c) the distribution of the critical time derived as a Monte-Carlo sample of the times when the layer height crosses the level of 2m.

7.5.1.2 The threatened

Next we assess the number of people that may be subjected to the critical conditions during the emergency evacuation of the building. This number is determined by two factors:

- the time it to takes for the persons to move from the inside of the building to a safe place outside of the building,
- the number of people that there may be at one time inside the building.

The time it takes for a person to evacuate in the case of fire may be divided to three parts [ABCB 2005]:

- The cue time, *i.e.*, the time that elapses from the fire initiation to the time when a person receives a cue (alarm, sensory perception, etc.) of a fire in the building.
- The response time (or reaction time), *i.e.*, time it takes to realise that the cue is an indication of a fire.
- The movement time, which can further be subdivided to a period taken by the initiation of movement and the time it takes to complete the movement to a safe place.

For the cue time we employ a simplification that it can be due to either a direct sensory perception (*e.g.*, seeing or smelling) of the fire or an alarm from fire detectors, depending on which one is shorter.

Sensory perception of the fire is naturally possible only during the times when there are people inside the building. We assume that this occupied time coincides with the times that the shop is open, *i.e.*, Monday-Friday from 7 p.m. to 9 a.m., on Saturday from 7 p.m. to 6 a.m. and closed on Sunday, making a total of 81 hours of occupied time per a week or 48 %. We tie the possibility of a direct sensory perception to the fire size, or, more precisely, to the heat release rate HRR, by assuming that the average fire size when it is perceived is about 200 kW and that it is rare (probability of 95 %) that the fire will not detected when it has grown to the size of 2,5 MW. The sensory perception is intentionally made rather wide to reflect the inherent uncertainty in human actions (see Figure 52). It can be modelled by the 3-parameter gamma distribution with $\alpha = 1{,}22$, $\beta = 0{,}99$ min and $x_{\min} = 0{,}32$ min.

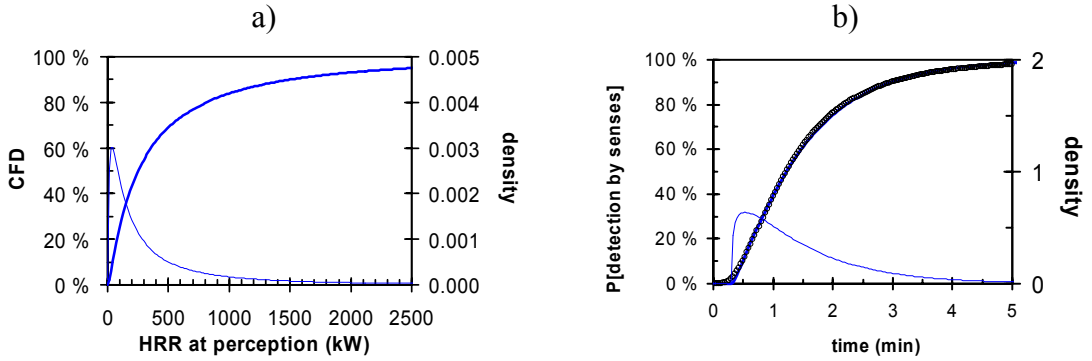

Figure 52. Statistical model for the sensory perception of the fire: a) probability of perception vs. the fire size expressed as the heat release rate (HRR) and b) time dependence of the probability of the sensory perception of the fire.

To model the cue from the alarms we considered three different options:

- The first case is that the alarm takes place when the heat detectors that trigger that smoke vents activate at 100 ˚C.
- As a second case we analyse the option that there would be additional, more sensitive, heat detectors which activate at 58 ˚C.
- The third detection case is that there would be additional smoke detectors. The activation is modelled according to the temperature rise [see, *e.g.*, Benjamin *et al*. 1979] with the temperature rises needed for activation ranging from 10 ˚C to 15 ˚C (uniform distribution).

The response time index, RTI = 25 $m^{1/2}s^{1/2}$ and the reliability to operate as intended on demand, 95 %, are assumed to be the same for the three detector types. The detector activation times resulting of a Monte-Carlo analysis of their performance are shown in Figure 53. The Monte Carlo samples are modelled using a 3-parameter gamma distribution with parameters $\alpha = 26{,}16$, $\beta = 0{,}060$ min and $x_{min} = 2{,}65$ min (case 1), $\alpha = 7{,}66$, $\beta = 0{,}101$ min and $x_{min} = 2{,}23$ min (case 2) and $\alpha = 8{,}06$, $\beta = 0{,}069$ min and $x_{min} = 1{,}42$ min (case 3).

The cue time distributions obtained as the minimum of the sensory perception time and the detector activation time are shown in Figure 54.

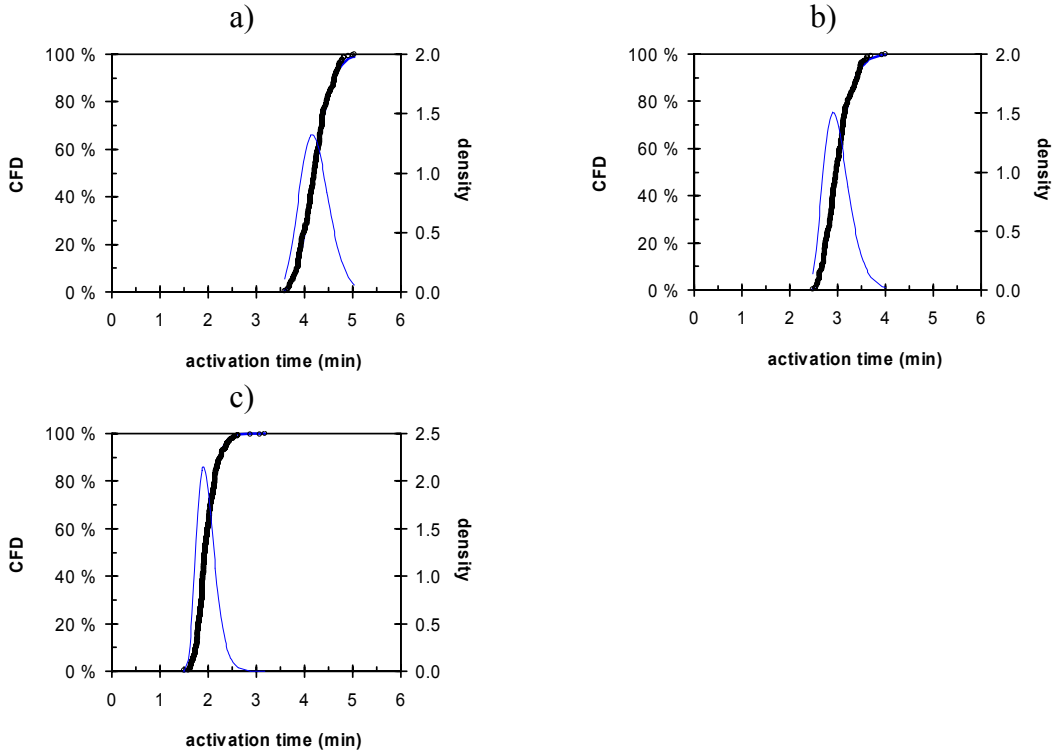

Figure 53. Statistical models for the fire detected activation times: a) heat detectors, activation at 100 ˚C, b) heat detectors, activation at 58 ˚C and c) smoke detectors, activation at temperature rise ranging between 10–15 ˚C.

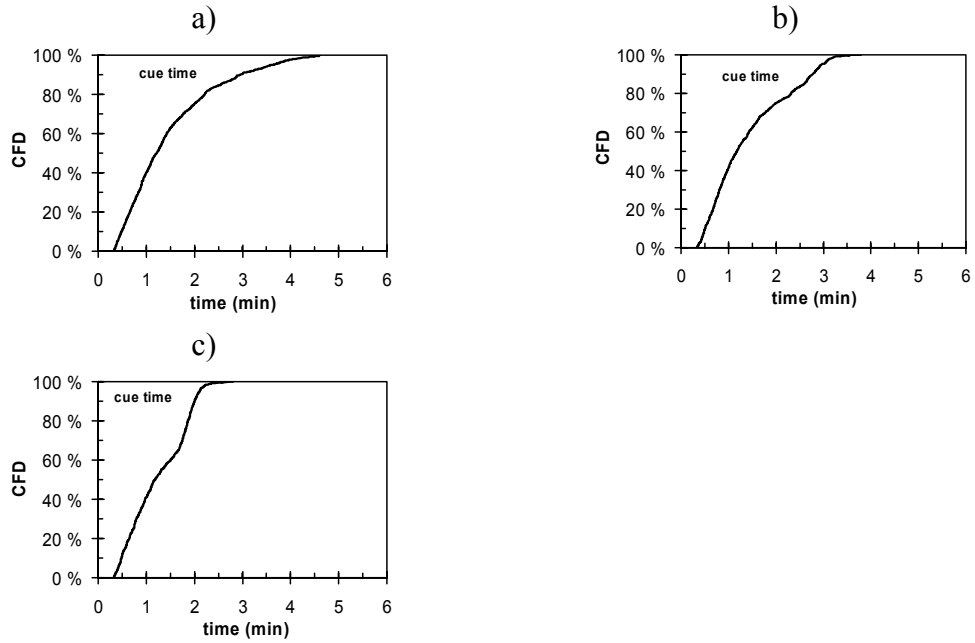

Figure 54. Statistical models for the cue times obtained using the distributions shown in Figure 52b and Figure 53: a) heat detectors activating at 100 ˚C, b) heat detectors activating at 58 ˚C and c) smoke detectors activating at temperature rise 10–15 ˚C.

The values cited in literature for the response time (or reaction time) vary considerably: e.g., a Finnish fire safety engineering guide [RIL 2003] gives values ranging between 120–180 s depending on the way how the fire cue has been received while the results of Frantzich obtained in three evacuation exercises in different Swedish furniture department stores [Frantzich 2001, Tabell 14] range between 15–54 s with the mean value of *ca*. 25–30 s. Purser & Bensilum [2001] provide quantified data (Figure 55 a) on the premovement time which corresponds to our response time. In this study we model the response time using the lognormal distribution characterising the data of Purser and Bensilum shown in Figure 55b.

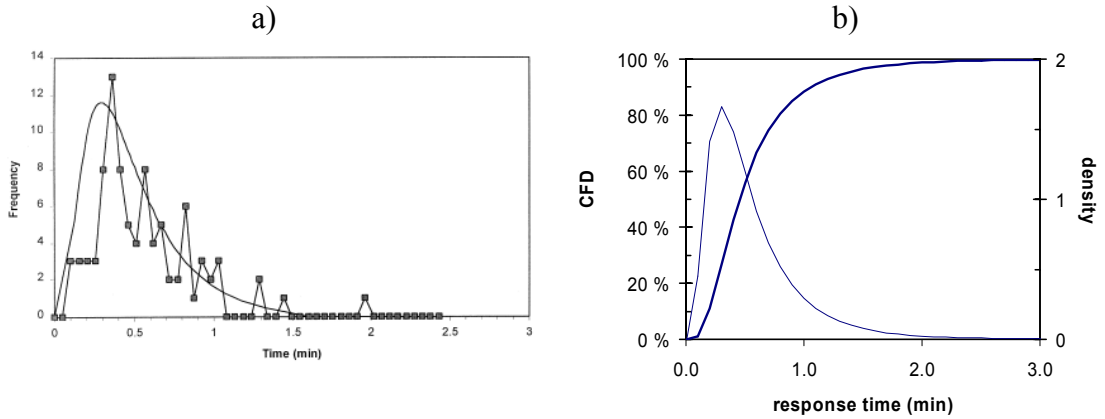

Figure 55. a) Data of Purser and Bensilum [2001] on the response time and b) modelling of the data using a lognormal distribution with mean value equal to 0,29 minutes and coefficient of variation of 74 %.

The time taken by the movement to the exit doors and further outside to safety was calculated using the new FDS-Evac evacuation simulation software tool developed at VTT Fire Research [Korhonen *et al.* 2005]. An example of the results of the FDS-Evac calculation is shown in Figure 56 and the results depicting the time-dependence of the number of people inside the building during the evacuation process are shown in Figure 57. In the further analysis we use the results obtained with $N(0) = 100$ persons modelled using a 3-parameter gamma distribution with parameters $\alpha = 2{,}28$, $\beta = 8{,}9$ s and $x_{\min} = 8{,}8$ s. The mean and coefficient of variation of this distribution are 29 s and 46 %, respectively[4].

[4] If the other exit is not available, the mean value of the movement time grows to about 39 s but the coefficient variation decreases slightly to 42 %.

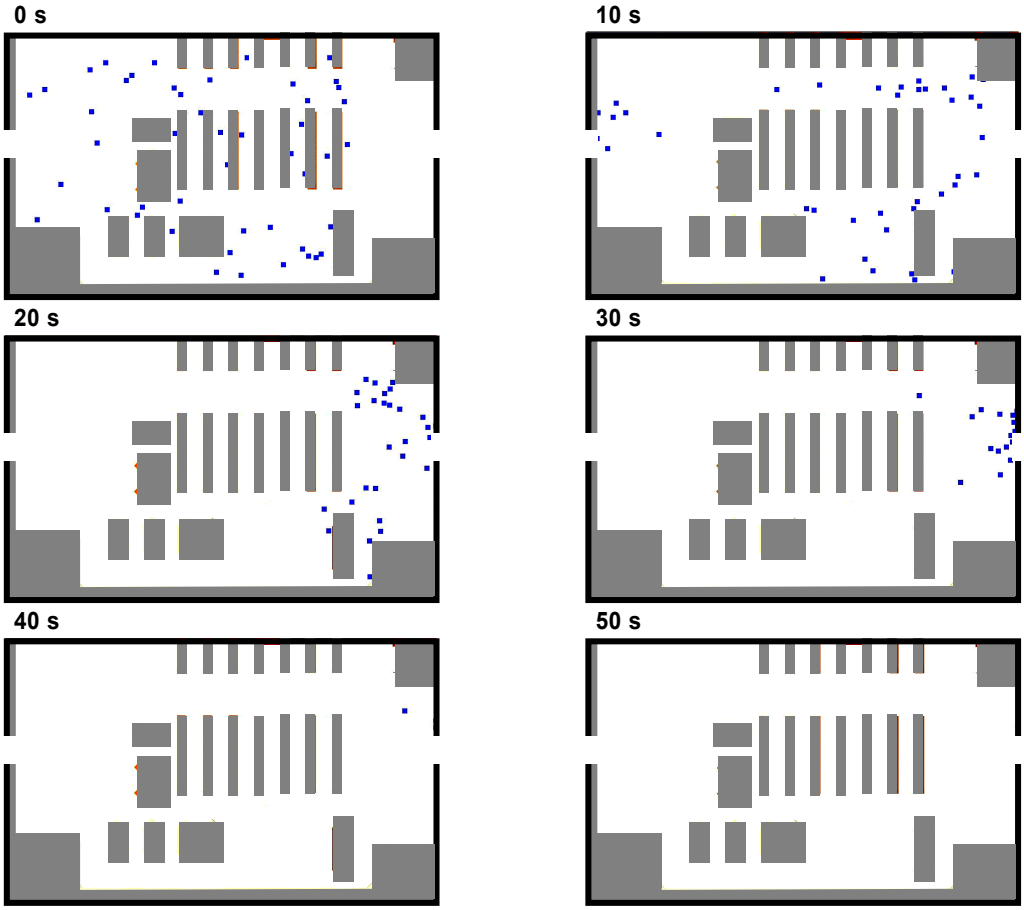

Figure 56. Example of the evacuation of the building calculated using the FDS-Evac program [Korhonen et al. 2005]. The initial number of people inside the building is 50 and both exits on the south and north wall of the building are available for escape.

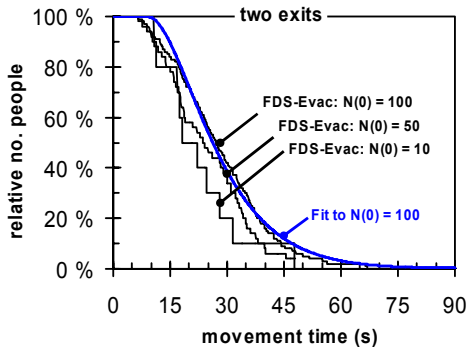

Figure 57. Results of the movement time calculations for selected initial populations in the building, N(0) = 10, 50 or 100 persons (no. people is shown as normalised by the initial number of people). The curve fitted to the results obtained with N(0) = 100 persons shows the functional shape (3-parameter gamma distribution) used in the following analysis.

The time required for the evacuation of the building is obtained as a sum of the cue time (Figure 54), the response time (Figure 55b) and the movement time (Figure 57). Figure 58a, b and c summarise the evacuation time distributions for the three detectors cases considered, *i. e.*, heat detectors activating at 100 ˚C (Figure 58a), heat detectors activating at 58 ˚C (Figure 58b) and smoke detectors activating at temperature rise ranging from 10 ˚C to 15 ˚C (Figure 58c). The distributions are modelled using a piece-wise defined 3-parameter gamma distribution with the density function given by

$$f(x) = 0,\ x < x_{\min,1}.$$
$$f(x) = \frac{1}{\Gamma(\alpha_1)\beta_1^{\alpha_1}}\left(x - x_{\min,1}\right)^{\alpha_1 - 1} e^{-\frac{x - x_{\min,1}}{\beta_1}},\ x_{\min,1} \le x < x_* \tag{38}$$
$$f(x) = \frac{1}{\Gamma(\alpha_2)\beta_2^{\alpha_2}}\left(x - x_{\min,2}\right)^{\alpha_2 - 1} e^{-\frac{x - x_{\min,2}}{\beta_2}},\ x_* \le x$$

with

$$x_* = F^{-1}(p) \tag{39}$$

where $F^{-1}(\cdot)$ denotes the inverse of the corresponding cumulative distribution and p is a parameter. Curve fit yields the following values for the distribution parameters α_1, β_1, $x_{\min,1}$, α_2, β_2, $x_{\min,2}$ and p:

- heat detectors activating at 100 ˚C: $\alpha_1 = 2{,}86$, $\beta_1 = 0{,}64$ min, $x_{\min,1} = 0{,}71$ min, $\alpha_2 = 22{,}7$, $\beta_2 = 0{,}29$ min, $x_{\min,2} = -4{,}29$ min and $p = 0{,}7$;

- heat detectors activating at 58 ˚C: $\alpha_1 = 1{,}70$, $\beta_1 = 0{,}92$ min, $x_{\min,1} = 1{,}00$ min, $\alpha_2 = 23{,}1$, $\beta_2 = 0{,}20$ min, $x_{\min,2} = -2{,}02$ min and $p = 0{,}75$;

- smoke detectors activating at temperature rise 10–15 ˚C: $\alpha_1 = 1{,}81$, $\beta_1 = 0{,}89$ min, $x_{\min,1} = 0{,}97$ min, $\alpha_2 = 23{,}0$, $\beta_2 = 0{,}14$ min, $x_{\min,2} = -0{,}92$ min and $p = 0{,}6$.

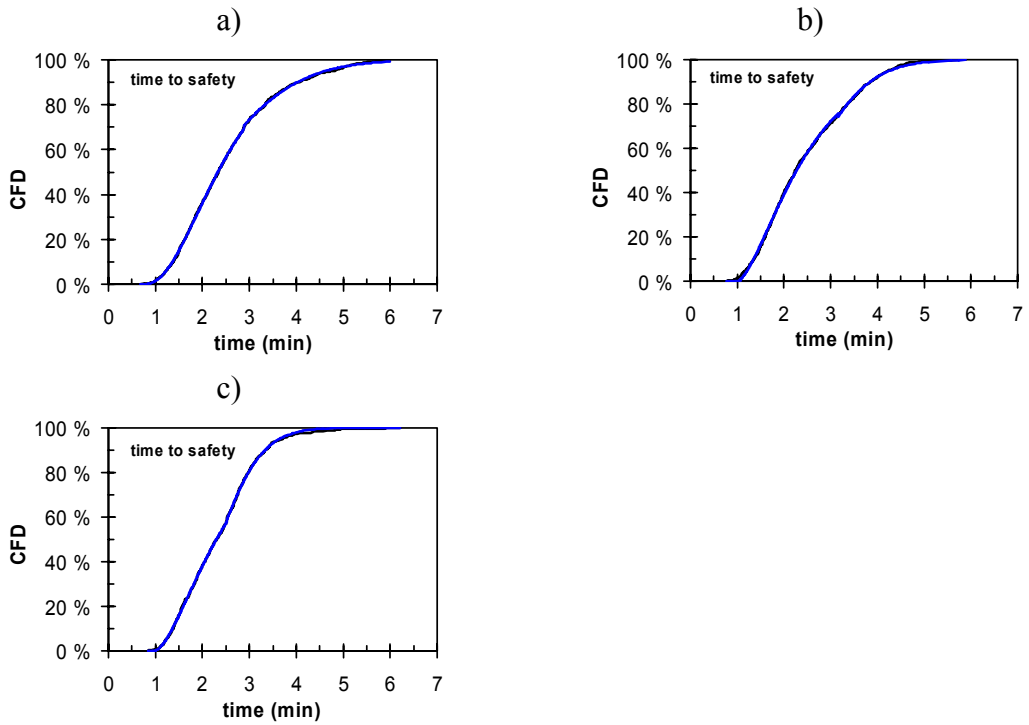

Figure 58. Statistical models for the time required for the evacuation of the building: a) heat detectors activating at 100 ˚C, b) heat detectors activating at 58 ˚C and c) smoke detectors activating at temperature rise 10–15 ˚C.

To convert the distributions shown above to risk to life we need to know what the expected number people inside the building during the shopping hours is. Here we make the following assumption regarding this factor: we assume that it is very rare to have more than 100 people at one time inside the building (probability 1 % or less) and further that there is 20 % probability of having more than 50 persons simultaneously inside the building. Figure 59 shows a lognormal distribution that fulfils these conditions.

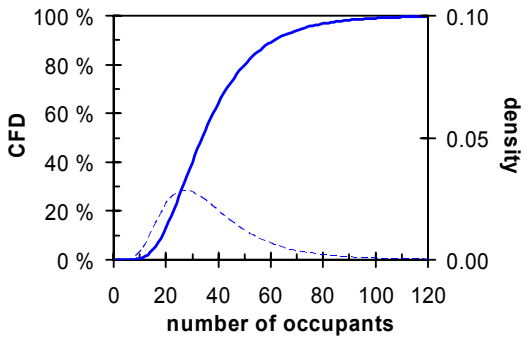

Figure 59. Assumed distribution of the number of people inside of the building at a given time during the shopping hours.

7.5.1.3 Risk to life

Now that we have models for the threat caused by the fire and the evacuation process, we may assess the related risks in a quantitative manner. Technically the calculation goes so that we execute Monte Carlo sampling of the expectation value of the number of people (N_c) that may be subjected to critical conditions[5]. The results of a Monte Carlo analysis using a sample size of 10 000 are shown in Figure 60. Plotted on a linear probability scale (Figure 60a), the results obtained for the heat detectors activating at 100 ˚C or 58 ˚C are practically indiscernible while for the smoke detector the probabilities are clearly lower: for N_c values larger than 1, the difference is roughly one order of magnitude (factor of 10). A plot using a logarithmic scale for the probabilities reveals that using more sensitive heat detectors activating at 58 ˚C instead of 100 ˚C would reduce the risks at the low end of the consequence spectrum.

The probability of having no persons subjected to critical conditions ($p(0)$) gives a further differentiation of the safety levels provided by the three fire detection and alarming options:

- heat detectors activating at 100 ˚C: $p(0)$ = 5 % or only once in 20 fires;
- heat detectors activating at 58 ˚C: $p(0)$ = 34 % or once in about 3 fires;
- smoke detectors activating at temperature rise 10–15 ˚C: $p(0)$ = 54 % or once in about every second fire.

[5] In each Monte-Carlo run we first select randomly the probabilty of the onset of the critical conditions, which using the inverse F_C^{-1} of the distribution defined by Eq. (36) gives us the corresponding time. Using the distributions shown in Figure 58 for the timing of the evacuation and in Figure 59 for the potential number of occupants we then can evaluate the number of people that may be subjected to critical conditions as well as the probability of this event.

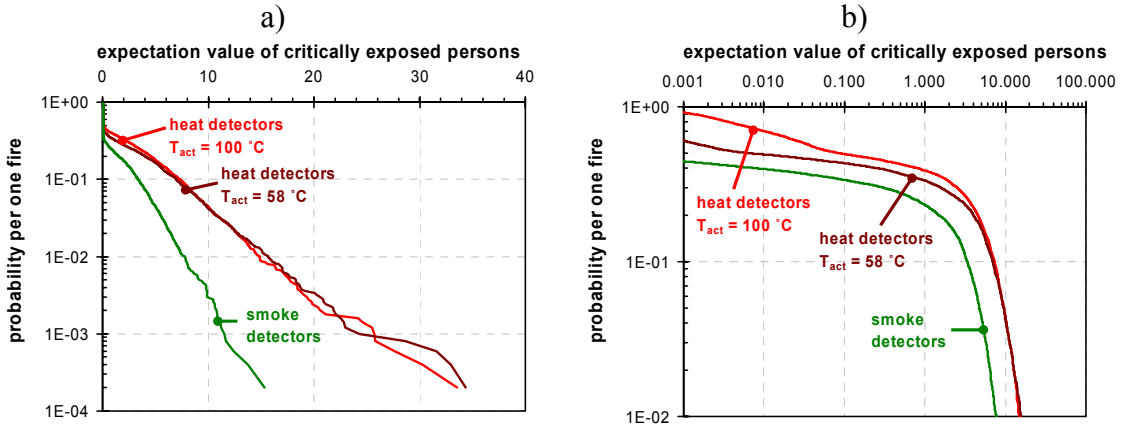

Figure 60. Risk to life assessed according to the potential number of people subjected to critical conditions: a) the probabilities shown on a linear scale and b) the probabilities shown on a logarithmic scale. Monte-Carlo analysis with sample size of 10 000.

To assess the significance of the risks we have to assess the probability, or more precisely, the frequency of occurrence of fires in such buildings as we consider here. Tillander [2004] and Tillander & Keski-Rahkonen [2001] have analysed Finnish fire statistics and obtained quantitative results of the specific ignition frequency f'' expressing the frequency of fire occurrences per unit floor area (in units of $a^{-1}m^{-2}$)[6] for different building categories:

$$f'' = c_1 \cdot A^r + c_2 \cdot A^s \qquad (1)$$

where A is the building floor area and the parameters c_1, c_2, r and s depend on the building category. While there is no building category matching precisely such a isolated hall-like shop building that we are considering, the closest match may be the category "commercial buildings" for which the parameters are $c_1 = 7 \cdot 10^{-5}$ $a^{-1}m^{-1,35}$, $c_2 = 6 \cdot 10^{-6}$ $a^{-1}m^{-1,95}$, $r = -0{,}65$ and $s = -0{,}05$. Alternatively one can consider the building as one belonging to the category "all buildings except residential and industrial buildings, warehouses and other buildings", introduced by Tillander [2004] to improve the statistical accuracy of the results, for which the parameters are $c_1 = 9 \cdot 10^{-4}$ $a^{-1}m^{-0,96}$, $c_2 = 6 \cdot 10^{-6}$ $a^{-1}m^{-1,05}$, $r = -1{,}04$ and $s = -0{,}05$. Inserting the floor area of 1700 m^2 to the above expression, we obtain the following two estimates for the specific ignition frequency:

- $f'' = 4{,}7 \cdot 10^{-6}$ $a^{-1}m^{-2}$ for the category "commercial buildings"
- $f'' = 4{,}5 \cdot 10^{-6}$ $a^{-1}m^{-2}$ for the category "all buildings except residential and industrial buildings, warehouses and other buildings".

[6] "a" stands for a year, coming from word *annus*, Latin for "year."

Thus we can conclude that the value $f'' = 5 \cdot 10^{-6}\ a^{-1}m^{-2}$ is an appropriate approximation for the specific ignition frequency. The corresponding ignition frequency is $f = f'' \cdot A = 5 \cdot 10^{-6} \cdot 1700\ a^{-1} = 8{,}5 \cdot 10^{-3}\ a^{-1}$ or one fire in 120 years. According to Statistics Finland there are about 470 single-storey shop halls in Finland with the floor area ranging from 1000 m^2 to 2000 m^2. In this population, the ignition frequency per building equal to $f = 8{,}5 \cdot 10^{-3}\ a^{-1}$ corresponds to $470 \cdot 8{,}5 \cdot 10^{-3}\ a^{-1} \approx 4$ fires per year in Finland. On the other hand the Finnish fire statistics reveal that during the 6-year period 1996–2001 there were there were 27 fires in single-storey shop-halls belonging to the fire class P2 according to the Finnish building fire classification. This corresponds to 4,5 fires per year in Finland confirming the fire frequency evaluated on the basis of the results of Tillander and Keski-Rahkonen. The annual scatter in the number of fires is ca. 30 %.

Our description of the fire is such that once ignited the fire grows unobstructed to engulf the whole building. Yet not all fires reported to the fire statistics are so severe, but some ignitions just do not spread or if they would be able to spread they are extinguished by the personnel/occupants or by the fire brigade. We have the data required to model quantitatively the fire brigade actions and hence we calculate the influence of the fire brigade in the next section (section 7.5.2) by using the Time-Dependent Event Tree Method. We could incorporate also the first-aid extinguishing into the Time-Dependent Event Tree analysis (see e.g. Hietaniemi *et al.* [2002] and Korhonen *et al.* [2003], but in this study we use a shorter route and take the first-aid extinguishing as well the fact that not all fires have the potential to spread into account by using statistical data to reduce the ignition frequency. According to property-damage distributions shown in Figure 61, the proportion of fires that cause only a small damage to the building contents, say less than 1000–2000 euros or 1–2 % of the value at risk, is about 50 %. Thus we obtain the final results for the frequency of fires with the potential to reach the severity of our simulated fire

$$f = 0{,}5 \cdot 8{,}5 \cdot 10^{-3}\ a^{-1} \approx 4 \cdot 10^{-3}\ a^{-1}. \qquad (41)$$

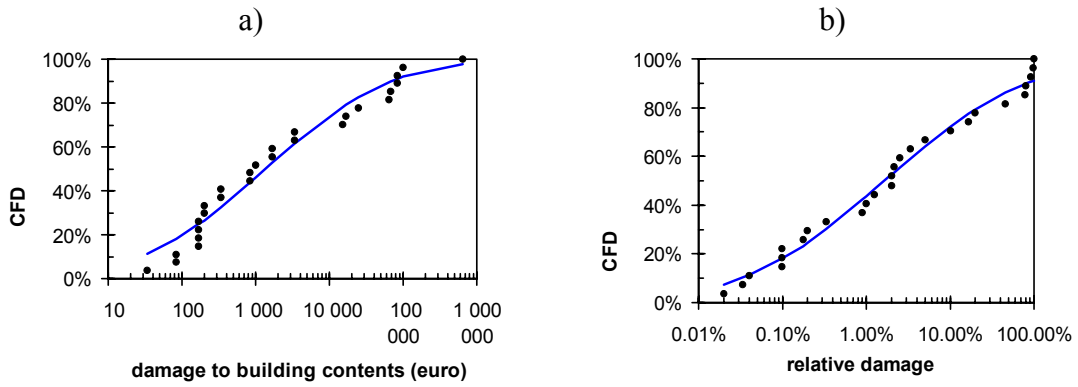

Figure 61. Assessment of the portion of fires that either self-extinguish or become extinguished via first-aid extinguishing action by personnel or shop customers: a) distribution of the damage to the building contents and b) distribution of the relative damage to the building contents (damage per value at risk). Data based on Finnish fire statistics between 1996–2001.

With the average severe fire rate of *ca*. 2 fires a year, for heat detectors, the results given above concerning the risk to life mean that annually in Finland the chance of having 10 persons at once being subjected to critical conditions is $2 \cdot 4 \cdot 10^{-2} = 0{,}08$ or roughly once in every 10–15 years. For the smoke detectors, the corresponding numbers are $2 \cdot 3 \cdot 10^{-3} = 0{,}006$ or about once in every 150 years for a 10-person exposure. Having 10 persons subjected to critical conditions while trying to escape from a fire as frequently as almost every 10th year does not seem as a sufficient level of safety while the risk level of once in 150 years seems much more tolerable in particular when one remembers that these exposures do not mean fatalities but severe impediments of the evacuation of those exposed.

Hence we may conclude that if the safety of lives against fire in such buildings that we are considering here relies on the heat detectors, the resulting risk level seems to high to be considered as tolerable while if the safety would be increased by the more sensitive smoke detectors, the resulting risk level is considerably lower and indeed most likely tolerably low.

7.5.2 Influence of the fire brigade

The ability of the first response units of the fire brigade (FB) to get the fire into control or extinguish it depends on the size of the fire when the FB stars fight it: the larger the fire, the more difficult it is to get under control. The size of the fire at the FB intervention depends on

- the growth rate of the fire,
- the time when the fire is detected,
- the time delay between fire detection and the time when the firemen are ready to spray water into he fire.

The time delay between fire detection and the time of the start can be factor down to the following time delays:

- the time when the emergency call reaches the FB,
- the time it takes from the FB to leave the fire station after the reception of the emergency call (turnout time),
- the travel time to the target,
- the time required at the fire scene to make the preparations for the water application (water set-up time),
- the time taken for search and rescue tasks extinguishing intervention (search and rescue time).

Concerning the first time delay, we assume that fire detection is associated with an alarm signal transmitted to the FB and if the emergency signal is a phone call, we assume that is made promptly after the fire detection. In the following we deal with the last four items as well as the probability that the FB can extinguish a fire of a certain size.

7.5.2.1 Turnout time

Due to the groundbreaking work of Tillander and Keski-Rahkonen in fire statistics analysis, we have in Finland a solid statistical base for the quantitative assessment of the influence of the fire brigade operations on the fire development. Figure 62 shows data of Tillander and Keski-Rahkonen [2000, Figure 40] for the fire brigade turnout time in the same region as the building we are considering is located. The data can be fitted by a 2-parameter gamma distribution (same as 3-parameter gamma distribution with $x_{\min}$ set to zero) with parameters $\alpha = 3{,}43$ and $\beta = 18{,}6$ s. The mean value of this distribution is 63 s and the coefficient of variation 54 %.

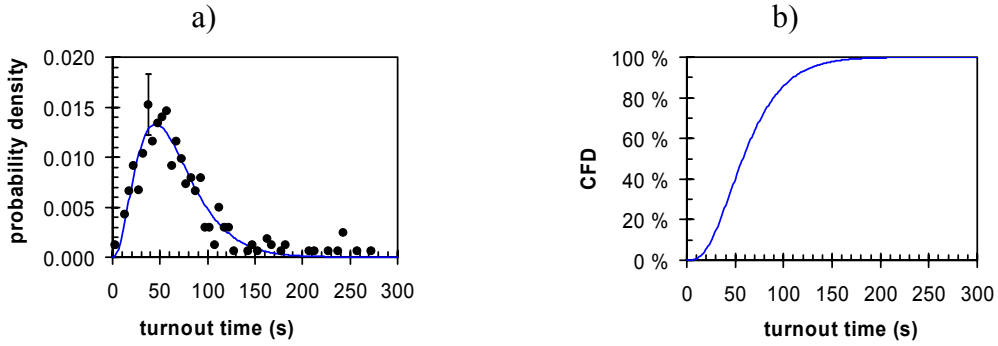

Figure 62. Distribution of the fire brigade turnout time: a) data of Tillander and Keski-Rahkonen [2000] with a 2-parameter gamma distribution fit and b) the corresponding cumulative frequency distribution.

7.5.2.2 Travel time

Tillander and Keski-Rahkonen [2000] provide also statistical data and their analysis concerning the fire brigade travel times. As the travel distance that we are considering is a very short one, only 0,5 km, we base our estimate on the travel time on a simple analysis of the data of Tillander and Keski-Rahkonen on the travel times of the rural fire brigades. Figure 63a shows a replotting of short-distance data of Figure 70 of Tillander and Keski-Rahkonen [2000] with a linear model fitted to the data. For simplicity we model the scatter of the data as quantified by the linear fit by a normal distribution. Figure 63b shows the resulting prediction of the travel time for the fire brigade distance of 0,5 km: the mean of distribution is 1,35 min and the standard deviation 0,44 min.

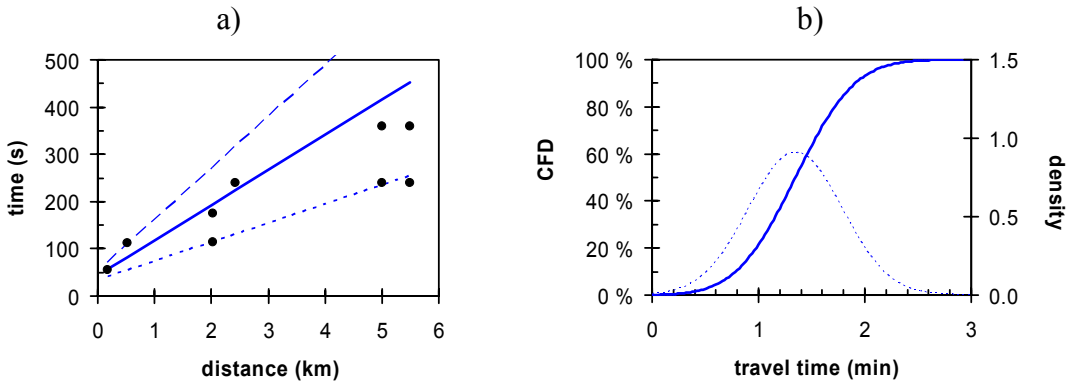

Figure 63. a) Short-distance data extracted from Figure 70 of Tillander and Keski-Rahkonen [2000] and a linear fit to the data (the dashed and dotted lines depict lines deviating from the best fit by one standard deviation).

7.5.2.3 Water set-up time

To model the time required at the fire scene to make the preparations for the water application, we apply the results from the Fire Brigade Intervention Model (FBIM) [Marchant *et al*. 2001]: Figure 64a shows their results on the time required to remove, connect and charge a 65-mm hose from hydrant to appliance and Figure 64b modelling of the results using the Weibull distribution with the density function given by

$$f(x) = \frac{\alpha}{\beta^{\alpha}} x^{\alpha-1} e^{-\left(\frac{x}{\beta}\right)^{\alpha}}, \; x \geq 0 \tag{42}$$

where according to a least-squares fit, $\alpha = 2{,}18$, $\beta = 68{,}0$ min. The mean of this distribution is 60 s and the coefficient of variation 48 %.

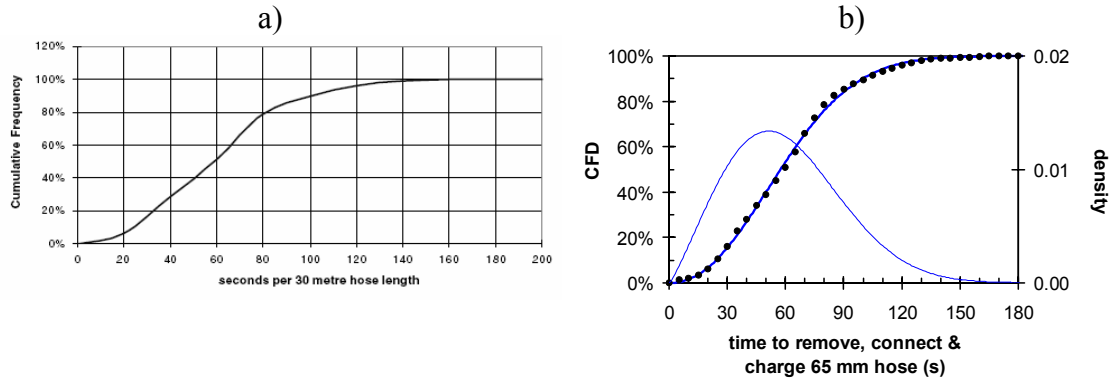

Figure 64. a) Result of Marchant et al. [2001] concerning the time required to remove, connect and charge a 65-mm hose from hydrant to appliance and b) statistical modelling using the Weibull distribution (the dots represent samples of the curve of Marchant et al. [2001].

7.5.2.4 Search and rescue time

Särdqvist [1998] analysed reports from 307 fires in non-residential buildings in London between years 1994 and 1997. He gives data on the time period from the FB arrival to the starting of the intervention. His general finding is that this time delay is generally short, which comes as no with the longest times to intervention, up to 5 to 10 minutes, being related for the small or medium-sized fires that are hard to find in possible large premises. The majority of the time delays between the arrival and the start of the intervention fall between 1 and 2 minutes. The building we are considering is a not-particularly-large, one-storey facility with a simple lay-out and hence, we can assume

that the pre-intervention time delay coincide with the smaller time range observed by Särdqvist [1998]. The search and rescue time comprises only a part of this time delay and in its quantification we assume that it corresponds to about half of the arrival-intervention delay, or about 1 minute. We characterise the scatter of this quantity by modelling it with the Weibull distribution assigning the value of 50 % to the coefficient of variation (mean equal to 1 min). This distribution is shown in Figure 65.

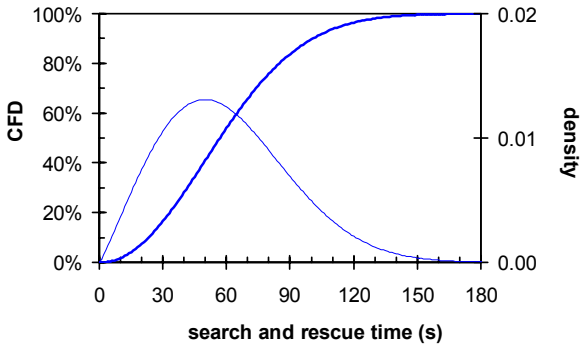

Figure 65. Distribution of the search and rescue time.

7.5.2.5 Time from fire detection to the fire brigade intervention

The time from fire detection to fire brigade intervention may be obtained by summing up the turnout time (Figure 62), the travel time (Figure 63b), the water set-up time (Figure 64b) and the search and rescue time (Figure 65). The resulting distribution is shown in Figure 66.

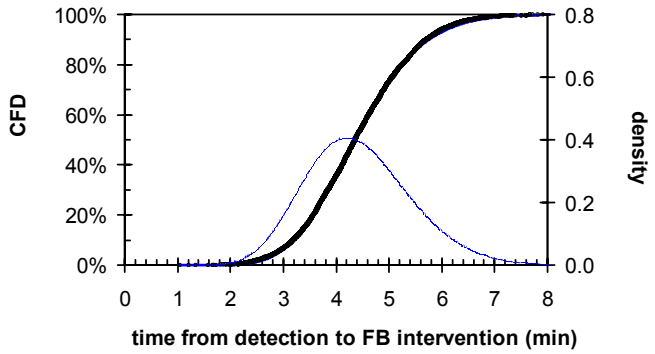

Figure 66. Distribution of the time from fire detection to fire brigade intervention.

7.5.2.6 Time from fire initiation the to fire brigade intervention

When add to the result shown in Figure 66 the time taken by the fire detection either by senses or a fire detector we obtain an estimate for the time lapsed from the beginning of the fire to the tie when the fire brigade starts its extinguishing trial. The results for the shopping hours when both sensory perception and detection by detectors are possible are shown in Figure 67 and the results for the unoccupied hours when only detection by detectors is possible are shown in Figure 68. The Monte Carlo results are modelled using 3-parameter gamma distributions with the following parameters:

- shopping hours:
  - heat detectors activating at 100 ˚C: $\alpha = 9{,}36$, $\beta = 0{,}46$ min, $x_{\min} = 1{,}56$ min (mean = 5,9 min, coefficient of variation = 24 %);
  - heat detectors activating at 58 ˚C: $\alpha = 19{,}0$, $\beta = 0{,}31$ min, $x_{\min} = 0{,}0$ min (mean = 5,8 min, coefficient of variation = 23 %);
  - smoke detectors activating at temperature rise 10–15 ˚C: $\alpha = 24{,}2$, $\beta = 0{,}24$ min, $x_{\min} = 0{,}0$ min (mean = 5,7 min, coefficient of variation = 20 %);
- unoccupied hours:
  - heat detectors activating at 100 ˚C: $\alpha = 32{,}7$, $\beta = 0{,}18$ min, $x_{\min} = 2{,}76$ min (mean = 8,7 min, coefficient of variation = 12 %);
  - heat detectors activating at 58 ˚C: $\alpha = 31{,}0$, $\beta = 0{,}19$ min, $x_{\min} = 1{,}58$ min (mean = 7,4 min, coefficient of variation = 14 %);
  - smoke detectors activating at temperature rise 10–15 ˚C: $\alpha = 31{,}0$, $\beta = 0{,}18$ min, $x_{\min} = 0{,}70$ min (mean = 6,4 min, coefficient of variation = 16 %).

Figure 69 compares the fire brigade intervention times to the fire size expressed as the heat release rate. Figure 70 shows the probability that an average fire brigade [Hietaniemi *et al*. 2004, Barry 2002] is able to extinguish the fire as a function of the fire size or as a function of time. When we compare Figure 69 and Figure 70 we can see that longer ends of the fire brigade intervention times extend to times when the fire is so big that the success in its extinguishing is uncertain (larger that 10 MW); for the unoccupied hours the fire brigade intervention times extend well into the region where the probability of extinguishing is zero.

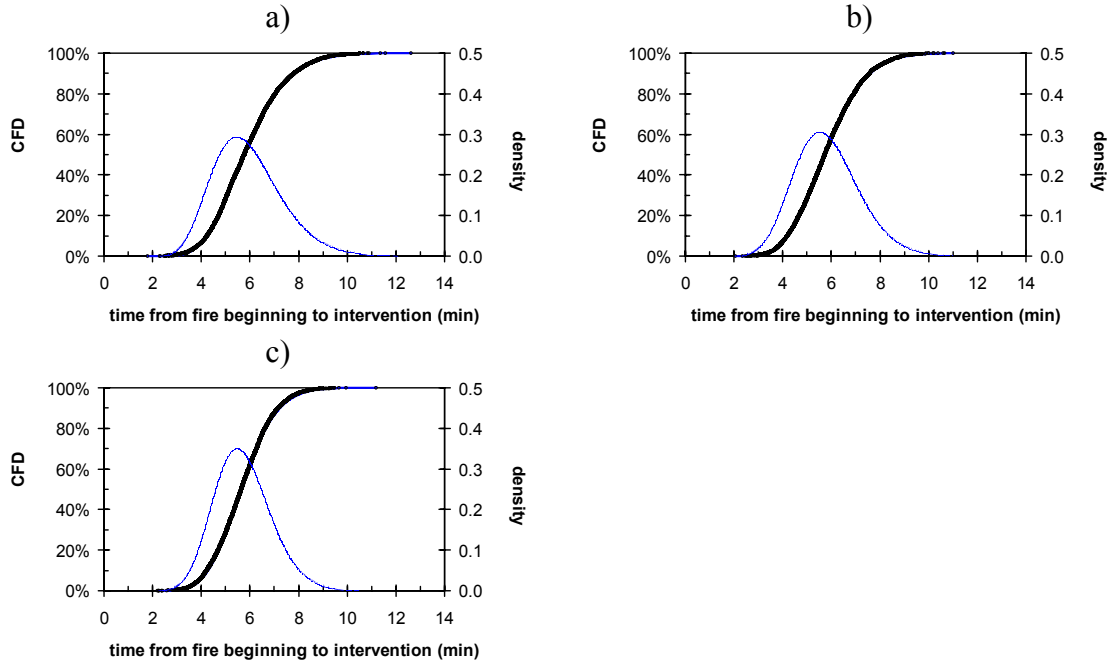

Figure 67. Time from fire initiation the to fire brigade intervention during shopping hours: a) heat detectors activating at 100 ˚C, b) heat detectors activating at 58 ˚C and c) smoke detectors activating at temperature rise 10–15 ˚C.

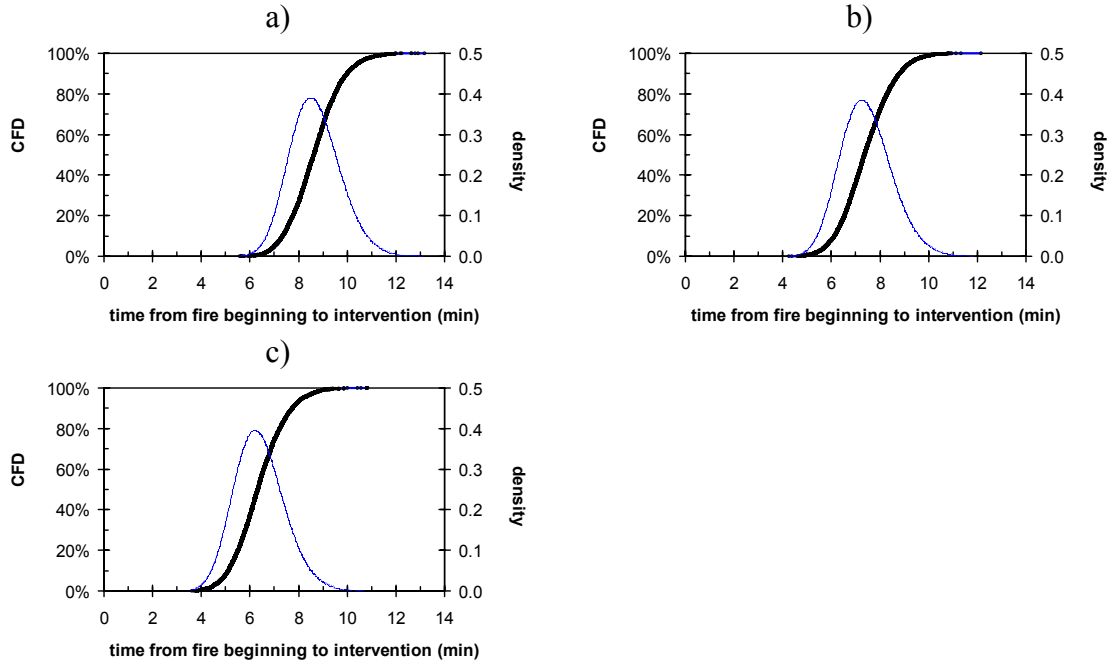

Figure 68. Time from fire initiation the to fire brigade intervention during unoccupied hours: a) heat detectors activating at 100 ˚C, b) heat detectors activating at 58 ˚C and c) smoke detectors activating at temperature rise 10–15 ˚C.

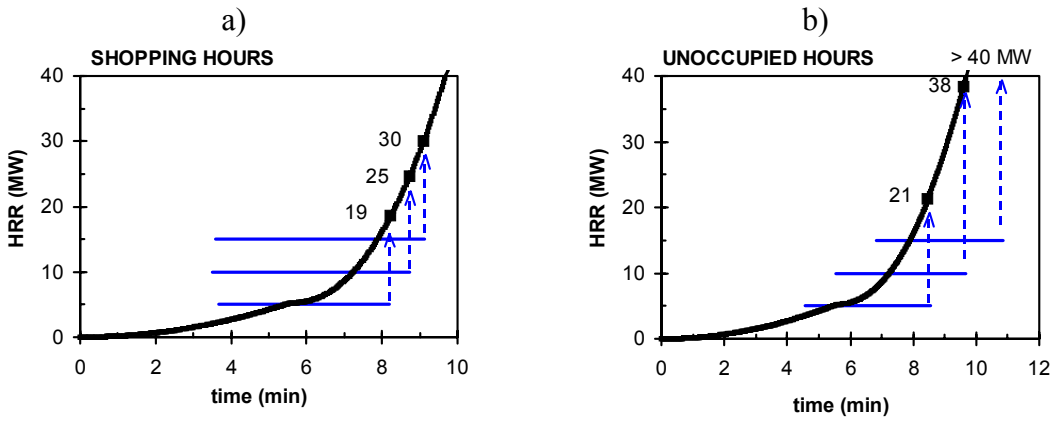

Figure 69. The fire brigade intervention times compared to the fire growth: a) shopping hours and b) unoccupied hours. The lines depict the 95 % confidence interval of the fire brigade intervention times.

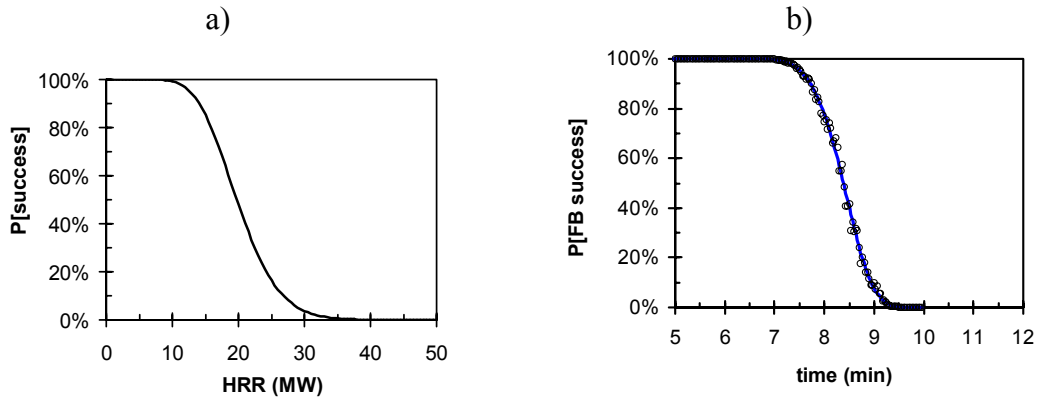

Figure 70. Probability that the fire brigade extinguishing intervention is successful: a) vs. the fire size expressed as the heat release rate (HRR) and b) vs. time.

7.5.3 Analysis of the structural failure probabilities using the Time-Dependent Event Tree Method

In the previous sections we have developed models for the fire detection (sensory perception or via detectors) and the fire brigade intervention as well as to the performance of the structures under the simulated fire exposure. Integrating all these description to a whole picture of the structural fire safety forms a non-trivial problem of probability calculus: one must track the temporal evolution of the interdependent events taking into account the conditioning of latter events by the former event, which builds

up a very complex problem of proper handling of the condition probabilities. VTT [Hietaniemi *et al*. 2002, Korhonen *et al.* 2003, Hietaniemi *et al*. 2005] has developed a Time Dependent Event Tree (TDET) Method which used the technique of Markovian Chains to handle the problem. This method is described in some details in Appendix D.

The primary event that TDET Method keeps track of is whether there still is a fire in the building or has it been extinguished or terminated because the fire load has burned out. It can be seen that during the shopping hours, the fire is likely to be detected so early that the fire brigade intervention can take place before the fire has grown too big to extinguish and thus the probability that there is a fire in the building drops to some percents during the early phases of its development (Figure 71). During the unoccupied hours, the early fire detection relies on the detectors. It can be seen that the heat detectors that trigger as smoke vents activate at 100 ˚C are too slow to guarantee efficient fire fighting leading to only about 30 % success probability of the fire brigade (Figure 72a). The detectors operating at 58 ˚C enhance the fire brigade success probability to about 70 % (Figure 72b) and for the smoke detectors the fire brigade success probability is about 90 % (Figure 72c), which may be considered sufficient as there are no associated risks to life.

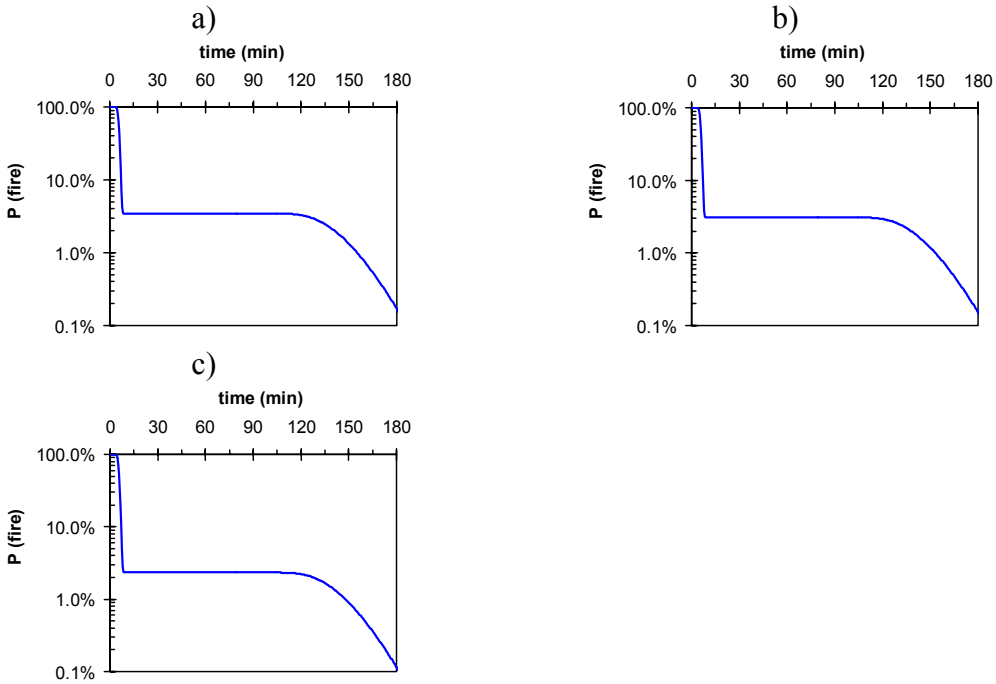

Figure 71. TDET results concerning the continuation of the fire during shopping hours: a) heat detectors activating at 100 ˚C, b) heat detectors activating at 58 ˚C and c) smoke detectors.

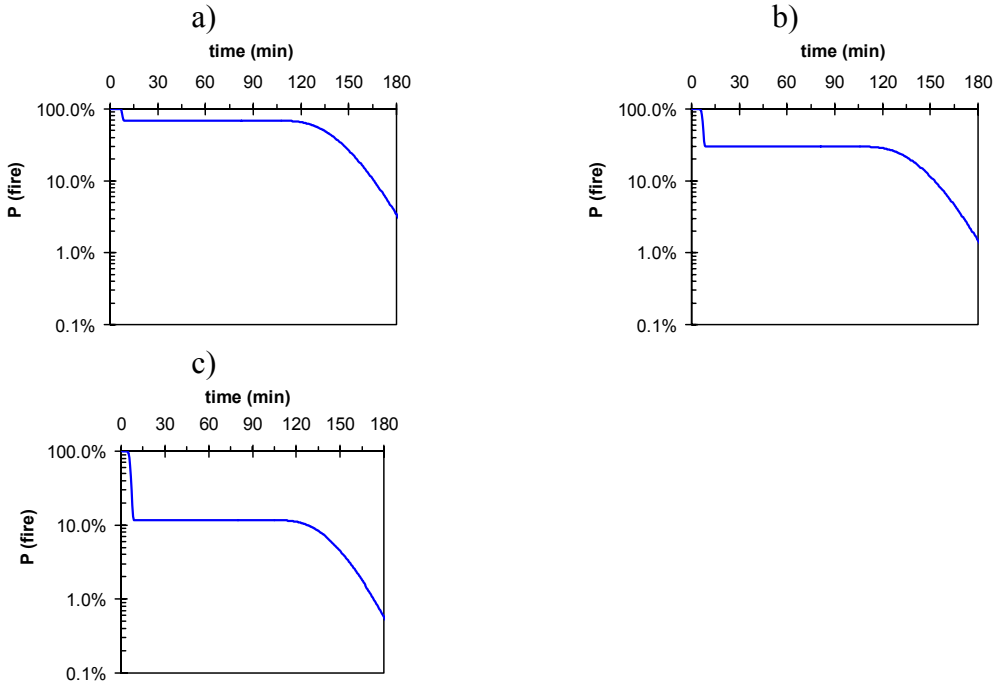

Figure 72. TDET results concerning the continuation of the fire during unoccupied hours: a) heat detectors activating at 100 ˚C, b) heat detectors activating at 58 ˚C and c) smoke detectors activating at temperature rise 10–15 ˚C.

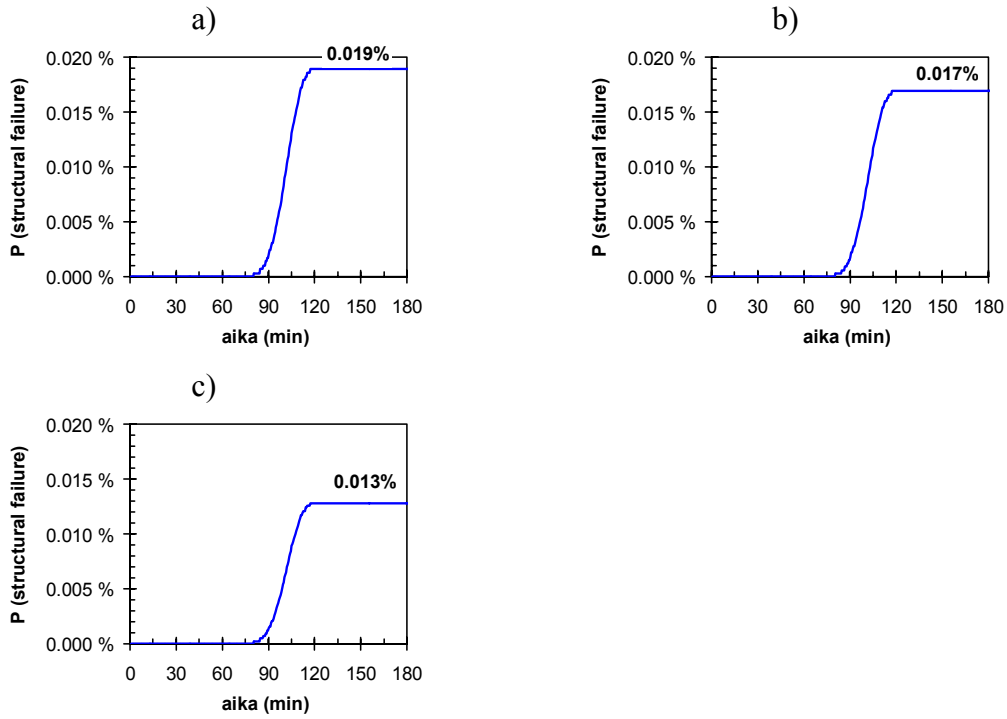

Figure 73. TDET results on the structural failure probability during shopping hours: a) heat detectors activating at 100 ˚C, b) heat detectors activating at 58 ˚C and c) smoke detectors.

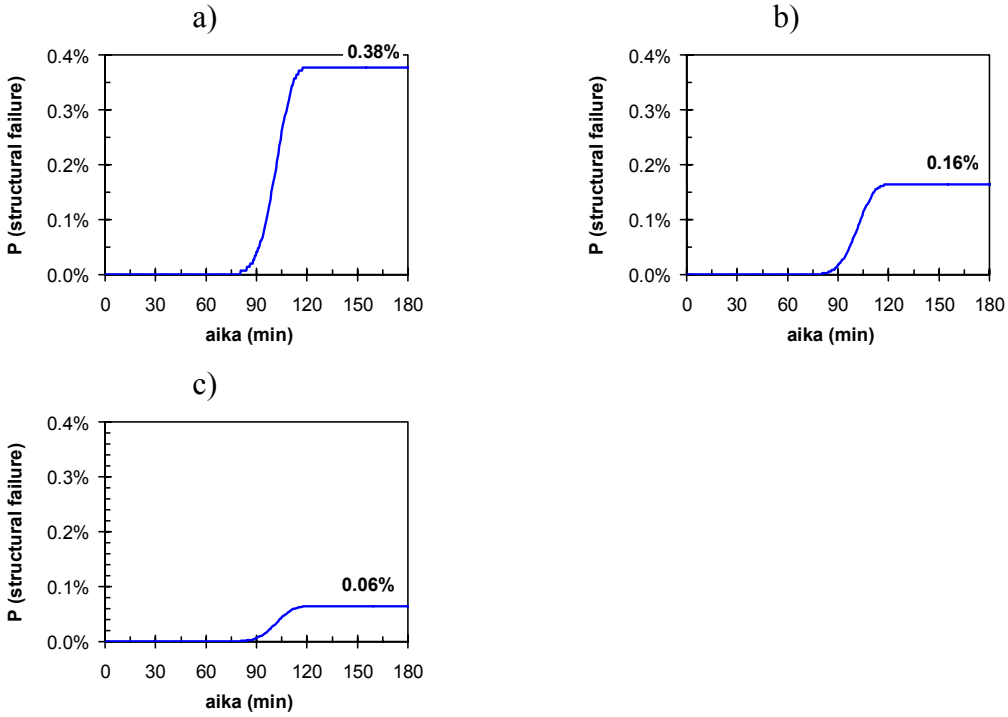

Figure 74. TDET results on the structural failure probability during unoccupied hours: a) heat detectors activating at 100 ˚C, b) heat detectors activating at 58 ˚C and c) smoke detectors.

TDET results on the structural failure probability are shown in Figure 73, Figure 74 and Table 8. It can be seen that during the shopping hours the failure probabilities per one fire are *ca*. 0,01–0,02 % or $1 \cdot 10^{-4} - 2 \cdot 10^{-4}$ per fire which with annual fire frequency of $4 \cdot 10^{-3}$ fires/year corresponds to annual failure probability of ca. $0{,}4 \cdot 10^{-6} - 0{,}8 \cdot 10^{-6}$. During the unoccupied hours the failure probabilities are higher ranging between *ca*. 0,06–0,4 % or $0{,}6 \cdot 10^{-3} - 4 \cdot 10^{-3}$ per fire. The corresponding annual failure probabilities are ca. $3 \cdot 10^{-6} - 15 \cdot 10^{-6}$. As the portions of the shopping hours and unoccupied hours are 48 % and 52 %, the resulting annual failure probabilities are as given in Table 8.

Table 8. Annual probability of failure due to fire calculated on the basis of the fire simulation.

$P_{f,fire,year}$	**Shopping hours**	**Unoccupied hours**	**Combination**
Heat detectors activating at 100 °C	$0{,}76 \cdot 10^{-6}$ 1/a	$15 \cdot 10^{-6}$ 1/a	$8{,}2 \cdot 10^{-6}$ 1/a
Heat detectors activating at 58 °C	$0{,}68 \cdot 10^{-6}$ 1/a	$6{,}6 \cdot 10^{-6}$ 1/a	$3{,}7 \cdot 10^{-6}$ 1/a
Smoke detectors	$0{,}51 \cdot 10^{-6}$ 1/a	$2{,}6 \cdot 10^{-6}$ 1/a	$1{,}6 \cdot 10^{-6}$ 1/a

The tolerability of these fire-related failure probabilities can be assessed, e.g., in the following ways:

- a comparison to the failure probabilities obtained for the normal-temperature design in Chapter 5 (see Figure 75) reveals that
  - if one considers the normal-temperature results obtained by using the Finnish norm B10, the fire-related failure probability obtained for the heat detectors activating at 100 °C exceed that of the normal-temperature design while the failure probabilities obtained for the heat detectors activating at 58 °C and the smoke detectors lie well below the normal-temperature design value;
  - for the normal-temperature results obtained by using the Eurocode 5, the fire-related failure probability obtained for the both heat detectors exceed that of the normal-temperature design while the failure probabilities obtained for the smoke detectors coincide with the normal-temperature design value.

- a comparison to the recommended target probability values in the ultimate limit state for a one year period (see Figure 76) reveals that
  - failure probabilities obtained for all detector options are well below the limit given by the probabilistic model code [JCCS 2001];
  - failure probabilities obtained for the heat detectors options exceed the limit value given in the Eurocode 0, while the failure probability obtained smoke detector is approximately equal to the limit value.

- in the building stock in Finland with about 500 such buildings as that consider in this study, the failure probabilities mean that the failure return periods[7] are
  - *ca*. 240 years for the heat detectors activating at 100 °C;
  - *ca*. 540 years for the heat detectors activating at 58 °C;
  - *ca*. 1300 years for the smoke detectors.

[7] Probability per year of having no failures is $P = (1\text{-}p_{f,fire,annual})^{500}$ and the return period equals $1/(1\text{-}P)$.

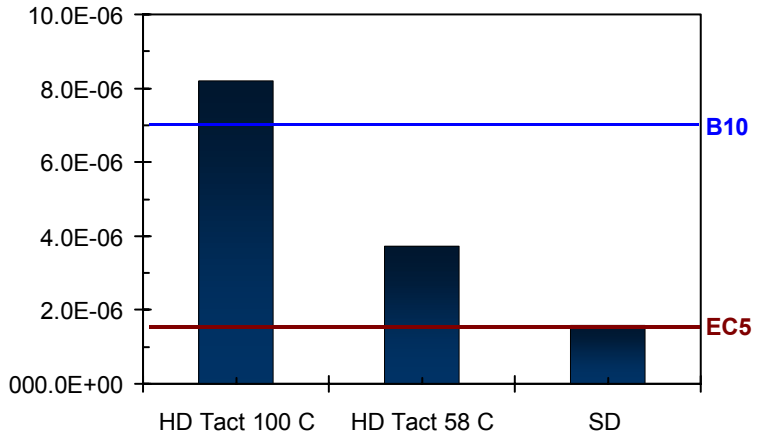

Figure 75. Comparison of the annual failure probabilities obtained on the basis of fire simulation to the normal-temperature failure probabilities.

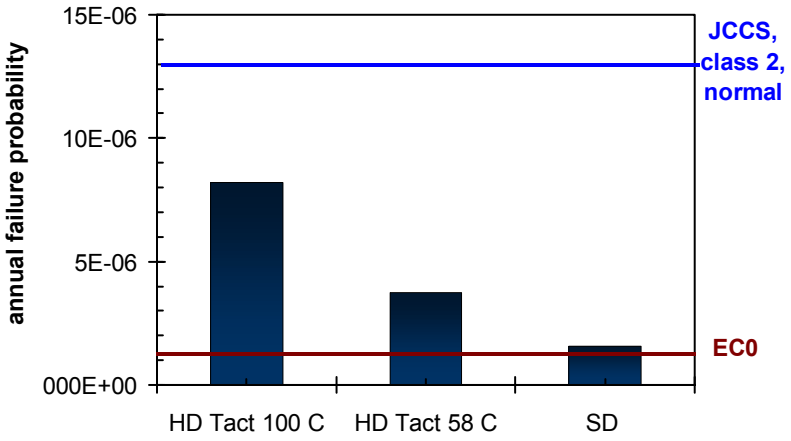

Figure 76. Comparison of the annual failure probabilities obtained on the basis of fire simulation to the recommended target probability values in the ultimate limit state for a one year period according to the probabilistic model code [JCCS 2001] and prEN 1990 [CEN 2001].

8. Summary

This report presents use of advanced, probabilistic calculation methods to assess of the fire endurance of structures applied to glulam wooden structures.

The first part of the report presents a reliability analysis based on the approximation of the fire exposure by the standard time-temperature curve with the results of Eurocode 5 and the Finnish norm B10 used as comparison benchmark to which the probabilistic method is compared to. The calculations address the effect of the strength variation of the glulam material as well as the treatment of the variability of the snow load. It is shown that the probability of failure resulting from a deterministic design based on Eurocode 5 is low compared to the target values and lower sections are possible if applying a probabilistic design method. In fire design, if a 60 minute resistance is required, this is not the case. Stochastic charring rates have a significant influence on the results as well.

The second part of this report deals with an approach based on fire simulation , which features several novel methods: 1) use of the state-of-art fire simulation program FDS4 to assess the course and influence of a natural fire, 2) analysis of the deterministic results obtained from the FDS4 simulations to a stochastic description of the natural fire and subsequent probabilistic calculations using the Probabilistic Fire Simulator developed at VTT and 3) the use of the Time-Dependent Event Tree (TDET) method developed at VTT to integrate the influence of fire-safety measures to the fire safety analysis. The simulation-based probabilistic fire endurance assessment presented in this report gives the reader a comprehensive and concrete exposition of the use of the methodology which represents the leading edge of modern fire technology. The results of the simulation-based probabilistic fire endurance assessment show that the glulam structures are actually able to withstand the fire exposure throughout the whole fire up to the burn-out of the fire load.

Acknowledgements

The authors gratefully acknowledge the financing to the work by the National Technology Agency of Finland (Tekes) and VTT Building and Transport. we are grateful to the persons who have been involved in the various phases of the fire safety analysis of the particular building: Drs. Timo Korhonen and Tuomas Paloposki and Mr. Henry Weckman from VTT Fire Research and Tapani Tuominen from SPU Systems Oy.

References

ABCB. 2005. International Fire Engineering Guidelines. National Research Council of Canada (NRC), International Code Council (ICC), United States of America, Department of Building and Housing, New Zealand and Australian Building Codes Board (ABCB). Australia: ABCB. 425 p.

Atreya, A. 2002. Convection heat transfer. In: DiNenno, P. J., Drysdale, D., Beyler, C. L. & Walton, W. D. (ed.). Quincy: SFPE Handbook for Fire Protection Engineering, 3. Edition, Pp. 1/39–1/64.

Barry, T. F. 2002. Risk – Informed, Performance -Based Industrial Fire Protection. Tennessee: Tennessee Valley Publishing. ISBN 1-882194-09-8.

Baum, H. 2005. Simulating Fire Effects on Complex Building Structures. Fire Safety Science. Proceedings of the Eighth International Symposium, 18–23 September 2005, Beijing, China. International Association for Fire Safety Science. (In print).

Benjamin, I., Heskestad, G., Bright, R. & Hayes, T. 1979. An analysis of environments of fire detectors. USA: Fire Detection Institute. 37 p.

Boverket. 2002. Boverkets byggregler, BFS 1993:57 med ändringar till och med 2002:19.

CEN. 2001. PrEN 1990 Eurocode – Basis of structural design – Final draft July 2001. Document CEN/TC 250/SC 5 : N 159.

CEN. 2002. prEN 1995-1-1, Eurocode 5, Design of timber structures, Part 1-1: General Rules, General rules and rules for buildings, Final Draft, 2002-10-09.

CEN. 2002b. Eurocode 1: Actions on Structures – Part 1–2: General Actions – Actions on structures exposed to fire. Brussels: CEN. 59 p. (EN 1991-1-2: 2002 E).

Drysdale, D. 1998. Introduction to Fire Dynamics. 2nd Ed. New York: John Wiley & Sons. 466 p.

Frantzich, H. 2001. Tid för utrymning vid brand. Karlstad, Sweden: Räddningsverket. 122 p. (P21-365/01) ISBN 91-7253-092-8.

Hietaniemi, J., Baroudi, D., Korhonen, T., Björkman, J., Kokkala, M. & Lappi. E. 2002. Yksikerroksisen teollisuushallin rakenteiden palonkestävyyden vaikutus paloturvallisuuteen. Riskianalyysi ajasta riippuvaa tapahtumapuumallia käyttäen (Fire safety impact of the fire resistance of the structures of a single-storey industrial building: risk analyisi using a time-dependent event tree method). Espoo: Technical Research Centre of Finland. 95 p. + app. 51 p. (VTT Tiedotteita – Meddelanden – Research Notes 2123.) ISBN 951-38-5935-5. (In Finnish). http://virtual.vtt.fi/inf/pdf/tiedotteet/2002/T2123.pdf.

Hietaniemi, J., Korhonen, T., Joyeux, D. & Ayme, N. 2004. Risk-based Fire Safety Engineering Approach to Obtain Balanced Structural Fire Resistance Requirements. In: Bradley, D., Drysdale, D. & Molkov, V. Fire and Explosion Hazards, Proceedings of the Fourth International Seminar. Londonderry, Northern Ireland, UK, September 8–12, 2003. Belfast, Northern Ireland, UK: University of Ulster. Pp. 505–514. ISBN 85923 186 1.

Hietaniemi, J. & Korhonen, T. 2004a. A case study of performance of load-bearing wooden structures in natural fire. Proceedings of the 8th World Conference on Timber Engineering, WCTE 2004, Volume II, Lahti, June 14–17, 2004. Helsinki: RIL, VTT, Wood Focus. Pp. 329–334.

Hietaniemi, J. & Korhonen, T. 2004b. Study of performance of load-bearing wooden structures in natural fire. Wood and Fire Safety, 5th International Scientific Conference, 18–22 April 2004, Strbské Pleso. Technical University in Zvolen, Department of Fire Protection, Faculty of Wood Sciences and Technology. 2004. 9 p.

Hietaniemi, J., Hostikka, S., & Korhonen, T. 2004c. Probabilistic Fire Simulation. In: Almand, K. H. (Ed.). Proceedings of the 5th International Conference on Performance-Based Codes and Fire Safety Design Methods. October 6–8, 2004. Luxembourg. Bethesda, MD. USA. Society of Fire Protection Engineers. Pp. 280–291.

Hietaniemi, J. 2005. A Probabilistic Approach to Wood Charring Rate. Espoo: VTT. 53 p. (VTT Working Papers 31) ISBN 951-38-6583-5.
http://virtual.vtt.fi/inf/pdf/workingpapers/2005/W31.pdf.

Hietaniemi, J., Cajot, L.-G., Pierre, M., Fraser-Mitchell, J. Joyeux, D. & Papaioannou, K. 2005. Risk-Based Fire Resistance Requirements. Final Report. Luxembourg: Office for Official Publications of the European Communities. 528 p. ISBN 92-894-9871-4. (EUR 21443 EN).

Hostikka, S. & Keski-Rahkonen, O. 2003. Probabilistic simulation of fire scenarios. Nuclear Engineering and Design. Vol. 224. Pp. 301–311.

Hostikka, S., Keski-Rahkonen, O. & Korhonen, T. 2003. Probabilistic Fire Simulator. Theory and User's Manual for Version 1.2. Espoo, VTT Building and Transport. VTT Publications 503. 72 p. + app. 1 p. ISBN 951-38-6235-6; 951-38-6236-4. http://virtual.vtt.fi/inf/pdf/publications/2003/P503.pdf.

JCSS. 2001. Probabilistic Model Code. Joint Committee of Structural Safety, JCSS. 2001. http://www.jcss.ethz.ch.

Korhonen, T., Hietaniemi, J., Baroudi, D. & Kokkala, M. 2002. Time-Dependent Event-Tree Method for Fire Risk Analysis: Tentative Results. 7th International Symposium of Fire Safety Science. Boston: 16–21 June 2002. Pp. 321–332.

Korhonen, T., Hietaniemi, J., Baroudi, D. & Kokkala, M. 2003. Time-dependent event-tree method for fire risk analysis: tentative results. Fire safety science : proceedings of the seventh international symposium. Worcester, Massachusetts, USA, 16–21 June 2002. Boston, MA, USA: International Association for Fire Safety Science. Pp. 321-332. ISBN 0-9545348-0-8.

Korhonen, T., Hostikka, S. & Keski-Rahkonen, O. 2005. A proposal for the goals and new techniques of modelling pedestrian evacuation in fires. Proceedings of the 8th International Symposium on Fire Safety Science. Beijing, China: September 18–23, 2005. International Association of Fire Safety Science. (In press).

Marchant, R., Kurban, N & Wise, S. 2001. Development and Application of the Fire Brigade Intervention Model. Fire Technology, Vol. 37, pp. 263–278.

McGrattan, K. B., Floyd, J. E., Forney, G. P., Baum, H. R. & Hostikka, S. 2001. Development of Combustion and Radiation Models for Large Scale Fire Simulation. Proceedings of Computer Applications in Fire Protection Engineering, 3rd Technical Symposium. Baltimore, USA, September 12–13, 2001. Bethesda, USA: Society of Fire Protection Engieners. Pp. 14–22.

McGrattan, K. B. (Ed.) 2004a. Fire Dynamics Simulator (Version 4): User's Guide. 104 p. (NIST Special Publication 1019).

McGrattan, K. B. (Ed.). 2004b. Fire Dynamics Simulator (Version 4): Technical Reference Guide. 101 p. (NIST Special Publication 1018).

McGrattan, K. B., Baum, H. R., Rehm, R. G., Hamins, A., Forney, G. P., Floyd, J. E., Hostikka, S. & Prasad, K. 2002a. Fire Dynamics Simulator (Version 3) – Technical

Reference Guide. Gaithersburg, MD. USA: National Institute of Standards and Technology. 51 p. (NISTIR 6783, 2002 Ed.).

McGrattan, K. B., Forney, G. P., Floyd, J. E., Hostikka, S. & Prasad, K. 2002b. Fire Dynamics Simulator (Version 3) – User's Guide. Gaithersburg, MD. USA: National Institute of Standards and Technology. 81 p. (NISTIR 6784, 2002 Ed.).

Ministry of the Environment. 2002. E1 The National Building Code of Finland. Fire safety of buildings. Regulations and guidelines 2002. Decree of the Ministry of the Environment on fire safety of buildings. Helsinki: Ministry of the Environment. 41 p.

Perälä J. & Reuna, R. 1990. Lumen vesiarvon alueellinen ja ajallinen vaihtelu Suomessa (Regional and temporal variation of snow water value in Finland). Vesi ja ympäristöhallitus. Julkaisuja – sarja A 56. Helsinki 1990. (In Finnish).

Purser, D. A. & Bensilum, M. 2001. Quantification of Behaviour for Engineering Design Standards and Escape Time Calculations, Safety Science, Vol. 38, pp. 157–182.

Ranta-Maunus A. 2001. Summary report of NI project on reliability of timber structures. Joint Nordic wood project meeting and Cost E24 workshop, October 2001, Copenhagen.

RCP GmbH 1999. Strurel, A structural Reliability Analysis Program System, COMREL & SYSREL Users Manual, RCP GmbH, 1999.

RIL 2001. Puurakenteiden suunnitteluohjeet B10 (Finnish timber structures design codes B10) RIL 120-2001. Helsinki 2001.

RIL. 2003. Paloturvallisuussuunnittelu – Oletettuun palonkehitykseen perustuva suunnittelu ja ratkaisuesimerkit. Helsinki: Suomen Rakennusinsinöörien Liitto RIL. 138 s. (RIL 221-2003). ISBN 951-758-433-3.

SAKO 1999. Basis of design of Structures – Proposals for modification of partial safety factors in Eurocodes. Joint committee of NKB and INSTA-B. NKB Committee and work reports, 1999:01 E.

Särdqvist, S. 1998. Real Fire Data: Fires in non-residential premises in London 1994–1997. Lund: Lund University. 62 p. (Report 7003) ISRN LUTVDG/TVBB--7003—SE.

Thelandersson S., Larsen H. J., Östlund L., Isaksson T. & Svensson S. 1999. Säkerhetsnivåer för trä och träproducter i konstruktioner. Lund Universität. Rapport TVBK-3039. 37 p. + app.

Tillander, K. & Keski-Rahkonen, O. 2000. Palokunnan saatavuuden merkitys rakennuksen paloriskitarkastelussa (Significance of the fire brigade availability to building fire risk assessment). Espoo: Valtion teknillinen tutkimuskeskus. 213 p. + app. 55 p. (VTT Tiedotteita 2013). ISBN 951-38-5634-8; 951-38-5635-6. (In Finnish). http://virtual.vtt.fi/inf/pdf/tiedotteet/2000/T2013.pdf.

Tillander, K. & Keski-Rahkonen, O. 2001. Rakennusten syttymistaajuudet PRONTO-tietokannasta 1996–1999 (Building ignition frequencies frome the PRONTO database 1996–1999). Espoo: Valtion teknillinen tutkimuskeskus. 66 p. + app. 16 p. (VTT Tiedotteita 2119). ISBN 951-38-5929-0; 951-38-5930-4. (In Finnish). http://virtual.vtt.fi/inf/pdf/tiedotteet/2001/T2119.pdf.

Tillander, K. 2004. Utilisation of statistics to assess fire risks in buildings. Doctor's Thesis. Espoo: VTT. VTT Publications 537. 224 p. + app. 37 p. ISBN 951-38-6392-1; 951-38-6393-X. http://virtual.vtt.fi/inf/pdf/publications/2004/P537.pdf.

Toratti, T. & Turk, G. 2005. COST E24 Final Seminar. (To be published).

Appendix A: Further analysis of the snow-load data

Figure A1 shows a comparison of the distributions of the maximum annual snow loading expressed as water equivalents obtained in two ways, one directly from the data of Perälä & Reuna and a Weibull distribution fit to that data and the other via a Monte Carlo analysis of the monthly snow data.

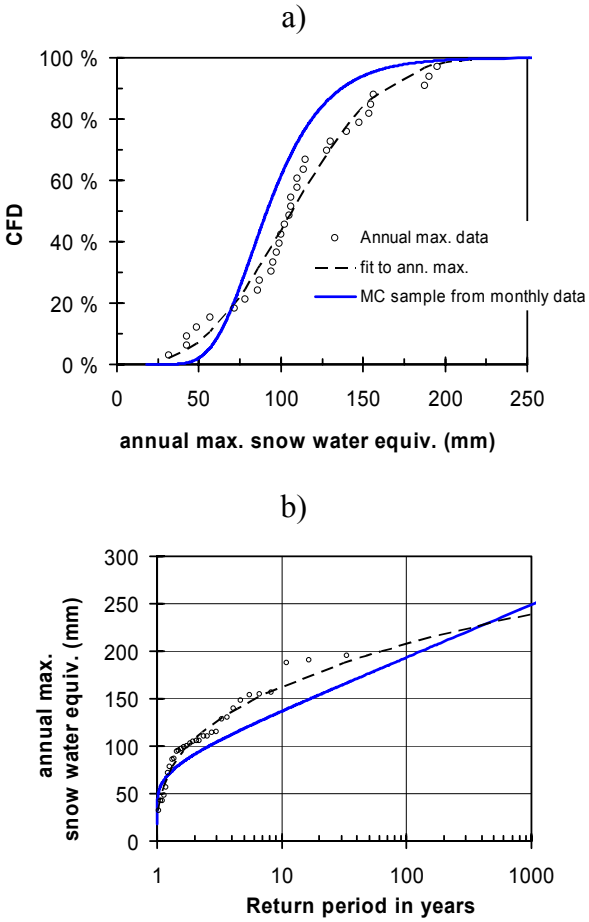

Figure A1. Comparison of the distributions of the maximum annual snow loading expressed as water equivalents obtained in two ways, one directly from the data of Perälä & Reuna and a Weibull distribution fit to that data and the other via a Monte Carlo analysis of the monthly snow data: a) a conventional form of plotting the cumulative frequency distribution vs. the variable value and b) an inverted plot using the return-period concept.

Appendix B: Detailed presentation of the FDS4 fire simulation results

This Appendix summarises the results of the FDS4 fire simulation runs in more details.

Time-temperature curves

Scenario with window breaking temperature set at 400 ˚C

a)

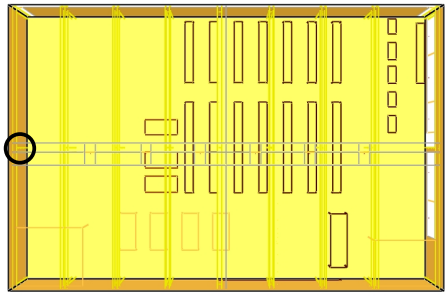

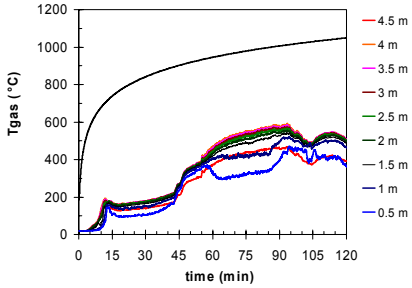

b)

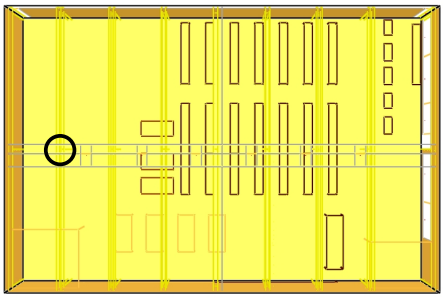

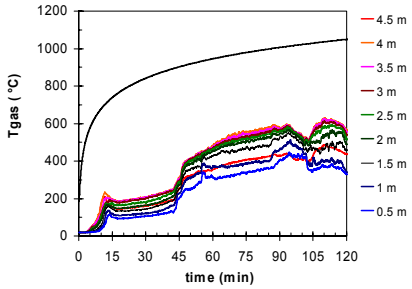

c)

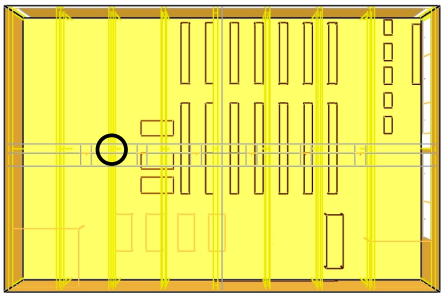

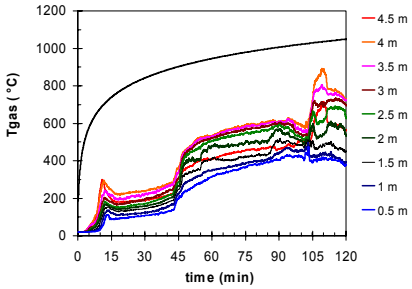

d)

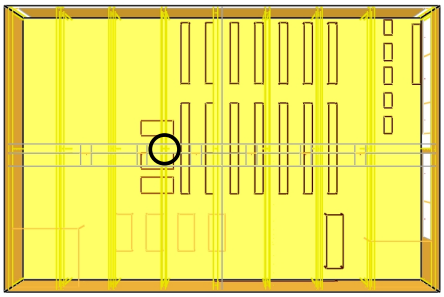

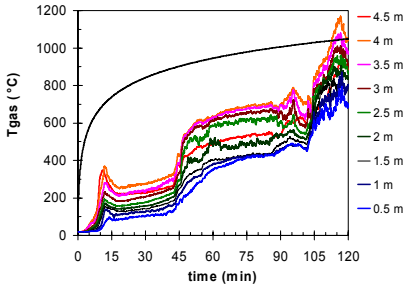

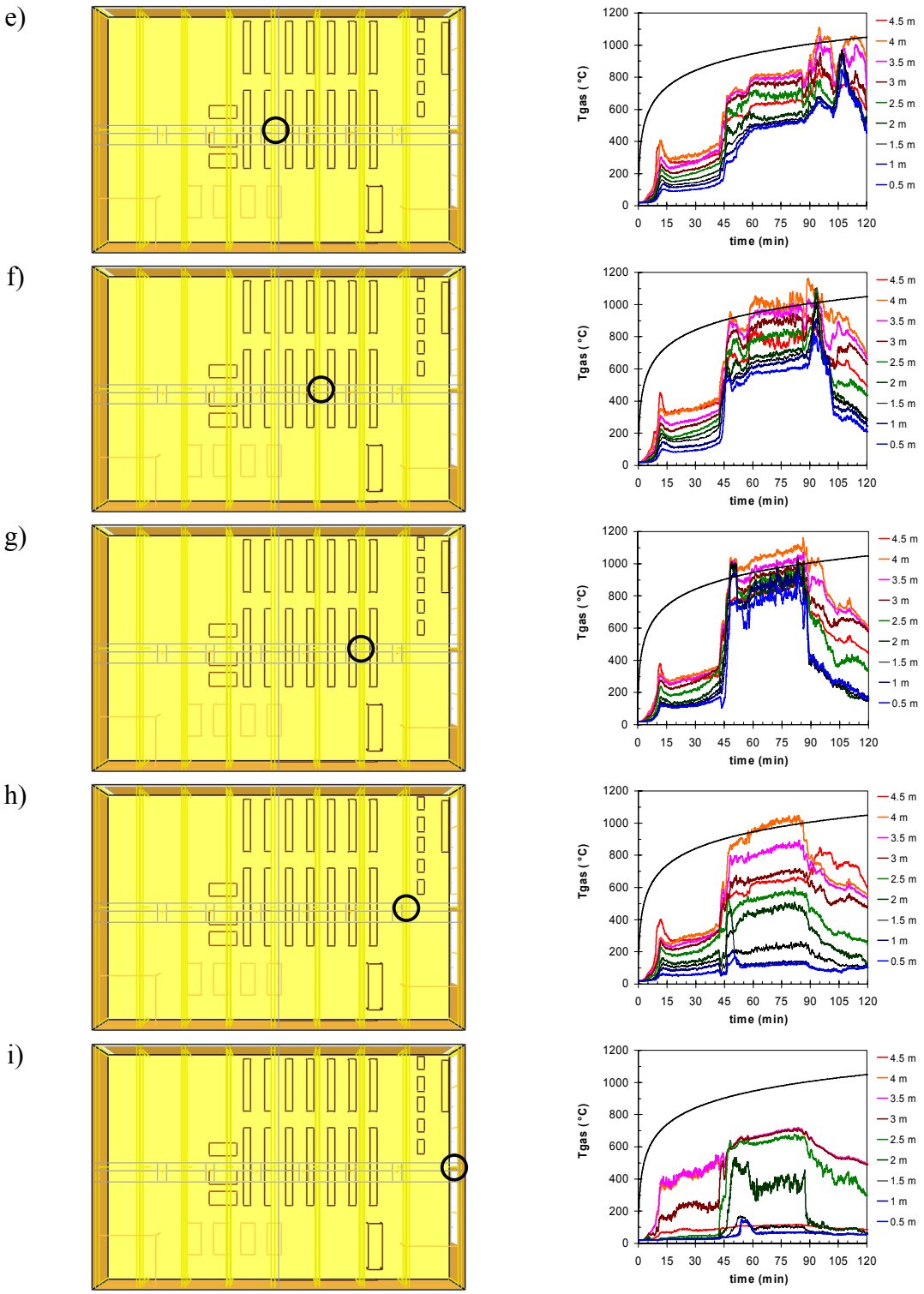

Figure B1. Time-temperature curves for the fire scenario with glass fallout temperature set at 300 °C: a) x = 0 m, b) x = 6 m, c) x = 12 m, d) x = 18 m, e) x = 24 m, f) x = 30 m, g) x = 36 m, h) x = 42 m and i) x = 48 m. To clarify the curves, the simulation results have been smoothed by using a 30-s sliding averaging procedure.

Scenario with window breaking temperature set at 500 ˚C

a)

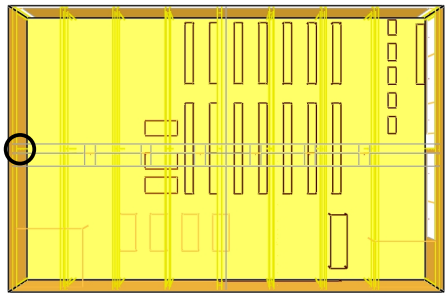

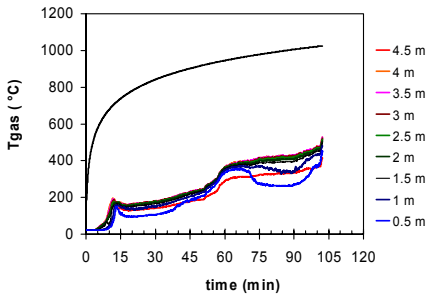

b)

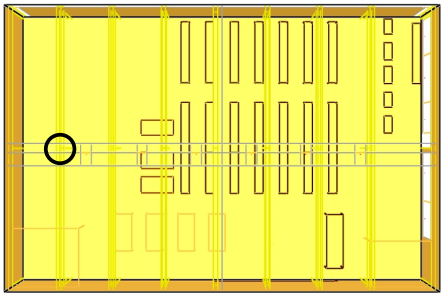

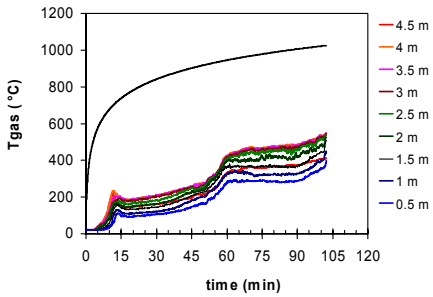

c)

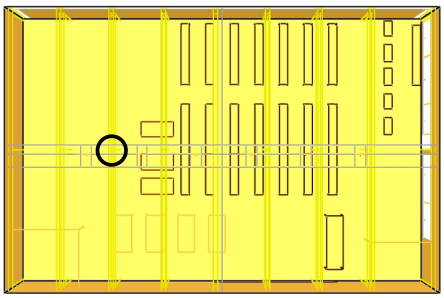

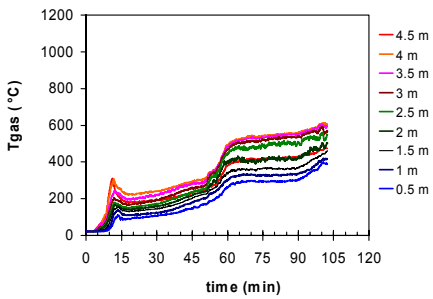

d)

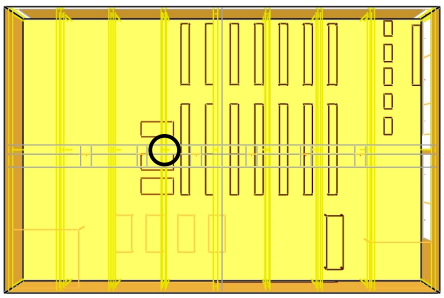

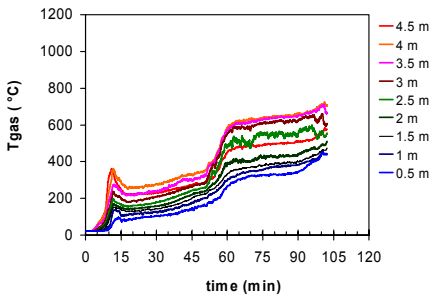

e)

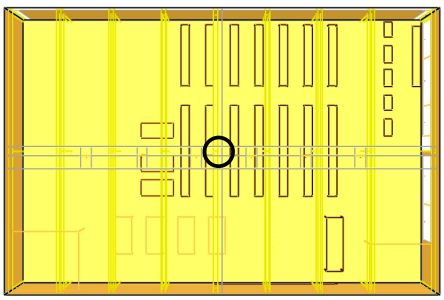

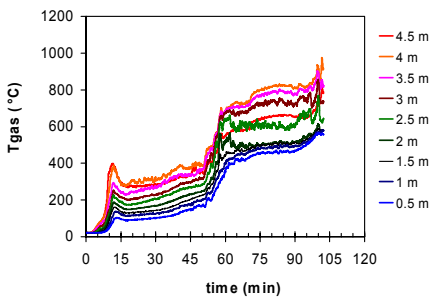

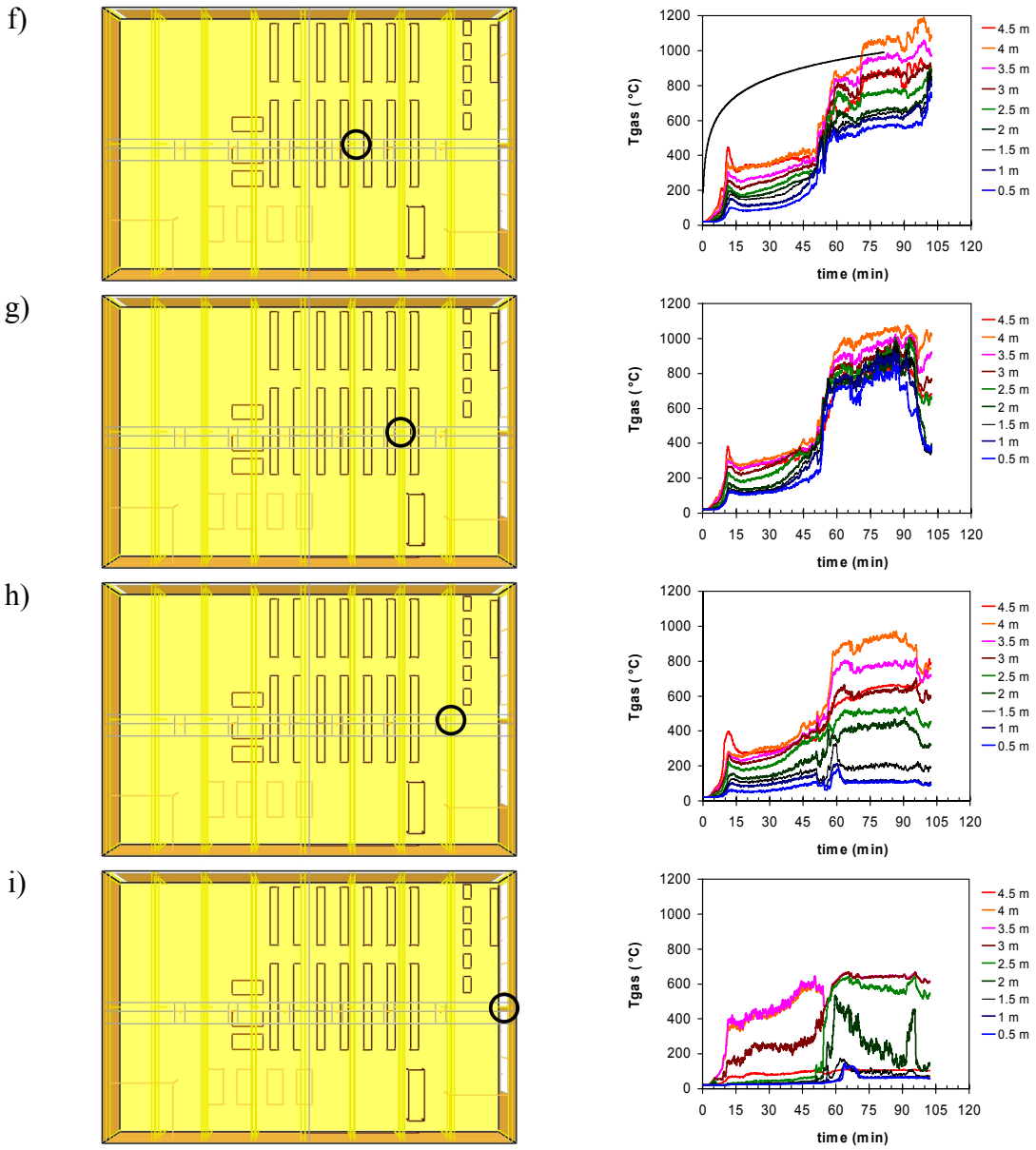

Figure B2. Time-temperature curves for the fire scenario with glass fallout temperature set at 400 °C: a) x = 0 m, b) x = 6 m, c) x = 12 m, d) x = 18 m, e) x = 24 m, f) x = 30 m, g) x = 36 m, h) x = 42 m and i) x = 48 m. To clarify the curves, the simulation results have been smoothed by using a 30-s sliding averaging procedure.

Smoke density

The smoke density is quantified by the extinction coefficient k_g defined as the product of a constant $K_m \approx 7600$ m^2/kg and the density of smoke particulates (kg/m^3) (McGrattan 2004a). It characterises the ability of the smoke to attenuate light: a beam of

monochromatic light with initial intensity I_0 traverses a smoke layer of thickness $\Delta\ell$, its intensity drops to a value $I_0 \cdot \exp(-k_g \cdot \Delta\ell)$.

Scenario with window breaking temperature set at 400 ˚C

a)

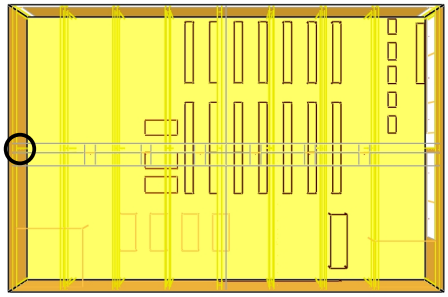

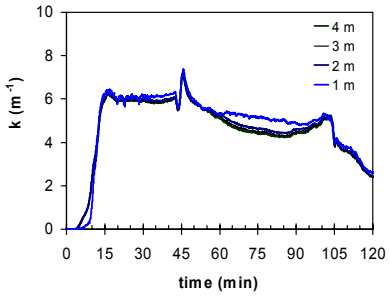

b)

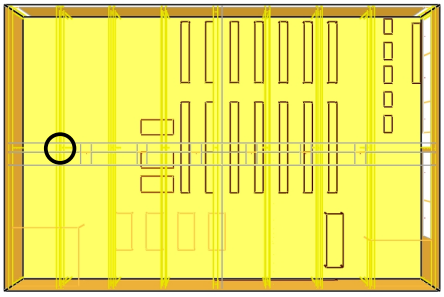

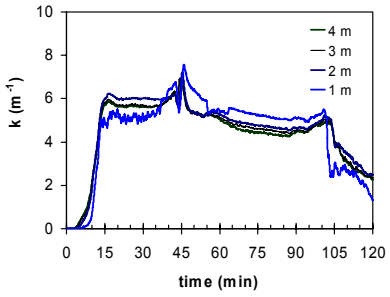

c)

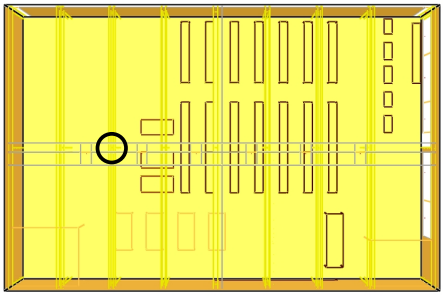

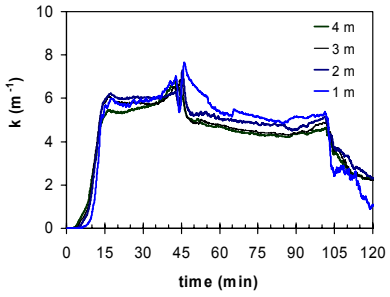

d)

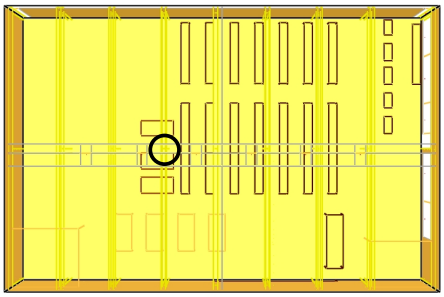

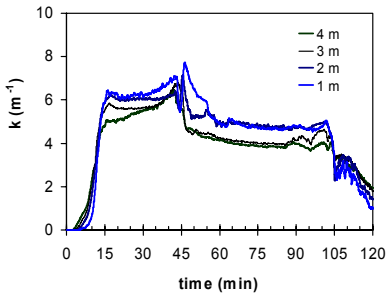

e)

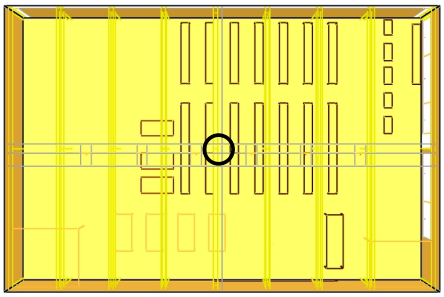

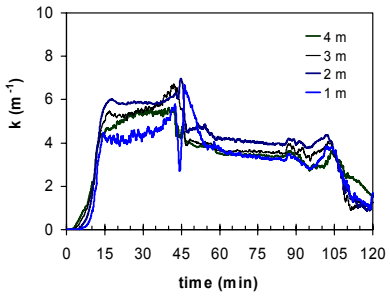

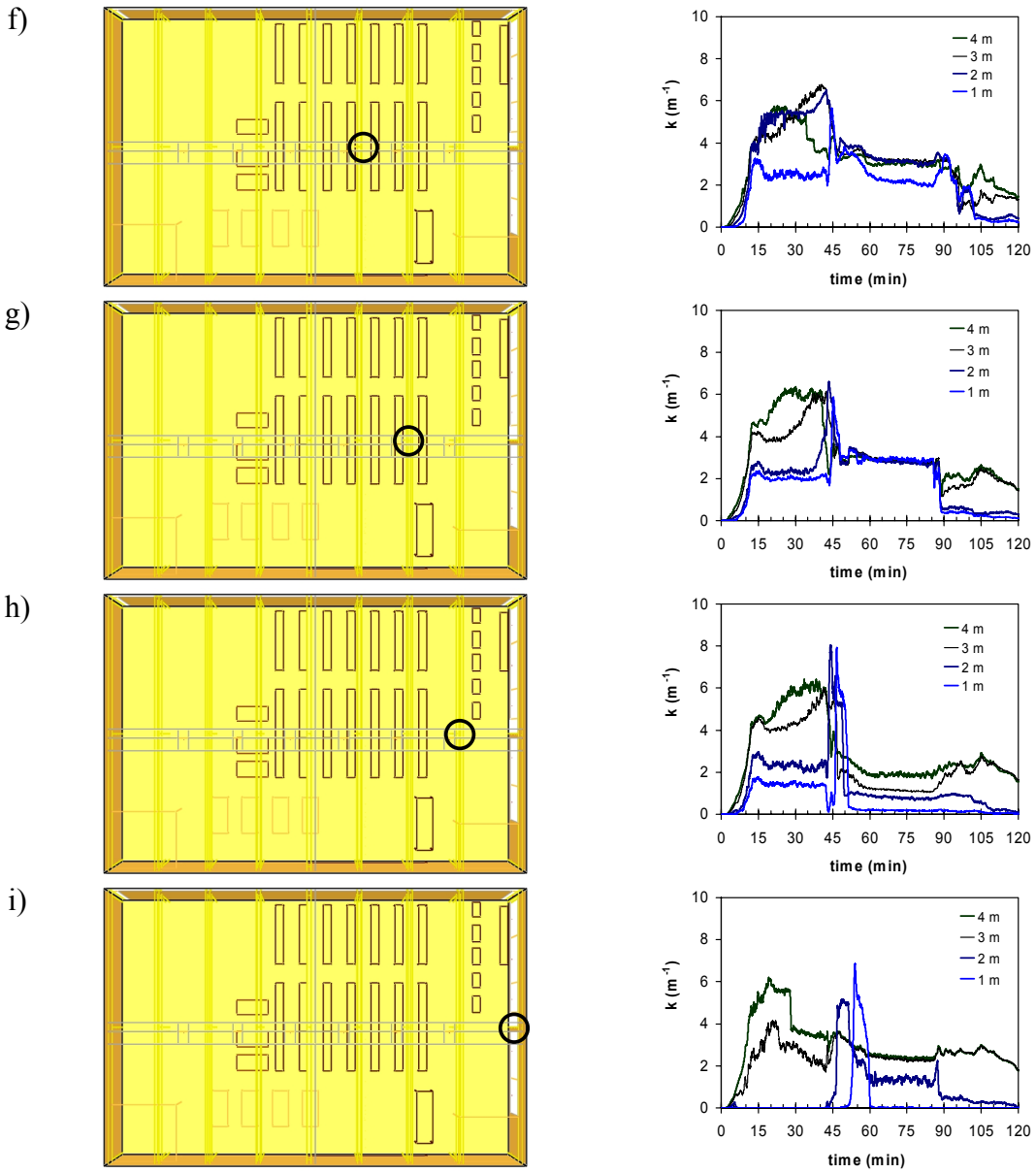

Figure B3. Time dependence of the extinction coefficient at different heights for the fire scenario with glass fallout temperature set at 400 °C: a) x = 0 m, b) x = 6 m, c) x = !2 m, d) x = 18 m, e) x = 24 m, f) x = 30 m, g) x = 36 m, h) x = 42 m and i) x = 48 m. To clarify the curves, the simulation results have been smoothed by using a 30-s sliding averaging procedure.

Scenario with window breaking temperature set at 500 ˚C

a)

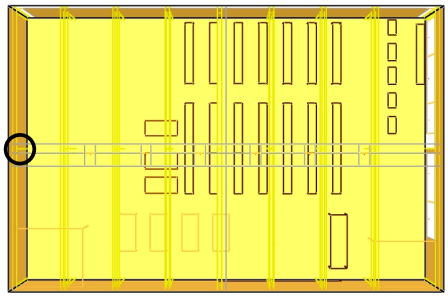

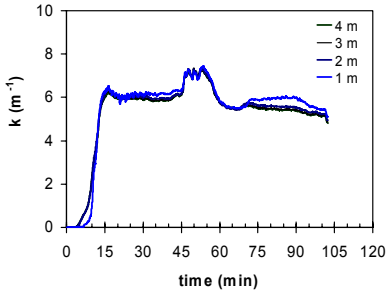

b)

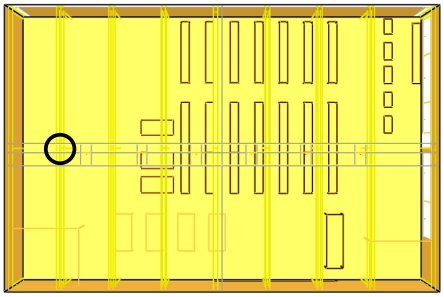

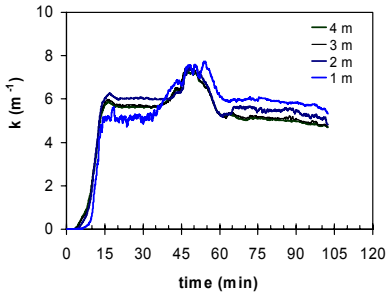

c)

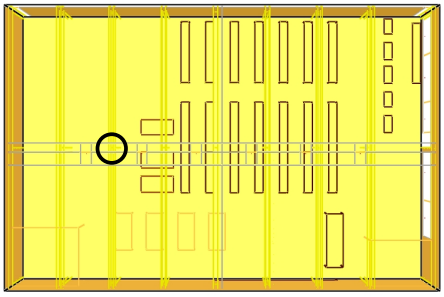

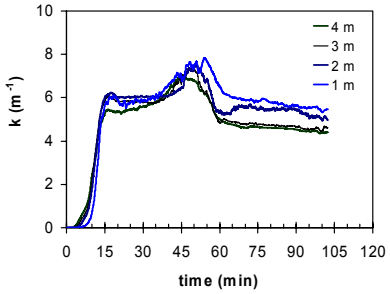

d)

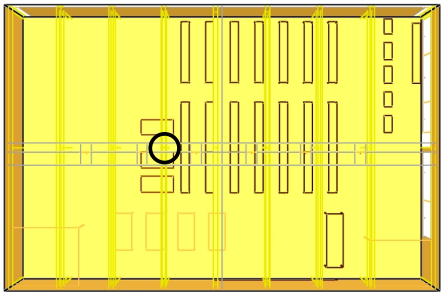

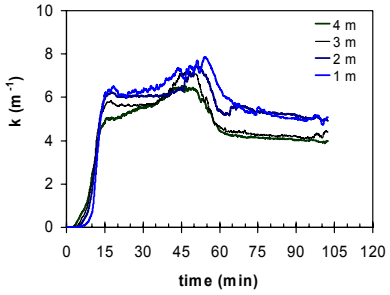

e)

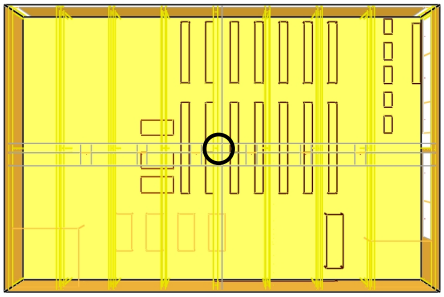

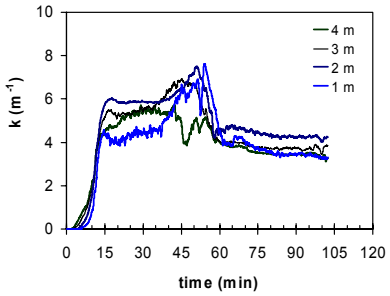

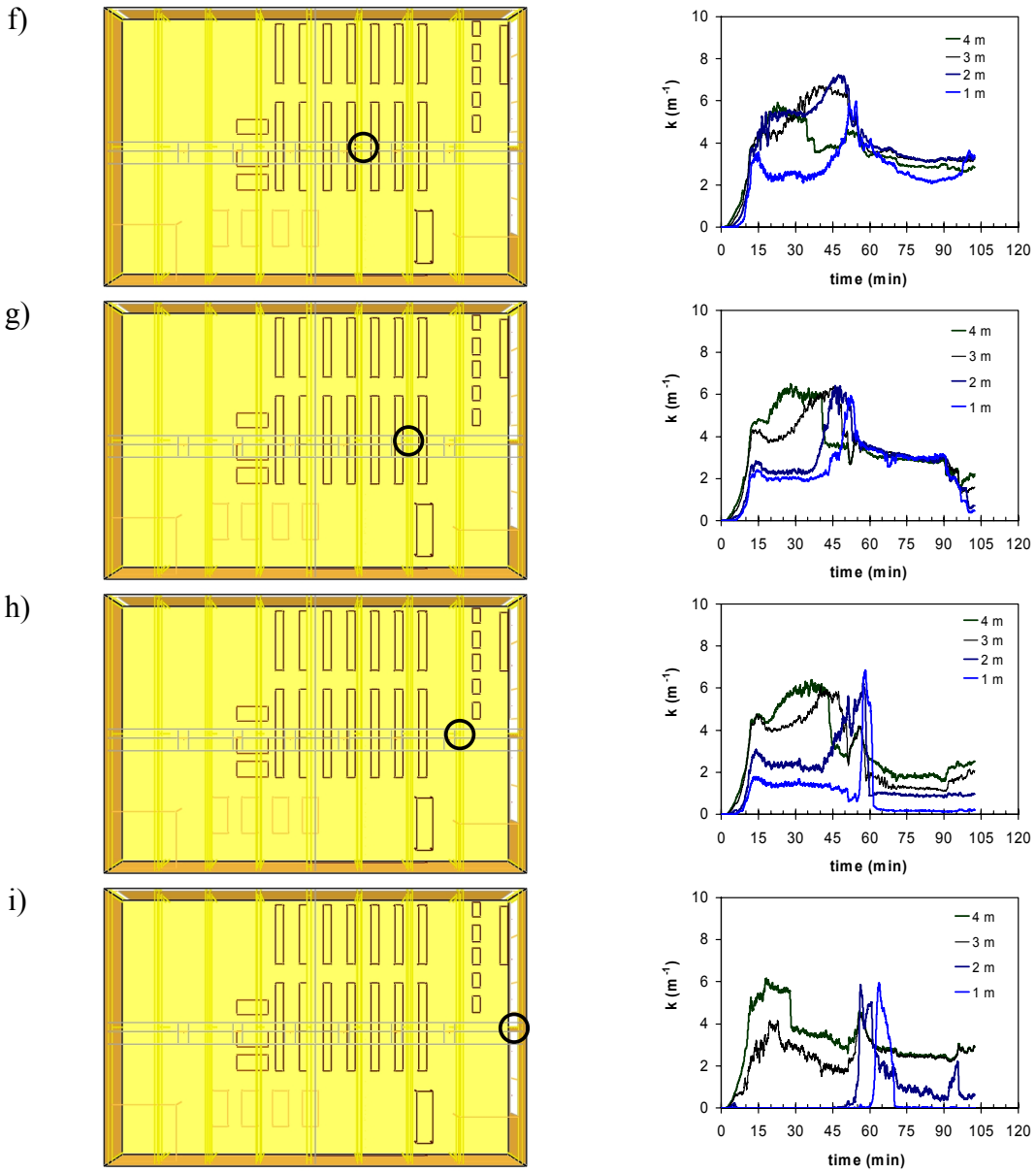

Figure B4. Time dependence of the extinction coefficient at different heights for the fire scenario with glass fallout temperature set at 500 °C: a) x = 0 m, b) x = 6 m, c) x = !2 m, d) x = 18 m, e) x = 24 m, f) x = 30 m, g) x = 36 m, h) x = 42 m and i) x = 48 m. To clarify the curves, the simulation results have been smoothed by using a 30-s sliding averaging procedure.

Flow field

The flow field is illustrated by a 2-dimensional planar cut at height z = 4,0 m as well as profiles along a line x = 29,5 m and z = 4,0 m.

Scenario with window breaking temperature set at 500 ˚C

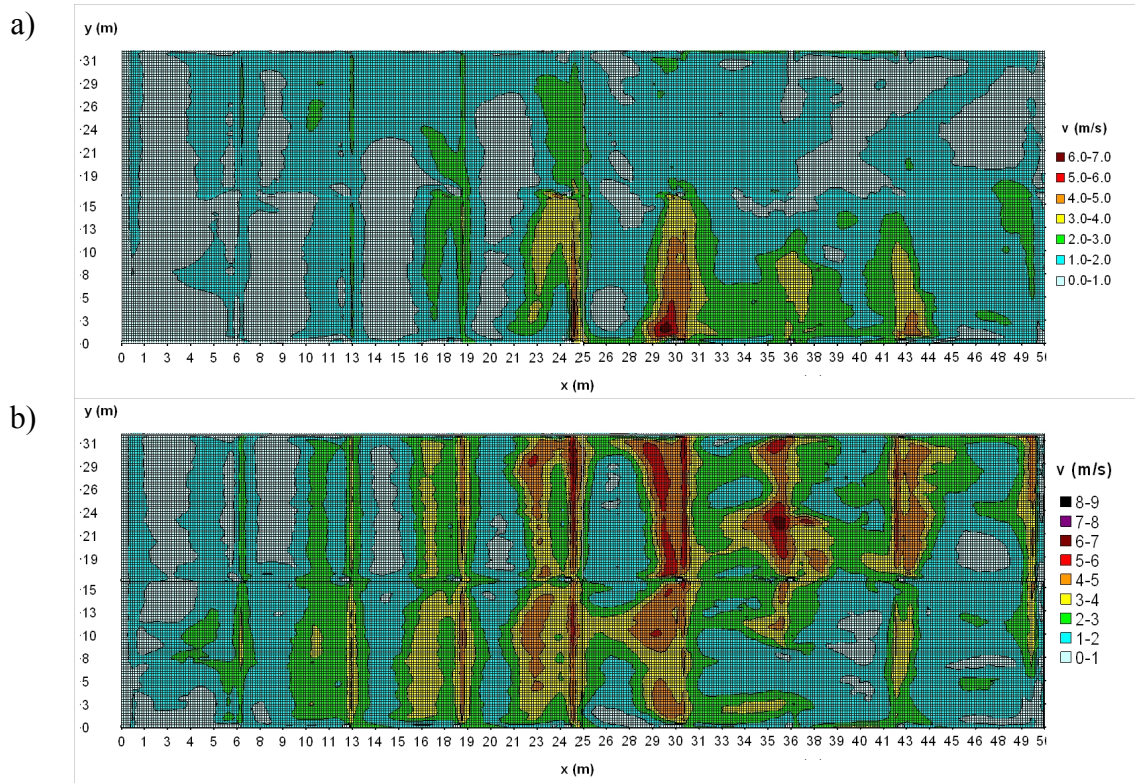

Figure B5. Flow velocity field at height z = 4,0 m, average values during a) 35–40 minutes and b) 85–90 minutes.

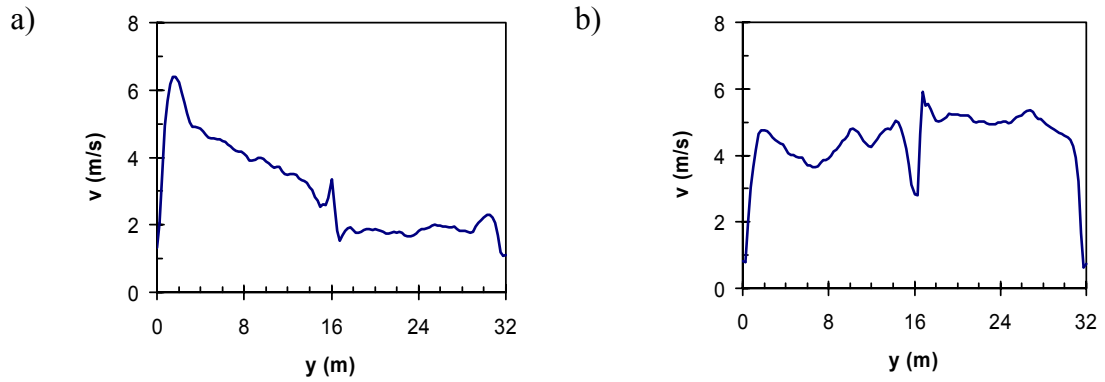

Figure B6. Flow velocity profiles along line x = 29,5 m and z = 4,0 m, average values during a) 35–40 minutes and b) 85–90 minutes.

Appendix C: Thermal properties of air

The heat transfer coefficient depends on the mean boundary layer temperature via the thermal conductivity, kinematic viscosity and thermal diffusivity of air. These values are tabulated in Table B1 (Atreya 2002). For the needs of the Monte Carlo simulations of the heat transfer coefficient, we model these data using a simple functional model

$$f(T) = f_0 + \sum_{n=1}^{2} A_n \tanh^{p_n}\left(\frac{T}{w_n}\right). \qquad \text{(C1)}$$

Results of the least-squares fittings are shown in Figure B1.

Table C1. Temperature dependence of the thermal conductivity, kinematic viscosity and thermal diffusivity of air.

T (˚C)	Thermal Conductivity λ_g ($Wm^{-1}K^{-1}$)	Kinematic Viscosity ν (m^2/s)	Thermal Diffusivity α (m^2/s)
27	0,0263	1,59E-05	2,25E-05
77	0,0300	2,10E-05	2,99E-05
127	0,0338	2,64E-05	3,83E-05
177	0,0373	3,24E-05	4,72E-05
227	0,0407	3,88E-05	5,67E-05
277	0,0439	4,56E-05	6,67E-05
327	0,0469	5,27E-05	7,69E-05
377	0,0497	6,02E-05	8,73E-05
427	0,0524	6,81E-05	9,80E-05
477	0,0549	7,64E-05	1,09E-04
527	0,0573	8,49E-05	1,20E-04
577	0,0596	9,38E-05	1,31E-04
627	0,0620	1,03E-04	1,43E-04
677	0,0643	1,12E-04	1,55E-04
727	0,0667	1,22E-04	1,69E-04
827	0,0715	1,42E-04	1,95E-04
927	0,0763	1,63E-04	2,24E-04
1027	0,0820	1,85E-04	2,57E-04
1227	0,1000	2,40E-04	3,50E-04

a)

b)

c)

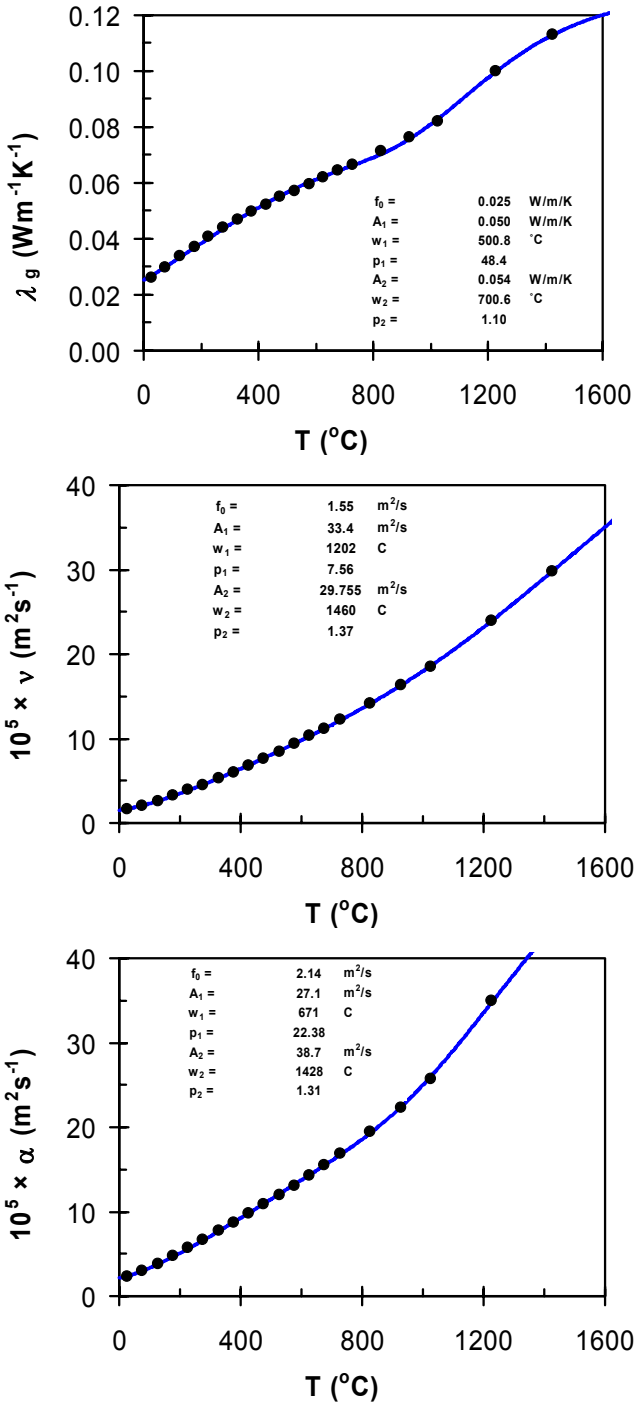

Figure C1. a) Thermal conductivity, b) kinematic viscosity and c) thermal diffusivity of air vs. temperature.

References of Appendix C

Atreya, A. 2002. Convection heat transfer. In: DiNenno, P. J., Drysdale, D., Beyler, C. L., Walton, W. D. (ed.). Quincy: SFPE Handbook for Fire Protection Engineering, 3. Edition, Pp. 1/39–1/64.

Appendix D: The time-dependent event tree risk analysis method

The basic idea of the method is to analyse the fire incident by dividing its progress to a relatively small number of discrete time intervals. At each time interval an event tree is constructed to describe the fire-related processes and potential actions (by humans or automatic systems) to detect and fight the fire. The details of the progress of the fire incident are described through the branching probabilities of the event trees.

The processes which may take place during a fire may be those driven by the fire, *e.g.*, build up of a smoke layer in the space, ignition of secondary objects, breaking of glass and heating of structures, etc. In a sense, also the evacuation efforts can be considered as an event driven by the fire. Simultaneously with the fire-driven processes – and in interaction with them – there occur either passive or active actions of detection and notification of the fire as well as efforts to suppress it.

To make their description suitable for event-tree analysis, the different processes are quantified so that they can be expressed in terms of a success-failure characterisation (such as whether smoke layer has reached a critical height or not). The successes or failures are assigned probabilities, which are derived from statistics, reliability data, Monte Carlo simulations, etc., depending on particular process considered.

Analysis of the fire incident using event trees at selected time intervals

General features

The event trees that describe the progress of a fire at a given time interval are subjected to a condition that the fire is not extinguished before the interval. If the fire is out at a given time then its behaviour is known trivially on later times and no event tree analysis is needed anymore. The time evolution of the fire incident is determined from the event trees either by employing conditional probabilities or by treating the system as a Markov-process. It should be also noted that all the probabilities of fire related phenomena (see below) are calculated using stochastic design fires. This means that these probabilities should be used with a condition that the fire is still freely burning design fire, *i.e.*, it is neither extinguished by humans nor by automatic extinguishing systems.

The branching probabilities of the event trees at a given time interval are calculated so that the stochastic design fires are freely developing fires up to the end of that time interval. Thus the only information related to the fire incident is the stochastic RHR

curves or the corresponding fire environment variables such as the hot-gas layer temperature, heat fluxes, etc., at that particular time.

Structure of the time-dependent event trees

There are many events that could change the behaviour of the fire incident as compared to a freely burning stochastic design fire. (The event that the fire is self-terminated is included implicitly in the stochastic design fires.) The principal factors that influence the structure of the event trees are the fire safety systems in the building, such as means of fire detection, alarms, manual first-aid extinction equipment, sprinklers, smoke ventilation systems, and the actions of the fire brigade.

The fire-driven processes in the building, such as smoke filling process and the influence of the fire to the structures, are not included in the event trees. They are described separately after the time development of the fire incident is known, i.e., they are not considered to change the evolution of the fire incident.

The event trees used to analyse the different time intervals are similar in structure, only the probabilities of the branches are different. The event tree structure used in this work is shown in Figure D1. The branches of the event trees correspond to the following events: 1) detection by senses, 2) extinguishing by personnel, 3) automatic detection by heat detectors, 4) actuation of sprinkler heads, 5) success of sprinklers ‘Sprinklers OK’, 6) presence of the fire brigade, 7) success of the fire brigade ‘Fire Br. OK’, and 8) burning out of the fire load ‘Self-term.’. Note that the branches where the fire stops include only one method of extinguishing. For example, the uppermost branch of the event tree, where the fire is manually extinguished by the personnel includes also the cases where the fire load would burn out (or sprinklers would work or fire brigade would success) during the same time interval as the personnel is successful.

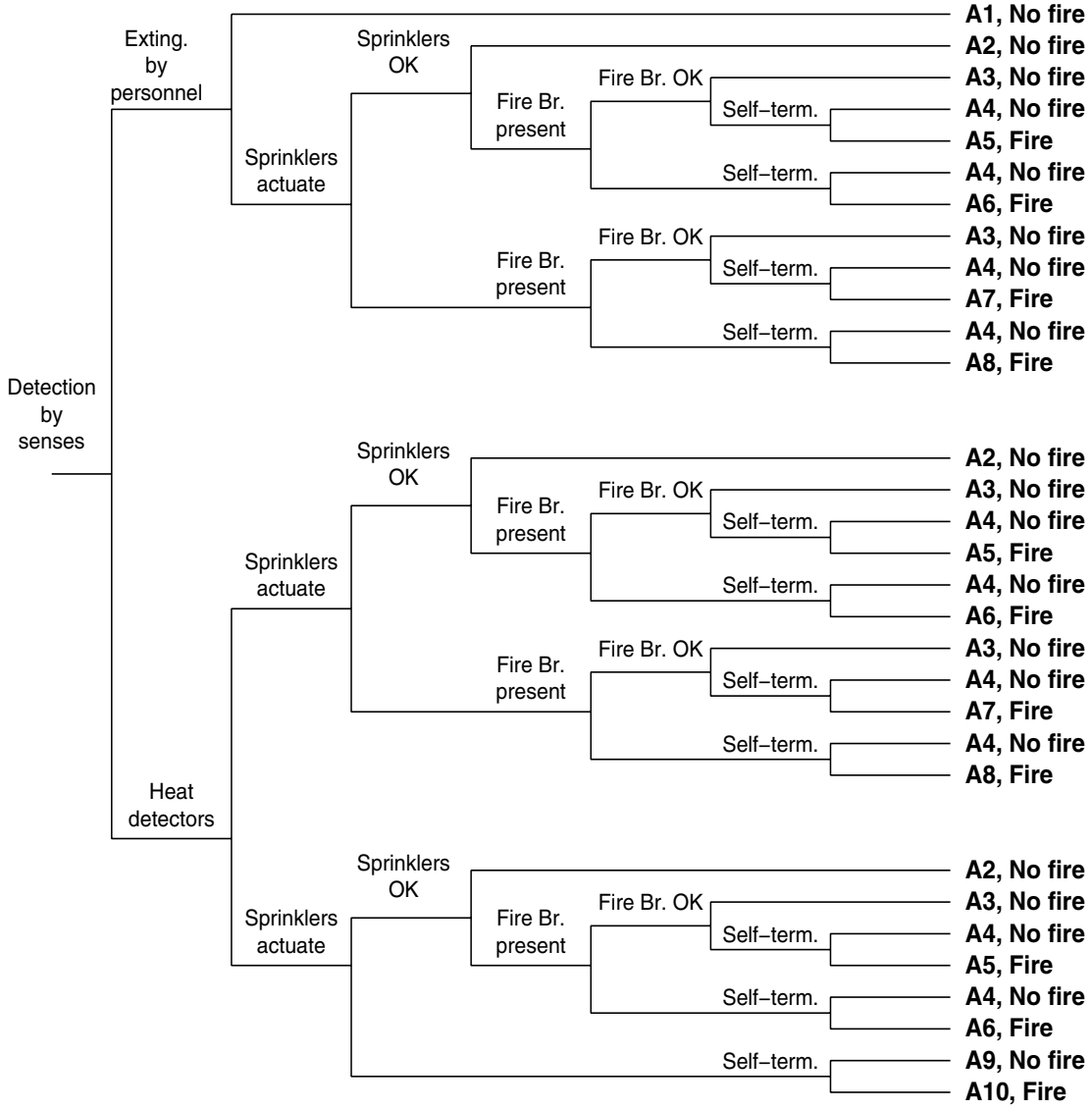

Figure D1. The event tree used to analyse the fire incident at a specific time interval. The upper branches corresponds to a successful operation and lower ones to a failure, e.g., 'Self-term' upper branch means that the fire is self-terminated due to the fact that the fuel load has burnt out. The labels A1-A10 refer to different states of the system.

Evaluation of the time evolution of the paths of events

The time evolution of the fire incident in the target building is calculated by using time-dependent event trees as described above. Let the fire incident be divided to n time intervals, t_1, t_2, …, t_n. The system can be only in ten mutually exclusive states at each time interval. These states are:

- A1: No fire, manual extinction by the personnel

- A2: No fire, extinction by sprinklers
- A3: No fire, extinction by the fire brigade
- A4: No fire, fire load has burnt out
- A5: Fire, personnel, fire brigade, and sprinklers have failed
- A6: Fire, personnel and sprinklers have failed
- A7: Fire, personnel and the fire brigade have failed
- A8: Fire, personnel has failed
- A9: No fire, not detected but no fire load left
- A10: Fire, not detected.

The notation used for the branching probabilities is listed below:

- a_i: Detection by senses
- k_i: Manual extinguishing done by the personnel is successful
- h_i: Detection by automatic (heat) detectors
- f_i: Fire load is burnt out
- s_i: Sprinkler heads actuate (This probability includes also the failure probability of sprinklers due to some malfunction in the system.)
- m_i: Sprinklers extinguish the fire (This probability is set to one, because it is assumed that when a sprinkler system operates correctly, it will extinguish the fire.)
- c_i: Fire brigade is present
- p_i: Extinguishing done by fire brigade is successful.

Manual extinguishing done by the personnel is assumed to occur when the fire is detected by senses. If the fire is first detected by an automatic system (heat detectors, sprinklers) then the personnel does not try to extinguish the fire, i.e., they do not try to find the location of the fire. Sprinklers operate at the time interval when the heads actuate. Fire brigade tries to extinguish the fire at that time interval when it arrives at the fire scene. There is only one extinguishing trial by each of the different extinguishing methods (personnel, sprinklers, fire brigade) during the fire incident. For example, if the fire brigade has arrived at a time interval t_i it does not try to extinguish the fire on the next time interval t_{i+1} anymore. This is a conservative assumption.

The values of the probabilities a_i, k_i, m_i, and p_i are probabilities that an extinguishing (or detection by senses) will be successful at a given time, i.e., they are supposed to depend only on the fire size and, thus, their values at different time intervals are independent of each other. These probabilities at different times are obtained as Monte Carlo averages. For example, the probability, that the manual extinguishing done by the personnel is

successful, is $k(t_i) = k\left(\dot{Q}(t_i)\right)$ at t_i. The branching probability k_i is calculated by an average over the simulated stochastic design fires:

$$k_i = \frac{1}{N_{MC}} \sum_{j=1}^{N_{MC}} k\left(\dot{Q}_j(t_i)\right), \tag{D1}$$

where N_{MC} is the number of the simulated RHR curves.

The branching probabilities h_i, s_i, and c_i are calculated differently. For example, the activation time of a heat detector depends on the whole RHR curve as it is calculated by solving a differential equation. The activation times are solved for each simulated design fires and thus, a probability distribution of the activation times is obtained. The response time of the fire brigade depends naturally on the detection times and thus also branching probability c_i is obtained as a probability distribution.

The values of the probabilities a_i, h_i, f_i, s_i, and c_i are tabulated as cumulative probability distributions. The cumulative probability distributions can not directly be used as branching probabilities, because one should use conditional probabilities at the branching points of the time-dependent event trees. For example, in order to detect the fire by senses at time interval 5–10 min, it should not be detected during the first 5 minutes. So at a time interval 5–10 min we have this additional (a priori) information (fire is not detected during 0–5 min) available and the probabilities will change, i.e., one can not just take the difference of the cumulative distribution between the times 10 and 5 minutes as the value of the branching probability.

To calculate conditional probabilities like those above one can use Bayes' theorem [Milton & Arnold, 1986], which states the probability of an event C_j with a condition that an event B is occurred is

$$P[C_j \mid B] = \frac{P[B \mid C_j] \cdot P[C_j]}{\sum_i P[B \mid C_i] \cdot P[C_i]} \tag{D2}$$

supposed that the probabilities fulfil conditions $P[B] \neq 0$, and that the events C_j are mutually exclusive, and that these states form a complete set. For example, the probability that a fire will be detected by senses during a time interval 5–10 min is calculated below by using Bayes' theorem. Let the cumulative detection probability be *A(t)* and the branching probability, which we need in the event trees, be presented with lower case, i.e., *a(5–10)* is the branching probability that the fire is detected during the time interval. Bayes' theorem reads now as

$$a(5-10) = P[5\text{-}10 \mid \text{not } 0\text{-}5] = \frac{P[\text{not } 0\text{-}5 \mid 5\text{-}10]P[5\text{-}10]}{P[\text{not } 0\text{-}5 \mid 0\text{-}5]P[0\text{-}5]+P[\text{not } 0\text{-}5 \mid 5\text{-}10]P[5\text{-}10]+P[\text{not } 0\text{-}5 \mid 10\text{-}\infty]P[10\text{-}\infty]} \quad \text{(D3)}$$

It is trivially seen that the events (detection during 0–5, 5–10, and 10–∞ min) are clearly mutually exclusive and form a complete set. Also P[not 0–5] $\neq 0$, as demanded. (If the probability of detection during the first time interval would be equal to one, then at later time one knows without any uncertainty that in which branch of the event tree the fire will be.) The probabilities P[not 0-5 | 5-10] and P[not 0–5 | 10–∞] are trivially equal to zero. Also P[not 0–5 | 0–5] is zero and the two other probabilities are P[5–10] = $A(10)–A(5)$ and P[10–∞] = $A(\infty)–A(10)=1–A(10)$. Finally the correct branching probabilities are

$$a(5-10) = \frac{A(10)-A(5)}{\big(A(10)-A(5)\big)+\big(A(\infty)-A(10)\big)} = \frac{A(10)-A(5)}{1-A(5)} \ . \quad \text{(D4)}$$

Calculations using conditional probabilities

The probabilities of states A_j after the break out of a fire are calculated by using the branching probabilities of the event trees. The following notation is used for these probabilities: $P\left[A_j^{ti}\right]$ is the probability that the system is at state A_j at the end point of the ith time interval. The fire is at state A_{10} , when the fire breaks out, so that the probability $P\left[A_{10}^{t0}\right] = 1$ and the probabilities of all the other states are equal to zero. At time t_1 = 5 min the probabilities of the states of the system are

$$P\left[A_1^{t1}\right] = P\left[A_1^{t0}\right] + a_1 k_1 \cdot P\left[A_{10}^{t0}\right] \quad \text{(D5)}$$

$$P\left[A_2^{t1}\right] = P\left[A_2^{t0}\right] + s_1 m_1 \cdot P\left[A_7^{t0}\right] + s_1 m_1 \cdot P\left[A_8^{t0}\right] + \left(a_1 \bar{k}_1 s_1 m_1 + \bar{a}_1 s_1 m_1\right) \cdot P\left[A_{10}^{t0}\right] \quad \text{(D6)}$$

$$\vdots \qquad\qquad \vdots$$

$$P\left[A_{10}^{t1}\right] = \bar{a}_1 \bar{h}_1 \bar{s}_1 \bar{f}_1 \cdot P\left[A_{10}^{t0}\right] \quad \text{(D7)}$$

Overbars above the branching probabilities mean complementary probabilities. Note also, that the sum of the probabilities is equal to one at each time, because the system must be in one of states. The probabilities at later times are calculated similarly, only

the time indices are increased on every time step. The transition probabilities between different states are tabulated in Table D1. Using this notation Equations (a)-(j) may be written as

$$P\left[A_j^t\right] = \sum_k M_{k\to j} \cdot P\left[A_k^{t-1}\right], \quad j = 1,\ldots,10 \ . \tag{D8}$$

Table D1. Transition probabilities related to the states A_i, i = 5, 6, 7, 8, 10, i.e., the states where the fire is still burning. The state A10 is the initial state of the system. An overbar means complement. Shown are only the allowed transitions. The transition probabilities for states A_i, i = 1,2,3,4,9, i.e., the states where the fire is extinguished, are all zero except the identity transitions $A_i \to A_i$, which equal to one.

transitions $A_{10} \to A_j$	**transition factor** $M_{10\to j}$
$A_{10} \to A_1$	ak
$A_{10} \to A_2$	$\mathrm{a\bar{k}sm} + \mathrm{\bar{a}sm}$
$A_{10} \to A_3$	$\mathrm{a\bar{k}s\bar{m}cp} + \mathrm{a\bar{k}\bar{s}cp} + \mathrm{\bar{a}hs\bar{m}cp} + \mathrm{\bar{a}h\bar{s}cp} + \mathrm{\bar{a}\bar{h}s\bar{m}cp}$
$A_{10} \to A_4$	$\mathrm{a\bar{k}(s\bar{m}c\bar{p}f} + \mathrm{s\bar{m}c\bar{f}} + \mathrm{\bar{s}c\bar{p}f} + \mathrm{\bar{s}\bar{c}f)} + \mathrm{\bar{a}\bar{h}(s\bar{m}c\bar{p}f} + \mathrm{s\bar{m}c\bar{f}) +}$ $\mathrm{\bar{a}h(s\bar{m}c\bar{p}f} + \mathrm{s\bar{m}c\bar{f}} + \mathrm{\bar{s}c\bar{p}f} + \mathrm{\bar{s}\bar{c}f)}$
$A_{10} \to A_5$	$\mathrm{a\bar{k}s\bar{m}c\bar{p}\bar{f}} + \mathrm{\bar{a}s\bar{m}c\bar{p}\bar{f}}$
$A_{10} \to A_6$	$\mathrm{a\bar{k}s\bar{m}c\bar{f}} + \mathrm{\bar{a}s\bar{m}c\bar{f}}$
$A_{10} \to A_7$	$\mathrm{a\bar{k}\bar{s}c\bar{p}\bar{f}} + \mathrm{\bar{a}h\bar{s}c\bar{p}\bar{f}}$
$A_{10} \to A_8$	$\mathrm{a\bar{k}\bar{s}\bar{c}f} + \mathrm{\bar{a}h\bar{s}\bar{c}f}$
$A_{10} \to A_9$	$\mathrm{\bar{a}\bar{h}\bar{s}f}$
$A_{10} \to A_{10}$	$\mathrm{\bar{a}\bar{h}\bar{s}\bar{f}}$
transitions $A_5 \to A_j$	**transition factor** $M_{5\to j}$
$A_5 \to A_4$	f
$A_5 \to A_5$	$\mathrm{\bar{f}}$
transitions $A_6 \to A_j$	**transition factor** $M_{6\to j}$
$A_6 \to A_3$	cp
$A_6 \to A_4$	$\mathrm{c\bar{p}f} + \mathrm{\bar{c}f}$
$A_6 \to A_5$	$\mathrm{c\bar{p}\bar{f}}$
$A_6 \to A_6$	$\mathrm{\bar{c}\bar{f}}$
transitions	

$A_7 \rightarrow A_j$	**transition factor** $M_{7\rightarrow j}$
$A_7 \rightarrow A_2$	sm
$A_7 \rightarrow A_4$	$\mathrm{s\overline{m}f} + \mathrm{\overline{s}f}$
$A_7 \rightarrow A_5$	$\mathrm{s\overline{m}\overline{f}}$
$A_7 \rightarrow A_7$	$\mathrm{\overline{s}\overline{f}}$
transitions $A_8 \rightarrow A_j$	**transition factor** $M_{8\rightarrow j}$
$A_8 \rightarrow A_2$	sm
$A_8 \rightarrow A_3$	$\mathrm{s\overline{m}cp} + \mathrm{\overline{s}cp}$
$A_8 \rightarrow A_4$	$\mathrm{s\overline{m}c\overline{p}f} + \mathrm{s\overline{m}\overline{c}f} + \mathrm{\overline{s}c\overline{p}f} + \mathrm{\overline{s}\overline{c}f}$
$A_8 \rightarrow A_5$	$\mathrm{s\overline{m}c\overline{p}\overline{f}}$
$A_8 \rightarrow A_6$	$\mathrm{s\overline{m}\overline{c}\overline{f}}$
$A_8 \rightarrow A_7$	$\mathrm{\overline{s}c\overline{p}\overline{f}}$
$A_8 \rightarrow A_8$	$\mathrm{\overline{s}\overline{c}\overline{f}}$

Calculations using a Markov process approach

By examining the equations above it is noticed that the probabilities of the states at a given time step depend only on the probabilities of the previous time step and on the known time-dependent branching probabilities. If the probabilities of the states are considered to be random variables then this system is a Markov process. A Markov process does not have memory, i.e., its future states are fully described by the present values of the random variables. The process is show schematically in Figure D2. The transition probabilities can be found in Table D1. For example, one can end up in the state A_2 (fire is extinguished by sprinklers) by three different ways: 1) from state A_7 if the sprinklers will actuate and be successful during a time interval. 2) form state A_8 if the sprinklers will actuate and be successful during a time interval. 3) from state A_{10} by two different ways, either no detection by senses, sprinklers will actuate and be successful or detection by senses but personnel fails and sprinklers will actuate and be successful. Similarly all the other transition probabilities between different states can be found.

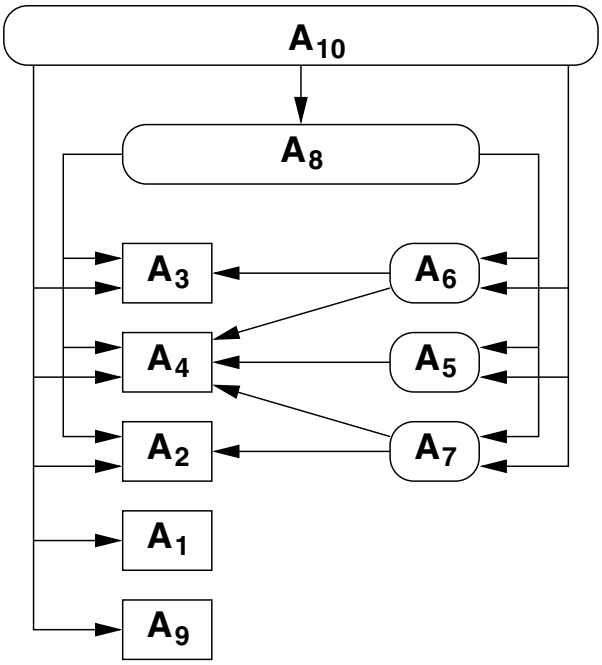

Figure D2. Allowed transitions between the states of the system. When the fire starts (time zero) the system is in the state A_{10}. States denoted by the sharp rectangles are final states of the system, i.e. states where the fire is extinguished. In states denoted by the rounded rectangles the fire is still burning.

Define a state vector $\mathbf{A}^i = \left(A_1^i, A_2^i, \ldots, A_p^i\right)^T$ and a corresponding probability vector $\mathbf{P}[\mathbf{A}^i] = \left(P[A_1^i], P[A_2^i], \ldots, P[A_p^i]\right)^T$, where superscripts label the time and subscripts label the states 1, 2,…, p (let the number of states be p). Using this notation the above process can be written as a Markov chain

$$\mathbf{P}[\mathbf{A}^i] = \mathbf{M}_i \, \mathbf{P}[\mathbf{A}^{i-1}], \quad i = 1, \ldots, n, \tag{D9}$$

where $\mathbf{M}_i$ is the transition matrix moving the system from time t_{i-1} to time t_i. The system is initially at state $\mathbf{A}^0$. In our example case the system is at the state A_{10} , so that the probability vector has a value $\mathbf{P}[\mathbf{A}^0] = (0,0,0,0,0,0,0,0,0,1)^T$ at time zero.

For the example case the matrix equation read as

$$\begin{pmatrix} P[A_1^i] \\ P[A_2^i] \\ P[A_3^i] \\ \vdots \\ P[A_{10}^i] \end{pmatrix} = \begin{pmatrix} m_{11}^i & m_{12}^i & m_{13}^i & \cdots & m_{1,10}^i \\ m_{21}^i & m_{22}^i & m_{23}^i & \cdots & m_{2,10}^i \\ m_{31}^i & m_{32}^i & m_{33}^i & \cdots & m_{3,10}^i \\ \vdots & \vdots & \vdots & \ddots & \vdots \\ m_{10,1}^i & m_{10,2}^i & m_{10,3}^i & \cdots & m_{10,10}^i \end{pmatrix} \begin{pmatrix} P[A_1^{i-1}] \\ P[A_2^{i-1}] \\ P[A_3^{i-1}] \\ \vdots \\ P[A_{10}^{i-1}] \end{pmatrix} . \qquad \text{(D10)}$$

Because the Markov process is dealing with probabilities and the used set of states is a complete one, the columns of the matrix **M** should sum up to one.

The elements of the transition matrix **M** are obtained by inspecting the Markov process. States surrounded with sharp rectangles (A_1, A_2, A_3, A_4, and A_5) are final states, i.e., states where the fire is extinguished. Once the fire has reached one of these states it will remain in that state, so the transition probabilities from these states to themselves, $M_{k\to k}$, are equal to one. All the other non-zero transition probabilities are listed below. The structure of the transition matrix is thus

$$\mathbf{M}_i = \begin{pmatrix} 1 & 0 & 0 & 0 & 0 & 0 & 0 & 0 & 0 & M_{10\to 1} \\ 0 & 1 & 0 & 0 & 0 & 0 & M_{7\to 2} & M_{8\to 2} & 0 & M_{10\to 2} \\ 0 & 0 & 1 & 0 & 0 & M_{6\to 3} & 0 & M_{8\to 3} & 0 & M_{10\to 3} \\ 0 & 0 & 0 & 1 & M_{5\to 4} & M_{6\to 4} & M_{7\to 4} & M_{8\to 4} & 0 & M_{10\to 4} \\ 0 & 0 & 0 & 0 & M_{5\to 5} & M_{6\to 5} & M_{7\to 5} & M_{8\to 5} & 0 & M_{10\to 5} \\ 0 & 0 & 0 & 0 & 0 & M_{6\to 6} & 0 & M_{8\to 6} & 0 & M_{10\to 6} \\ 0 & 0 & 0 & 0 & 0 & 0 & M_{7\to 7} & M_{8\to 7} & 0 & M_{10\to 7} \\ 0 & 0 & 0 & 0 & 0 & 0 & 0 & M_{8\to 8} & 0 & M_{10\to 8} \\ 0 & 0 & 0 & 0 & 0 & 0 & 0 & 0 & 1 & M_{10\to 9} \\ 0 & 0 & 0 & 0 & 0 & 0 & 0 & 0 & 0 & M_{10\to 10} \end{pmatrix} . \qquad \text{(D11)}$$

The (non-zero) transitions probabilities $M_{j\to k}$ can be formed by inspecting the dynamics of the process. For example, transition probability $M_{10\to 2}$ (from state 'fire burning unnoticed' to state 'fire extinguished by sprinklers') has two contributions: 1) detection by senses, manual extinguishing fails, sprinklers actuate and extinguish the fire has probability $a\bar{k}sm$ and 2) fire is not detected by senses, sprinklers actuate and extinguish the fire has probability $\bar{a}sm$. (Note, that the later case includes both the case where (heat) detectors alarm and do not alarm, $h + \bar{h} = 1$.)

After the transition matrices $\mathbf{M}_i$ are formed for each time step t_i it is easy to calculate the probabilities of states A_k at any time step as follows. One starts at the initial state probability vector $\mathbf{P}[\mathbf{A}^0]$ and multiplies this by the transition matrix $\mathbf{M}_1$ to get the

probabilities $\mathbf{P}[\mathbf{A}^1]$ at time t_i. The probabilities at all later times are obtained similarly, i.e., by multiplying previous probability vector with the corresponding transition matrix:

$$\begin{aligned}
\mathbf{P}[\mathbf{A}^1] &= \mathbf{M}_1\mathbf{P}[\mathbf{A}^0], \\
\mathbf{P}[\mathbf{A}^2] &= \mathbf{M}_2\mathbf{P}[\mathbf{A}^1] = \mathbf{M}_2\mathbf{M}_1\mathbf{P}[\mathbf{A}^0], \\
&\vdots \\
\mathbf{P}[\mathbf{A}^n] &= \mathbf{M}_n\mathbf{P}[\mathbf{A}^{n-1}] = \mathbf{M}_n\cdots\mathbf{M}_2\mathbf{M}_1\mathbf{P}[\mathbf{A}^0].
\end{aligned} \tag{D12}$$

VTT Working papers

33 Pötry, Jyri, Törmälä, Aarno, Salo, Raija & Hemilä, Jukka. Toimitusketjun hallinnan ja hankinnan toimintamalleja Italiassa. Vierailukokemuksia keväältä 2005. 2005. 32 s. + liitt. 4 s.

34 Leppälä, Kari, Kääriäinen, Jukka, Takalo, Juha & Savolainen, Pekka. Challenging global competition: tune up your product development. 2005. 36 p.

35 Rosqvist, Tony. Fatigue Analysis for Fleet Management using Bayesian Networks. 2005. 25 p.

36 Forsström, Juha, Lehtilä, Antti. Skenaarioita ilmastopolitiikan vaikutuksista energiatalouteen. 2005. 71 s. + liitt. 9 s.

37 Hietaniemi, Jukka & Rinne, Tuomo. Tulipalojen yksittäispäästöt ilmaan: laskennallinen lähestymistapa. 2005. 78 s.

38 Kevarinmäki, Ari, Oksanen, Tuuli & Yli-Koski, Rainer. Ruostumattomasta teräksestä valmistettujen puurakenteiden liitosten suunnittelu. Yleiset ohjeet ja palomitoitus. 2005. 51 s. + liitt. 12 s.

39 Mroz, Arkadiusz & Kärnä, Tuomo. Mitigation of ice loading. Feasibility study of semi-active solution. 2005. 34 p.

40 Paloposki, Tuomas, Tillander, Kati, Virolainen, Kimmo, Nissilä, Minna & Survo, Kyösti. Sammutusjätevedet ja ympäristö. 2005. 75 s. + liitt. 10 s.

41 Hietaniemi, Jukka. Probabilistic simulation of glass fracture and fallout in fire. 2005. 88 p. + app. 33 p.

42 Belloni, Kaisa, Villberg, Kirsi, Tillander, Kati, Saarela, Kristina & Paloposki, Tuomas. Tulipalon jälkihajujen poisto. 2005. 124 s.

43 Tsupari, Eemeli, Tormonen, Kauko, Monni, Suvi, Vahlman, Tuula, Kolsi, Aimo & Linna, Veli. Dityppioksidin (N_2O) ja metaanin (CH_4) päästökertoimia Suomen voimalaitoksille, lämpökeskuksille ja pienpoltolle. 2006. 94 s. + liitt. 7 s.

44 Saarinen, Jani, Rilla, Nina, Loikkanen, Torsti, Oksanen, Juha & Alasaarela, Jaakko. Innovaatioympäristö tänään ja huomenna. 2006. 32 s.

45 Heinonen, Jaakko. Preliminary Study of Modelling Dynamic Properties of Magnetorheological Fluid Damper. 2006. 36 p.

46 Häkkinen, Kai & Salmela, Erno. Logistiikkapalveluyhtiömalleja Suomen metalliteollisuudessa. Havaintoja vuonna 2005. SERVIISI-projektin osaraportti. 2006. 17 s.

47 Kurtti, Reetta & Reiman, Teemu. Organisaatiokulttuuri logistiikkapalveluorganisaatiossa. Tutkimus viidessä palveluvarastossa. 2006. 30 s.

48 Soimakallio, Sampo, Perrels, Adriaan, Honkatukia, Juha, Moltmann, Sara & Höhne, Niklas. Analysis and Evaluation of Triptych 6. Case Finland. 2006. 70 p. + app. 8 p.

49 Saarinen, Jani, Rilla, Nina, Loikkanen, Torsti, Oksanen, Juha & Alasaarela, Jaakko. Innovation environment today and tomorrow. 2006. 32 p.

50 Törnqvist, Jouko & Talja, Asko. Suositus liikennetärinän arvioimiseksi maankäytön suunnittelussa. 2006. 46 s. + liitt. 33 s.

51 Aikio, Sanna, Grönqvist, Stina, Hakola, Liisa, Hurme, Eero, Jussila, Salme, Kaukoniemi, Otto-Ville, Kopola, Harri, Känsäkoski, Markku, Leinonen, Marika, Lippo, Sari, Mahlberg, Riitta, Peltonen, Soili, Qvintus-Leino, Pia, Rajamäki, Tiina, Ritschkoff, Anne-Christine, Smolander, Maria, Vartiainen, Jari, Viikari, Liisa & Vilkman, Marja. Bioactive paper and fibre products. Patent and literary survey. 2006. 83 p.

52 Alanen, Raili & Hätönen, Hannu. Sähkön laadun ja jakelun luotettavuuden hallinta. State of art -selvitys. 2006. 84 s.

53 Pasonen, Markku & Hakkarainen, Toni. Kaukolämpölinjojen elinikä ja NDT. 2006. 27 s.

54 Hietaniemi, Jukka, Toratti, Tomi, Schnabl, Simon & Turk, Goran. Application of reliability analysis and fire simulation to probabilistic assessment of fire endurance of wooden structures. 2006. 97 p. + app. 23 p.

ISBN 951–38–6606–8 (URL: http://www.vtt.fi/publications/index.jsp)
ISSN 1459–7683 (http://www.vtt.fi/publications/index.jsp)